

Winter Maintenance of Permeable Interlocking Concrete Pavement: Examining Opportunities to Reduce Road Salt Pollution and Improve Winter Safety

by

Jeffrey Thomas Marvin

A thesis submitted in conformity with the requirements
for the degree of Master of Applied Science
Department of Civil & Mineral Engineering
University of Toronto

© Copyright by Jeffrey Marvin 2019

Winter Maintenance of Permeable Interlocking Concrete Pavement: Examining Opportunities to Reduce Winter Road Salt Pollution and Improve Winter Safety

Jeffrey Marvin

Master of Applied Science

Department of Civil & Mineral Engineering
University of Toronto

2019

Abstract

Permeable Interlocking Concrete Pavement (PICP) rapidly drains surface water through its paver joint spaces and therefore has the potential to prevent ice from forming during winter conditions. As a result, PICP may reduce the amount of road salt needed for de-icing paved surfaces, and it may also reduce the risk of pedestrian slipping and vehicle skidding. PICP also has the potential to reduce chloride concentrations released to the environment from winter salting practices, as melted ice and snow are temporarily retained within the aggregates of its base and subbase layers. This study evaluates the performance of an outdoor PICP and asphalt test pad over two winter seasons in Vaughan, Ontario by assessing differences in surface conditions, surface friction, surface temperatures, and chloride concentrations. PICP was found to prevent melted ice and snow from refreezing, have less drastic reductions in surface temperatures at sunset, and attenuate and delay chloride concentrations.

Acknowledgments

I would first like to thank Dr. Jennifer Drake for being such an outstanding research supervisor who has always supported me and who provided me with many great opportunities during my time in academia. Thank you for all your help and generosity, and for being available during such a busy phase of your life. Thank you also to Dr. Elodie Passeport for your substantial help in refining my state-of-the-art bioretention review paper for publication. I am more than grateful to have worked with such a knowledgeable and supportive individual in accomplishing such a momentous task. I would also like to thank Dr. Shoshanna Saxe for her review of my thesis. Coming from a different field of research, her feedback greatly helped to put everything back into a bigger picture perspective.

I want to thank all those in our research group who were involved with my field work during the past two winters, particularly Jody Scott who braved many storms with me, as well as Sylvie Spraakman and Kelsey Smyth who joined me on some of the coldest days of the year. I also want to extend a huge thanks to Mark Hummel and Dean Luciani at the Toronto and Region Conservation Authority (TRCA) for the massive amount of support they provided on this project, as well as the other TRCA staff at the Kortright Centre for Conservation who helped me with odds and ends and provided warm company during the cold Vaughan winters.

I also want to thank all my friends and family for their continuous support. I particularly want to thank my martial arts instructors and peers who provided a very welcoming, informative, and entertaining community during my stay in Toronto. Most of my time outside of the university was spent training and hanging out with this great group of individuals who kept my mind sharp and refreshed rather than being too narrowly focused on my work. Finally and most importantly, I want to thank my partner Jo for being so loving and supportive while she was also completing her own thesis, and I am very grateful that we were able to achieve our goals together.

This work was funded by the Interlocking Concrete Pavement Institute (ICPI), the Natural Sciences and Engineering Research Council of Canada (NSERC) Strategic Project Grant awarded to Jennifer Drake, and both the Gordon F. Newell Scholarship donated by Professor Gerald N. Steuart and the NSERC Graduate Scholarships-Master's awarded to Jeffrey Marvin. Research was carried out in partnership with ICPI and TRCA. Pavement materials for the research site were donated by Lafarge and Brampton Brick.

Table of Contents

Acknowledgments.....	iii
Table of Contents.....	iv
List of Tables.....	vi
List of Figures.....	vii
List of Appendices.....	ix
Chapter 1.....	1
1 Introduction.....	1
1.1 Winter Performance and Operation of Permeable Interlocking Concrete Pavement.....	1
1.2 Research Objectives.....	2
1.3 Thesis Structure.....	3
Chapter 2.....	4
2 Winter Maintenance of Permeable Interlocking Concrete Pavement: Evaluating Opportunities to Reduce Road Salt Pollution and Improve Winter Safety.....	4
2.1 Introduction.....	5
2.2 Methodology.....	7
2.2.1 Test Site Configuration.....	7
2.2.2 Winter Operations.....	10
2.2.3 De-Icing Treatments.....	12
2.2.4 Surface Temperature and Surface Condition Monitoring.....	13
2.2.5 Surface Friction Measurements.....	15
2.3 Results and Discussion.....	17
2.3.1 Surface Temperatures.....	17
2.3.2 Melting Processes during Undisturbed Snow Conditions.....	22
2.3.3 Surface Friction during Dry Pavement Conditions.....	24
2.3.4 Shovelled Snow Experiments.....	24

2.3.5	Ice Cover Experiments.....	27
2.4	Conclusions and Recommendations	32
Chapter 3	34
3	Additional Data and Observations	35
3.1	Evaluation of Chloride Concentrations in PICP Outflows	35
3.1.1	Methodology.....	35
3.1.2	Results and Discussion	37
3.1.3	Conclusions and Recommendations	47
3.2	Evaluation of Non-Contact Infrared Sensors for Measuring PICP Surface Temperatures.....	48
3.2.1	Methodology.....	48
3.2.2	Results and Discussion	51
3.2.3	Conclusions and Recommendations	55
3.3	Evaluation of Surface Friction Measuring Devices for PICP under Winter Conditions ...	56
3.3.1	Methodology.....	56
3.3.2	Results and Discussion	56
3.3.3	Conclusions and Recommendations	58
Chapter 4	59
4	Conclusions	60
References	63
Appendices	66

List of Tables

Table 1: Thermal properties of PICP and asphalt.	9
Table 2: Winter maintenance activities carried out on pavement cells.	11
Table 3: De-icer type and application rate for each test cell.....	13
Table 4: Comparison of air temperatures at research site with climate normal values.	18
Table 5: Comparison of surface temperatures between PICP and asphalt surfaces.	19
Table 6: Pavement melt times for undisturbed conditions.....	23
Table 7: List of included and excluded data from shovelled snow experiments.	25
Table 8: Mean DCOF and TCOF values for shovelled snow experiments.	25
Table 9: Comparison of PICP cell variables for shovelled snow experiments.....	26
Table 10: Comparison of friction between pavement cells for 16/Feb/2019 experiment.....	29
Table 11: Background and peak winter conductivities in pavement cell outflows.	38
Table 12: Chloride concentrations measured in water samples.....	43
Table 13: Estimations of peak winter chlorides in pavement cell outflows.	47
Table 14: Monthly averages of contact and infrared sensor data.	53

List of Figures

Figure 1: Surface layout of outdoor pavement test pad (facing south).....	8
Figure 2: Cross-sectional layout of (a) PICP and (b) asphalt test cells.	10
Figure 3: Surface friction measuring devices in use on ice covered PICP surfaces: (a) SlipAlert and (b) Mark IIIB.....	15
Figure 4: Box plot comparison of all surface temperature data and of data collected during clear conditions when no ice and snow were present.	18
Figure 5: Air and surface temperatures during (a) typical diurnal pattern in March 2018, (b) snow-covered period in February 2019.	20
Figure 6: Box plot comparison of daily sunset hour surface temperatures.....	21
Figure 7: Means and ranges of (a) DCOF and (b) TCOF measurements collected during 16/Feb/2019 experiment.	28
Figure 8: Ice and snow coverage during melting and refreeze on 16/Feb/2019.....	29
Figure 9: Installation of traps for housing conductivity sensors.....	36
Figure 10: Conductivity measurements collected during the 2019 winter and spring.	38
Figure 11: Water depth measurements collected during the 2019 winter and spring.....	41
Figure 12: Water temperature measurements collected during the 2019 winter and spring.	41
Figure 13: Linear regressions of conductivity and chloride data.....	45
Figure 14: Estimated chloride concentrations during the 2019 winter and spring.	46
Figure 15: Infrared sensor installation showing approximate extent of 75% data capture on PICP-RS-M and Asph-RS-M.	50
Figure 16: Box plot comparison of surface temperatures measured by contact sensors and infrared sensors for (a) all surface cover conditions and (b) clear conditions.	52

Figure 17: Surface temperature measurements collected from contact sensors and infrared sensors after a snowfall event on 27/Feb/2019, subsequent snow compaction on 28/Feb/2019, and partial melting of the asphalt cell on 01/Mar/2019. 53

Figure 18: Surface temperature measurements collected from contact sensors and infrared sensors during clear conditions on 24/Mar/2019. 54

List of Appendices

Appendix A: Site Photos.....	67
Appendix B: Surface Friction Data.....	85
Appendix C: Normality Testing of Friction Data on PICP Cells for Shovelled Snow Experiments	99
Appendix D: State-of-the-Art Review Paper on Phosphorus Sorption Amendments in Bioretention Media	105

Chapter 1

1 Introduction

1.1 Winter Performance and Operation of Permeable Interlocking Concrete Pavement

Permeable Interlocking Concrete Pavement (PICP) is a type of Permeable Pavement (PP) system and Low Impact Development (LID) stormwater practice that uses the joint spaces between pavers to drain water from the surface into an aggregate base and subbase layer. Water collected by the aggregate layers are stored and treated before infiltrating into the native soil below or being discharged to the downstream drainage system through a perforated underdrain. PICP systems are commonly used for roadways, walkways, driveways, and parking lots in lieu of conventional pavement systems for their added benefit of reducing and treating stormwater runoff. This helps to preserve the pre-development hydrological conditions of a paved area, which mitigates downstream flooding and reduces the amount of pollutants discharged to the environment. PICP systems can be designed to allow for zero infiltration, partial infiltration, or full infiltration into the underlying soils, all of which provide some level of both water quality and water quantity benefits. These benefits have also been demonstrated during winter periods in cold climate regions (Drake et al. 2013; Drake et al. 2014; Henderson and Tighe 2012; Huang et al. 2016; Roseen et al. 2012, Zhu et al. 2017), suggesting that their applicability to these regions is appropriate.

Despite their continued functionality during the winter, implementation of PICP in cold climate regions has been hindered by a lack of consensus on winter operations and concerns of groundwater contamination from winter de-icing practices due to the poor treatment of chlorides in PP systems (Borst and Brown 2014; Drake et al. 2014; Horst et al. 2010). Moreover, much of the winter maintenance research to date has focused on PP types that use poured surface materials such as pervious concrete and porous asphalt, and not interlocking products. Studies on poured PP materials have suggested that the rapid drainage of water from their surfaces can prevent melted ice and snow from refreezing and can increase melt rates, potentially reducing the amount of de-icing materials needed for maintaining winter safety (Kevern et al. 2012; Roseen et al. 2014). PP systems have also been shown to experience higher temperatures below the surface

during the winter as a result of increased insulation from void spaces in the aggregates and increased moisture content, which can reduce the risk of freezing and improve resistance to frost heave (Bäckström 2000; Kevern et al. 2009; Rohne and Lebens 2009). While similar winter safety and de-icing material reduction benefits are expected for PICP, minimal research has been carried out on this type of PP technology, and no research has been carried out in a controlled outdoor environmental. Surface friction, which is an indicator of pedestrian and vehicular safety on pavements, has also not been evaluated on PICP surfaces during winter conditions, and methods for measuring friction on PICP surfaces have not been established. Finally, while the total mass of chlorides is not expected to be reduced by PICP or other PP systems, the aggregate layers have been shown to attenuate and delay the release of peak chloride concentrations during the winter (Borst and Brown 2014; Drake et al. 2014; Zhu 2017). However, research on chloride attenuation in PICP systems is also needed in a controlled setting.

1.2 Research Objectives

The purpose of this study is to evaluate the winter safety and environmental benefits of PICP using test pavement cells in an outdoor environment where traffic and de-icing treatments are controlled. Data and observations were collected on PICP and conventional asphalt test cells throughout two winter seasons (2017/2018 and 2018/2019) at the Toronto and Region Conservation Authority (TRCA) Kortright Centre for Conservation, which is located in Vaughan, Ontario. The two primary objects of this research were to:

1. Evaluate the potential for PICP surfaces to require lower quantities of de-icing materials and provide increased slip and skid resistance during the winter compared to conventional asphalt surfaces; and,
2. Evaluate the ability of partial infiltration PICP systems to attenuate chloride concentrations from winter de-icing activities and delay their release to downstream drainage systems.

Results from this study are intended to help provide guidance for winter maintenance of PICP in cold climate regions, which in turn may help remove current implementation barriers for PICP in these locations. The findings will also be used to develop a PICP Best Management Practices manual for the Interlocking Concrete Pavement Institute.

1.3 Thesis Structure

The remaining chapters of this thesis are provided as followings:

- Chapter 2 is a standalone manuscript that presents the overall methodology, results, discussion, and recommendations from this research on the topics of winter maintenance and winter safety. The manuscript will be submitted for publication in the Journal of Cold Regions Engineering.
- Chapter 3 is a compilation of additional evaluations on data and observations that were collected at the research site but were not included in the manuscript. The chapter contains an evaluation of the chloride monitoring data, an evaluation of additional surface temperature data collected using infrared sensors, and an evaluation of the surface friction measuring devices that includes materials previously presented at the 12th International Conference on Concrete Block Pavement in Seoul, South Korea (Marvin and Drake 2018).
- Chapter 4 summarizes the conclusions and recommendations from the previous chapters.
- Appendix A presents a collection of site photos captured throughout the two winters that illustrate the various observations discussed throughout the thesis.
- Appendix B presents a summary of the surface friction data collected for each experiment.
- Appendix C presents the normality tests that were carried out on the friction data collected during the shovelled snow experiments on the PICP cells. These tests were needed to assess whether the normality assumptions were valid for carrying out two-way repeated measures ANOVA tests on the friction datasets.
- Appendix D presents the final draft of a state-of-the-art review paper on phosphorus sorption amendments in bioretention media that was accepted for publication in the Journal of Sustainable Water in the Built Environment on 14/May/2019 following peer-review. While this bioretention research is unrelated to the PICP research discussed throughout the thesis, it is included here such that this thesis provides all work that was completed by Jeffrey Marvin for the degree of Master of Applied Science. The manuscript was expanded from a systematic literature review paper that was completed as part of a reading course taught by Professor Drake during the Winter 2018 session. Professor Passeport and Professor Drake provided revisions to the version of the manuscript submitted for publication.

Chapter 2

Chapter 2 is comprised of a manuscript that will be submitted to the Journal of Cold Regions Engineering for future publication. Appendix A and Appendix B of this thesis will be submitted with the manuscript as Supplementary Data.

2 Winter Maintenance of Permeable Interlocking Concrete Pavement: Evaluating Opportunities to Reduce Road Salt Pollution and Improve Winter Safety

Jeffrey T. Marvin¹, Jennifer Drake²

¹Department of Civil & Mineral Engineering, University of Toronto, 35 St. George St., Toronto ON M5S 1A4, Canada

¹Associate Professor, Department of Civil & Mineral Engineering, Daniels Faculty of Architecture, Landscape & Design, University of Toronto, 35 St. George St., Toronto ON M5S 1A4, Canada

Abstract: Permeable Interlocking Concrete Pavement (PICP) is a type of permeable pavement system that uses the joint spaces between pavers to drain water from the surface into an aggregate base and subbase layer below. Because of its ability to rapidly drain surface water, PICP has the potential to reduce the amount of ice formed on the surface during winter conditions compared to traditional impervious pavements. As a result, PICP may reduce the amount of road salt needed for de-icing paved surfaces and may also reduce the risk of pedestrian slipping and vehicle skidding throughout the winter. This study evaluates the performance of an outdoor PICP and asphalt test pad during two winter seasons in Vaughan, Ontario by assessing differences in surface conditions, surface friction, and surface temperatures. Findings from the two winters suggest that PICP surfaces do not experience refreezing of surface water from previously melted ice and snow, whereas refreezing of conventional asphalt surfaces occurs as a result of prolonged wet conditions and lower surface temperatures at sunset. The use of de-icers on PICP surfaces is therefore only recommended when ice cover has formed from rapid freezing of partially melted compacted snow or freezing rain, although de-icers can be used

as needed to rapidly melt remaining snow on shovelled surfaces if surface temperatures are below freezing. PICP provides further opportunities to reduce de-icer quantities, as the drier conditions of PICP surfaces were found to prevent excess de-icing salts from dissolving, and observations from this study suggest that ice is less bonded to PICP surfaces compared to asphalt surfaces, indicating that ice may be easier to mechanically break up and remove on PICP surfaces.

2.1 Introduction

Permeable pavement (PP) systems are a type of Low Impact Development (LID) stormwater management practice that allow stormwater to drain through pavement surfaces into aggregate base and subbase layers. The aggregate layers temporarily store and treat the collected stormwater before discharging it into the downstream drainage system via a perforated underdrain or allowing it to infiltrate into the native soil below. As a result, PP systems are commonly used in lieu of conventional impervious pavements to reduce and treat stormwater runoff while still providing paved surfaces for vehicles and pedestrians. Some types of PP such as porous asphalt and pervious concrete use poured materials for the pavement layer, whereas other types of PP such as permeable interlocking concrete pavement (PICP) use impervious materials separated by porous spaces.

In cold climate regions, PPs have been demonstrated to function during the winter season by draining, treating, and infiltrating melted ice and snow (Drake et al. 2013; Drake et al. 2014; Henderson and Tighe 2012; Huang et al. 2016; Roseen et al. 2012), and they have also been shown to be more resistant to frost heave than conventional pavements (Bäckström 2000). Subsurface temperature characteristics of PP systems differ from conventional pavements, as the void spaces of the aggregates within the base and subbase layers insulate these layers against changes in ambient air temperatures (Kevern et al. 2009; Rohne and Lebens 2009). Water from the surface also increases the moisture content and latent heat of the aggregate layers and underlying soil, which reduces the potential for freezing and may expedite thawing processes (Bäckström 2000; Kevern et al. 2009; Rohne and Lebens 2009; Tyner et al. 2009). The combination of increased insulation and moisture content within PP systems causes the aggregate layers to experience warmer winter temperatures than the base and subbase layers below conventionally paved surfaces (Bäckström 2000; Rohne and Lebens 2009).

PP surfaces are typically treated during the winter season with conventional pavement de-icing materials such as road salts to melt ice and snow. Sand treatments are not recommended for PPs because sand particles can cause clogging and loss of infiltration capacity (Al-Rubaei et al. 2013; Huang et al. 2012), although washed aggregates that are identical to the joint material aggregates have been suggested for PICP as an alternative to sand (American Society of Civil Engineers [ASCE] 2018; Smith 2017). It is hypothesized that PP surfaces have the potential to require less de-icing materials than conventional pavement surfaces since melted ice and snow drain more rapidly from PP surfaces, reducing the risk of refreeze (Kevern et al. 2012). One study on porous asphalt suggests that road salt can be reduced by up to 77% while achieving a similar level of safety as conventional asphalt, as porous asphalt surfaces do not experience standing water and are clear of melted ice and snow sooner than conventional asphalt (Roseen et al. 2014). Based on this study, current best practices in North America for winter maintenance of all types of PP systems recommend to reduce the use of de-icing materials compared to when treating conventional pavements (ASCE 2018, Eisenberg et al. 2015, Smith 2017).

Melting and freezing processes on paved surfaces are also impacted by pavement surface temperatures, which depend on the thermal properties of the pavement material. Pavements with lower albedos, higher emissivities, and higher thermal conductivities reflect less heat and therefore warm up more rapidly during the day, whereas pavements with higher heat capacities store more heat during the day and are therefore warmer during the night (Li 2015). The poor thermal connection of PPs that use poured materials with large void spaces result in increased warming and cooling, and the increased moisture exposure of these poured products can increase evaporate cooling during wet conditions (Kevern et al. 2009, Li 2015). Differences between permeable and impermeable versions of pavement materials are expected to be minimal or much less extreme for concrete pavers and other modular PP systems where highly porous joint spaces surround impervious materials.

The desire to use lower amounts of de-icing products for PP surfaces stems from concerns that stormwater infiltration practices may further increase the amount of chloride pollutants in groundwater systems. While the use of winter road salts on conventionally paved surface are widely known to threaten ecosystems and human health by drastically increasing chloride concentrations in nearby surface waters, groundwater, and soils, dissolved chlorides are also poorly treated by PP systems (Borst and Brown 2014; Drake et al. 2014; Horst et al. 2010). If the

PP system allows for infiltration, there are concerns that winter salting will elevate chloride concentrations in the local groundwater. However, recent field research on porous asphalt systems suggest that the increased volume of infiltrated stormwater can dilute chloride concentrations in shallow groundwater if the upgradient groundwater is already polluted with high chloride concentrations from other winter salting activities (Dietz et al. 2017). Additionally, PP systems have been shown to attenuate peak chloride concentrations during the winter and delay their release to downstream drainage systems (Borst and Brown 2014; Drake et al. 2014; Zhu 2017), as further demonstrated by the chloride monitoring results presented in Section 3.1. Despite these reduced chloride concentrations, the total mass of chlorides released to the environment remains a concern and can only be addressed through a reduction of winter de-icing materials.

While PPs have been demonstrated to function hydraulically during the winter season in cold climate regions, their implementation in these areas has been hindered by a lack of consensus on winter operations. Moreover, most winter performance and operational research to date has focused on PP types that use porous surface materials, whereas minimal guidance currently exists for PICP systems that instead use the joint spaces between impervious paving stones to drain stormwater and meltwater from the surface. Most studies have also only compared differences between permeable and impermeable versions of the same pavement material, whereas PICP is often also installed as an alternative for impermeable asphalt. This study evaluates the potential for PICP to reduce the application of road salt while maintaining a safe and non-slippery surface during winter conditions in comparison with conventional asphalt pavement. Data collection and observations were made throughout two winters at an outdoor pavement test pad located in Vaughan, Ontario. The findings from this study are intended provide guidance for winter maintenance of PICP in cold climate regions, which in turn may help remove current implementation barriers for PICP in these locations.

2.2 Methodology

2.2.1 Test Site Configuration

An outdoor pavement test pad was constructed in August 2017 at the Toronto and Region Conservation Authority (TRCA) Kortright Centre for Conservation, located in Vaughan, Ontario. The Köppen climate classification at the site is Dfb, which is defined as a fully humid

continental climate with a warm summer (Kottek et al. 2006). The pavement test pad consisted of four 2 m by 2 m PICP cells and an asphalt control cell, and the cells were laid out in series along a strip, as shown in Figure 1. The names displayed in the figure for each pavement cell correspond to their respective pavement type, de-icer type, and application rate, as later described in Section 2.2.3. Each pavement cell was enclosed within an impervious concrete barrier such that water below the surface was unable to flow between the cells. All four PICP cells were constructed with a level surface, whereas the asphalt cell was sloped at 2% to allow for meltwater to drain to a catch basin. The cells were installed within an open field where they received no pedestrian or vehicular traffic throughout the study period. Thermal properties of the PICP and asphalt materials are provided in Table 1.

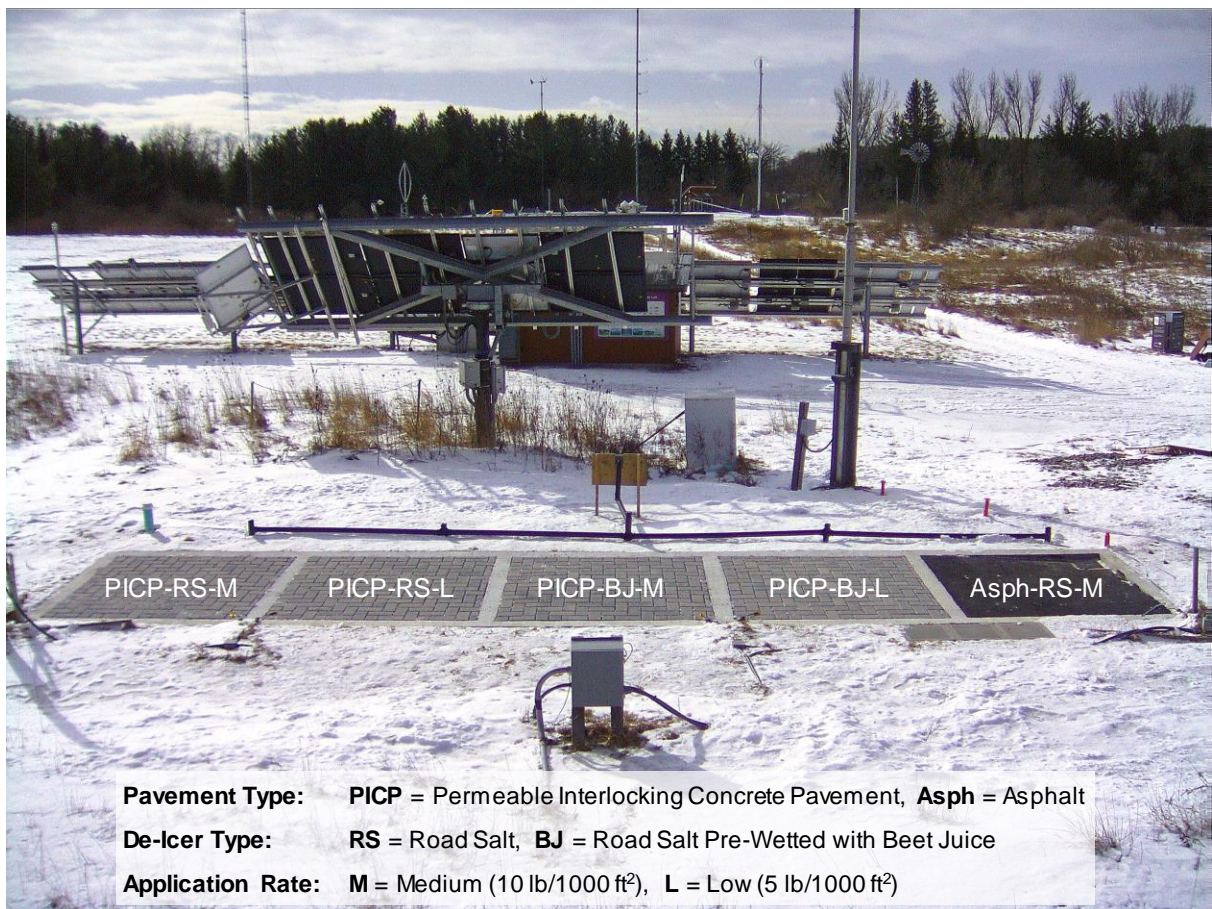


Figure 1: Surface layout of outdoor pavement test pad (facing south).

Table 1: Thermal properties of PICP and asphalt.

Pavement Type	Albedo	Emissivity	Thermal Conductivity (W/m-°C)	Specific Heat Capacity (J/kg-°C)
PICP	0.26 ^a	0.97 ^a	1.83 ^b	1001 ^b
Asphalt ^c	0.09	0.80	1.73 (0.74)	852

^a Value provided by manufacturer for Enviro Midori PICP product.

^b Values estimated based on data from Li et al. (2015) for newly constructed concrete surface.

^c Values estimated based on data from Li et al. (2015) for newly constructed asphalt surface.

Cross-sectional layouts of the PICP and asphalt cells are provided in Figure 2. The PICP cells followed design recommendations outlined by the Interlocking Concrete Pavement Institute. Paver materials used for the PICP cells were 80 mm thick, 120 mm x 240 mm grey Enviro Midori concrete paving stones laid out in a 90° herringbone pattern with 8.1 ± 0.6 mm joint spaces filled with ASTM No. 8 crushed stone. The pavers were installed above a 50 mm thick bedding layer that was also comprised of ASTM No. 8 crushed stone. A 100 mm thick base layer consisting of ASTM No. 57 crushed stone and a 150 mm thick subbase layer consisting of ASTM No. 2 crushed stone were installed below the bedding layer. All aggregate materials were washed. The total depth from the PICP surface to the native soil was therefore 380 mm, which places the installation well above the typical winter frost line in Vaughan of approximately 1.4 m (Ministry of Transportation of Ontario 2010). A 75 mm diameter perforated underdrain was installed in an approximately 100 mm deep sump below the subbase and was bedded with ASTM No. 57 stone. A permeable geotextile with a permittivity of 1.2 s^{-1} was installed below the subbase and underdrain to separate the aggregates from the native soil. The PICP cells therefore allowed for partial infiltration into the native soil, which was characterized as clayey with a measured saturated hydraulic conductivity of approximately 2 mm/hr.

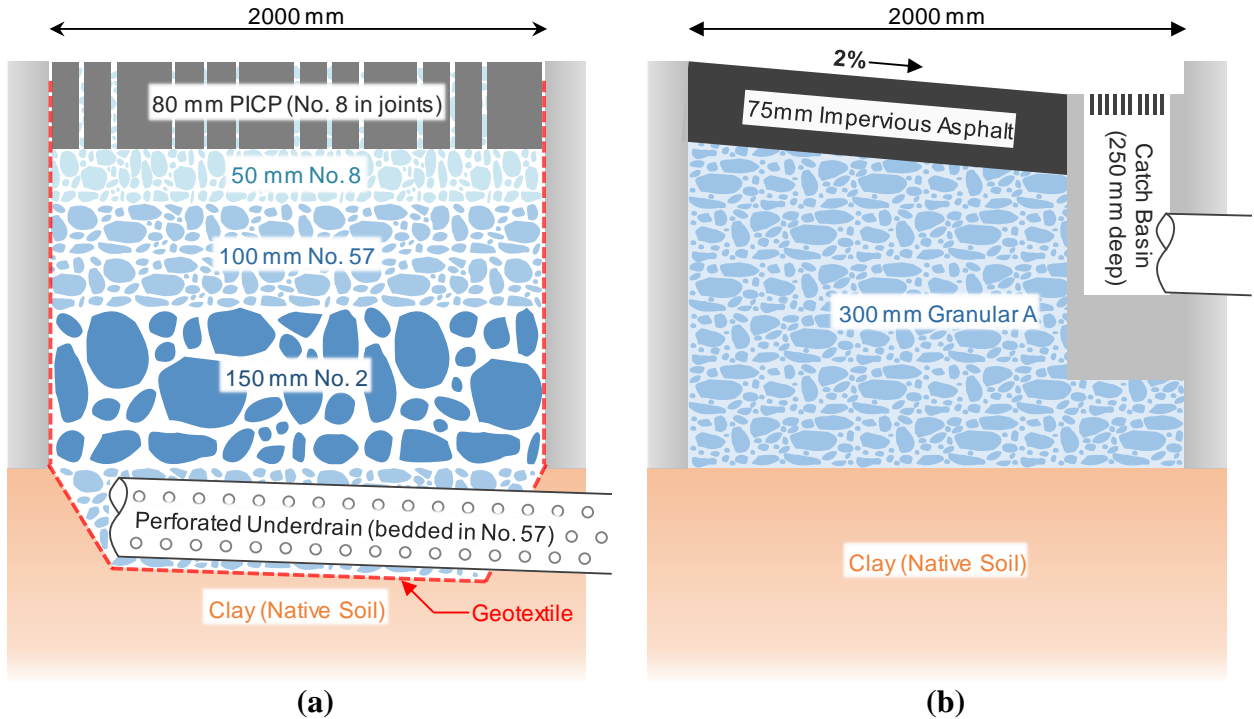


Figure 2: Cross-sectional layout of (a) PICP and (b) asphalt test cells.

The asphalt cell consisted of a 75 mm thick hot mix asphalt pavement layer installed above a 300 mm thick Granular A aggregate layer. This specification was typical of local residential driveway installations. The catch basin had surface dimensions of 250 mm x 250 mm and a depth of 250 mm with no sump, representing a shallow catch basin installation often found on private properties. A 75 mm diameter pipe was used for the catch basin outlet. Both the catch basin outlet pipe and the PICP underdrains were sloped at 1% from the cells into individual traps for water quality monitoring (see Section 3.1) before connecting to the downstream drainage system.

2.2.2 Winter Operations

A variety of snow clearing and de-icing practices were performed on the PICP and asphalt cells throughout the 2017/2018 and 2018/2019 winters to collect data and observations on different types of surface cover conditions that are commonly encountered on roadways, walkways, driveways, and parking lots. These practices generally consisted of shovelling snow from the pavement surfaces with or without prior compaction of the snow and then applying de-icing chemicals to each pavement cell. No anti-icing practices were evaluated in this study. A summary of the winter maintenance activities carried out during the two winters is provided in

Table 2. Maintenance activities began in January for both winters. The term *salting* in the table and throughout this thesis refers to the application of de-icing chemicals.

Table 2: Winter maintenance activities carried out on pavement cells.

Date	Snow Compaction	Shovelling (to thin layer of snow or ice)	Shovelling (to dense layer of snow or ice)	Salting
17/Jan/2018		✓		✓
01/Feb/2018		✓		
05/Feb/2018		✓		✓
08/Feb/2018		✓		✓
12/Feb/2018	✓		✓	
15/Apr/2018		✓		✓
18/Jan/2019	✓			
19/Jan/2019	✓			
21/Jan/2019	✓	✓		✓
28/Jan/2019	✓			
29/Jan/2019	✓		✓	✓
30/Jan/2019		✓		✓
07/Feb/2019		✓		✓
13/Feb/2019	✓			
14/Feb/2019	✓			
16/Feb/2019			✓	✓
28/Feb/2019	✓			
03/Mar/2019			✓	
04/Mar/2019			✓	✓

Shovelling and salting activities were carried out during the daytime hours after the cells were clear of all shadows and precipitation. The winter maintenance was mostly focused on the months of February and March because the cells were impacted by shadows during the mornings and late afternoons from November to January (see Figure A1). No shovelling or salting activities were performed during the night since the site was not accessible during this time. The pavement cells were not walked on while they were being shovelled and treated with de-icing chemicals. As a result of these limitations, pavement behaviour was not evaluated for conditions where surfaces are cleared and salted during the night or while snow is still falling. This study also does not assess pavement responses to additional ice, snow, and/or road salt introduced by regular pedestrian and vehicular disturbances.

Snow compaction was carried out by repeatedly walking over the cells using an equal walking pattern until a maximum compaction was visually observed. The number of passes required to achieve maximum compaction varied between events based on the thickness and condition of the snow. No devices or vehicles were used to compact the snow, as the walking pattern was found

to be a fast, simple, and effective method for such a small pavement area, and it was also representative of paved surfaces that receive high pedestrian traffic. The purpose of the snow compaction was to simulate winter pavement conditions where vehicles and pedestrians pass over snow covered surfaces before or while the surfaces are plowed or shovelled. Compacted snow is often not fully removed during plowing and shovelling activities, resulting in a leftover layer of dense snow. Water from partial melted snow, rainfall, or traffic can be trapped by compacted snow layers and then refreeze, forming a tight bond with the pavement surface. Snow compaction activities on the pavement cells therefore included two events where ice formed on the surfaces from partially melted compacted snow that was left undisturbed for several days.

Multiple other snowfall and mixed precipitation events of varying magnitudes occurred throughout the two winters where melting occurred the following day due to positive air and surface temperatures. While no maintenance was carried out for these events, they provided information on how snow melts on PICP surfaces when left undisturbed.

2.2.3 De-Icing Treatments

Each pavement cell received a specific de-icing treatment throughout the two winters, as outlined in Table 3. PICP-RS-M and PICP-RS-L refer to the PICP cells that received road salt (RS) at medium (M) and low (L) application rates, respectively, whereas PICP-BJ-M and PICP-BJ-L refer to the PICP cells that received road salt pre-wetted with beet juice (BJ) at medium and low application rates, respectively. Asph-RS-M refers to the asphalt control cell, which received road salt at a medium application rate and could be directly compared with PICP-RS-M. The medium and low application rates of 10 and 5 pounds of de-icer per 1000 square feet (lb/1000 ft²) used in this study were based on equipment calibration values used in the Salt Application Verified Equipment program administered by the Sustainable Technologies Evaluation Program. De-icer application rates were therefore consistent with local best practices.

Table 3: De-icer type and application rate for each test cell.

Test Cell	De-Icer	Application Rate (lb/1000 ft²)^a
PICP-RS-M	Road Salt	10
PICP-RS-L	Road Salt	5
PICP-BJ-M	Road Salt Pre-Wetted with Beet Juice	10
PICP-BJ-L	Road Salt Pre-Wetted with Beet Juice	5
Asph-RS-M	Road Salt	10

^aUnit for application rate is pounds of de-icer per 1000 square feet.

The road salt used in this study was a locally available commercial product (Sifto® Safe Step® Ice Salt™) composed of pure sodium chloride (NaCl). Pure NaCl was selected because it remains the most common and inexpensive de-icing chemical used throughout the world, and because it is locally available for property owners. The beet juice product used in this study to pre-wet the road salt was Fusion™ Liquid De-Icer. Pre-wetting was carried out by mixing at a ratio of 14 L of beet juice to one metric tonne of road salt, as recommended by the manufacturer. The purpose of using road salt that has been pre-wetted with beet juice was to evaluate a common and more environmentally friendly de-icing alternative to pure NaCl, and the product manufacturer claims that using beet juice to pre-wet road salt can reduce the amount of road salt that is needed. Beet juice also lowers the freezing point of water to lower values compared to NaCl, allowing ice and snow to melt when temperatures are too low for pure NaCl to function. Despite the potential salt reduction benefits of pre-wetting with beet juice, the low and medium application rates were kept the same between both treatment types such that the potential salt reduction benefits of beet juice on PICP could be directly compared.

2.2.4 Surface Temperature and Surface Condition Monitoring

Surface-mount thermistors were installed on the corner of each cell to continuously monitor pavement surface temperatures every five minutes throughout the winter periods. The use of contact sensors allowed for temperatures to be monitored below any ice or snow accumulation, which helped to identify surface conditions and the potential for the ice and snow to melt. No subsurface temperature data was collected in the cells, as frost penetration was not evaluated for this study. The thermistor model used in this study was 110PV, which has a tolerance of ± 0.2 °C for temperatures collected in the -40 to 70 °C range. Surface temperature measurements were collected throughout the 2017/2018 winter beginning 01/Mar/2018 and throughout the

2018/2019 winter beginning 08/Nov/2018. Ambient air temperature data at five minute intervals was collected from a climate station operated by the TRCA located approximately 500 m from the study site.

Daily mean, maximum, minimum, and sunset hour surface temperatures were calculated from the thermistor data. The sunset hour temperatures were determined by calculating the mean temperature during the time period spanning from 30 minutes before sunset to 30 minutes after sunset. The purpose of calculating sunset hour temperatures was to evaluate the potential for melted ice and snow to refreeze when solar radiation rapidly drops at the end of the day. Monthly means were then calculated for the daily mean, maximum, minimum, and sunset hour temperatures.

Surface conditions were monitored by capturing photos of the site every five minutes using a field camera and by manually capturing photos with handheld cameras during site visits. The field camera was equipped with infrared lighting to also capture photos during the night. Photos were collected by the field camera throughout the 2017/2018 winter beginning 24/Jan/2018 and throughout the 2018/2019 winter beginning 08/Nov/2018. Selected field camera and site photos are provided in Appendix A and are referred to throughout this chapter.

The amount of surface cover was visually estimated from each photo and grouped into one of the four following categories: full cover (< 1% clear), partial cover (between 1% and 95% clear), trace cover (between 95% and 99% clear), and clear (> 99% clear). No automated tools were used to estimate the surface cover percentages, as the grey colour of the pavers combined with the varying light conditions and resolution of the photos created challenges in developing a program that could distinguish between icy, snowy, slushy, wet, and clear conditions. The camera photos were also used to determine when each of the temperature sensors were impacted by surface cover throughout the monitoring period to eliminate the impacts of ice, snow, and slush on surface temperatures. Monthly and winter means of daily mean, maximum, minimum, and sunset hour surface temperatures were calculated for clear conditions by omitting all time steps where one or more of the five sensors were impacted by ice or snow.

2.2.5 Surface Friction Measurements

Surface friction was measured on the pavement cells using two devices, SlipAlert and Mark IIIB. Photos of the two devices are shown in Figure 3. SlipAlert is a British tribometer adopted by BS 8204 (British Standards Institution 2003) that measures the dynamic coefficient of friction (DCOF) by simulating the sliding action of a vehicle. Mark IIIB is an American tribometer certified to ASTM F2508 (ASTM International 2016) that measures the transitional coefficient of friction (TCOF) by simulating the biomechanical movement of a pedestrian when slipping on a surface. Measurements are collected at a single location when using Mark IIIB, whereas measurements are collected over the sliding distance of the instrument when using SlipAlert. While all TCOF measurements on the asphalt cell were able to be collected across its slope, corrections were made to sloped DCOF measurements using conversions provided by the manufacturer.



Figure 3: Surface friction measuring devices in use on ice covered PICP surfaces: (a) SlipAlert and (b) Mark IIIB.

SlipAlert and Mark IIIB were selected for this study since friction measurements needed to be collected within a 2 m length, in rapid succession, with minimal disturbance to surface conditions, and with minimal operator error. These criteria eliminated the use of other friction measuring devices that collect long continuous measurements, require a large amount of adjustments, or do not easily collect repeatable measurements. Moreover, the objective of

collecting friction measurements was to quantify slip and skid resistance values that were representative of both a pedestrian slipping and a vehicle skidding.

Surface friction was measured after shovelling, after salting, at various time intervals until the pavements were dry or experienced no further changes in surface cover, as well as before and after sunset if refreezing conditions occurred. Each friction measurement set consisted of collecting five replicate DCOF measurements and five replicate TCOF measurements per cell at locations that provided overall spatial representations of the pavement surfaces. The cell order in which the measurements were collected was randomized each day, and measurements were collected at approximately the same time on all cells. The DCOF measurements were collected prior to the TCOF measurements for each measurement set. The purpose of this data collection procedure was to equally account for any changes to surface cover that may occur during a measurement set. This was important because surface conditions can change within minutes, whereas the friction measurement sets took approximately 10 minutes to collect using SlipAlert and 20 minutes to collect using Mark IIIB.

Mean, minimum, and maximum values of DCOF and TCOF were calculated for each cell and measurement set using the five replicate measurements. Two additional SlipAlert measurements were collected on the asphalt cell, one across the top of the slope on the east side where drying would typically first occur, and one diagonally across the cell towards the catch basin to collect a measurement that was overall more representative of the entire cell. Additional Mark IIIB measurements were collected if the five measurements did not cover all observed types of surface cover such as isolated patches of ice or dry spots. This frequently occurred for TCOF measurements because Mark IIIB is only able to collect spot measurements. The additional SlipAlert and Mark IIIB measurements were only used to calculate minimum and maximum values for the cells and were not included in the calculation of mean values or in statistical hypothesis testing. Graphs of all processed surface friction data are provided in Appendix B.

2.3 Results and Discussion

2.3.1 Surface Temperatures

Surface temperatures between the four PICP cells were compared using the Friedman test, as temperature measurements were dependant on collection time and daily fluctuations in air temperatures resulted in the data being nonparametric. PICP surface temperatures were found to be significantly different ($p < 0.05$) between individual cells both with and without the impacts of ice and snow cover, although the reason for this difference could not be determined. Surface temperatures on the four PICP cells were therefore averaged for each measurement set prior to calculating the monthly averages, and all further discussion on PICP surface temperatures is based on average values calculated for the four cells.

Box plots of all surface temperature data and of data collected during clear conditions when no ice or snow were present on the pavement surfaces are presented in Figure 4 for each month and for the 2018/2019 winter (01/Dec/2018 to 31/Mar/2019). The December 2018 to March 2019 months were grouped together for analysis because they are the only months of the year where daily average air temperatures are below 0 °C in Vaughan (see Table 4). These months are also when most de-icing activities are carried out. However, surface temperatures reached as high as 28 °C on the PICP and 30 °C on the asphalt in March, suggesting that less de-icing is needed during this month compared to the previous winter months. As shown in Table 4, air temperatures at the research site were colder during the 2018/2019 winter than climate normal values.

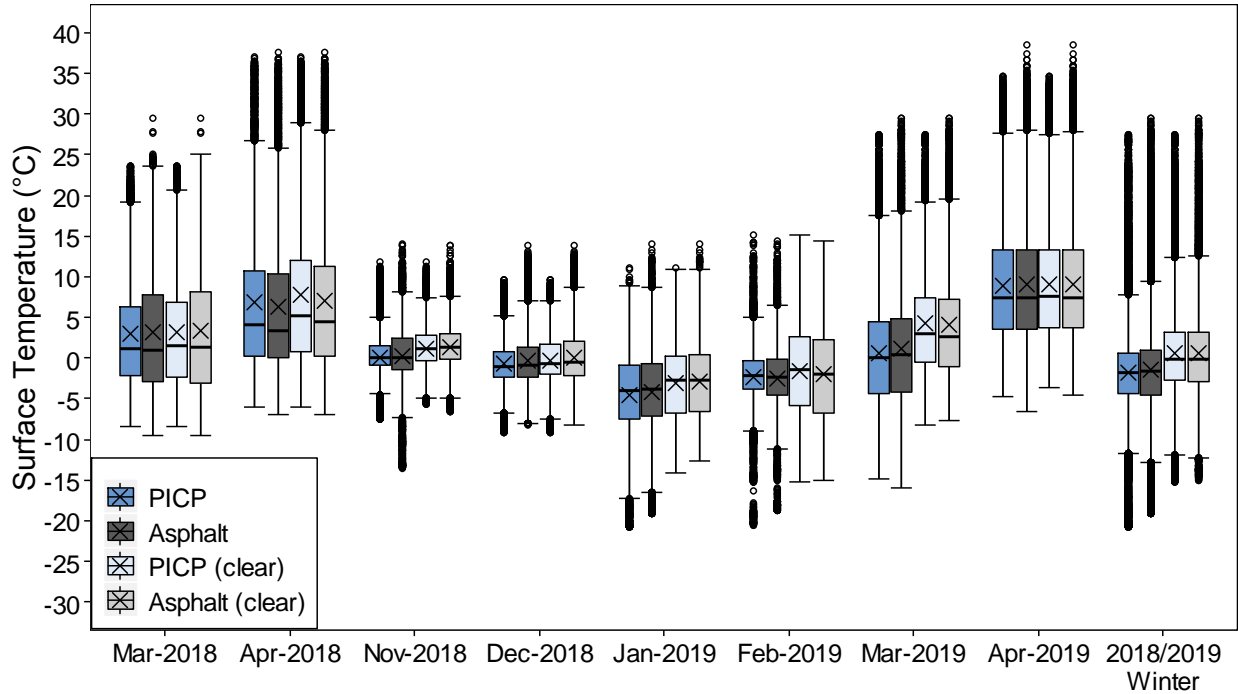


Figure 4: Box plot comparison of all surface temperature data and of data collected during clear conditions when no ice and snow were present.

Table 4: Comparison of air temperatures at research site with climate normal values.

Month	Daily Mean Air Temperature (°C)		Daily Maximum Air Temperature (°C)		Daily Minimum Air Temperature (°C)	
	Climate Normal ^a	2018/2019 Period ^b	Climate Normal ^a	2018/2019 Period ^b	Climate Normal ^a	2018/2019 Period ^b
	Nov	3.1	0.7	6.9	3.6	-0.8
Dec	-2.8	-0.9	0.8	2.2	-6.4	-4.3
Jan	-6.6	-7.6	-2.5	-3.3	-10.7	-12.4
Feb	-4.8	-5.0	-0.5	-0.7	-9.2	-9.7
Mar	-0.4	-1.8	4.3	3.1	-5.2	-6.7
April	6.6	5.7	12.0	10.4	1.2	0.8

^aClimate normal values are from the Woodbridge climate station operated by Environment Canada. The station is located approximately 6 km away from the research site.

^b2018/2019 temperatures are from a climate station operated by the TRCA. The station is located approximately 500 away from the research site.

Average differences in daily mean, maximum, minimum, and sunset hour surface temperatures between the two pavement types are presented in Table 5 for each month and for the 2018/2019 winter. Statistical comparisons of these differences were carried out using the Wilcoxon signed-rank test ($\alpha = 0.05$), and differences that were found to be significant are indicated in the table.

The Wilcoxon signed-rank test was used because temperature values were dependent on the day and because the datasets were nonparametric as a result of climate fluctuations throughout the monitoring period. Two-tailed tests were used to compare the daily mean values, whereas one-tailed tests were used to compare the daily maximum, minimum, and sunset hour values. For the one-sided tests, daily maximum temperatures were hypothesized to be higher on the asphalt due to its higher albedo, lower emissivity and lower thermal conductivity, whereas daily minimum and sunset hour temperatures were hypothesized to be lower on the asphalt due to its lower heat capacity.

Table 5: Comparison of surface temperatures between PICP and asphalt surfaces.

Month	Surface Temperature Difference between PICP Cells and Asphalt Cell (°C) ^a							
	Daily Mean ^b		Daily Maximum ^c		Daily Minimum ^c		Daily Sunset Hour ^c	
	All Days	Clear Days	All Days	Clear Days	All Days	Clear Days	All Days	Clear Days
Mar-2018	NS	NS	-3.2	-3.2	0.7	0.7	1.6	1.6
Apr-2018	0.5	0.7	-0.6	-0.6	1.0	1.1	1.9	2.1
Nov-2018	NS	NS	-3.1	-1.0	0.9	NS	NS	NS
Dec-2018	NS	NS	-1.8	-1.7	NS	NS	NS	NS
Jan-2019	NS	NS	-1.4	-1.9	NS	NS	NS	0.8
Feb-2019	NS	NS	-0.6	NS	NS	NS	0.8	1.1
Mar-2019	NS	NS	-2.9	NS	0.4	NS	0.9	1.4
Apr-2019	NS	NS	-1.2	-1.2	NS	NS	0.9	0.9
2018/2019 Winter	NS	NS	-1.7	-1.0	NS	NS	0.4	0.7

^a NS indicates that the difference was not significant ($p < 0.05$) or was not within the combined sensor accuracy of ± 0.4 °C. Positive values indicate that surface temperatures were higher on the PICP cells than on the asphalt cell, and negative values indicate that surface temperatures were lower on the PICP cells than on the asphalt cell.

^b Based on a two-tailed test.

^c Based on a one-tailed test.

Differences in daily mean surface temperatures between the two pavement types were not significant ($p > 0.05$) for the 2018/2019 winter. However, daily maximum surface temperatures for this winter were significantly lower ($p < 0.05$) on the PICP cells, indicating that peak melt rates during the day could be lower on PICP surfaces. As shown in Figure 5, the rise in morning PICP temperatures after sunrise were frequently delayed behind the asphalt, regardless of surface cover. PICP surface temperatures were therefore typically lower each day throughout the winter from around sunrise to mid-afternoon. The slower rise in surface temperature of the PICP compared to the asphalt was likely because the PICP had a lower albedo, higher emissivity, and higher thermal conductivity. The mean difference in daily maximum surface temperatures for the winter period was 1.7 and 1.0 °C with and without the impacts of surface cover, respectively,

indicating that a single degree change in air temperature could impact whether or not melting occurs on both types of pavements or just on the asphalt.

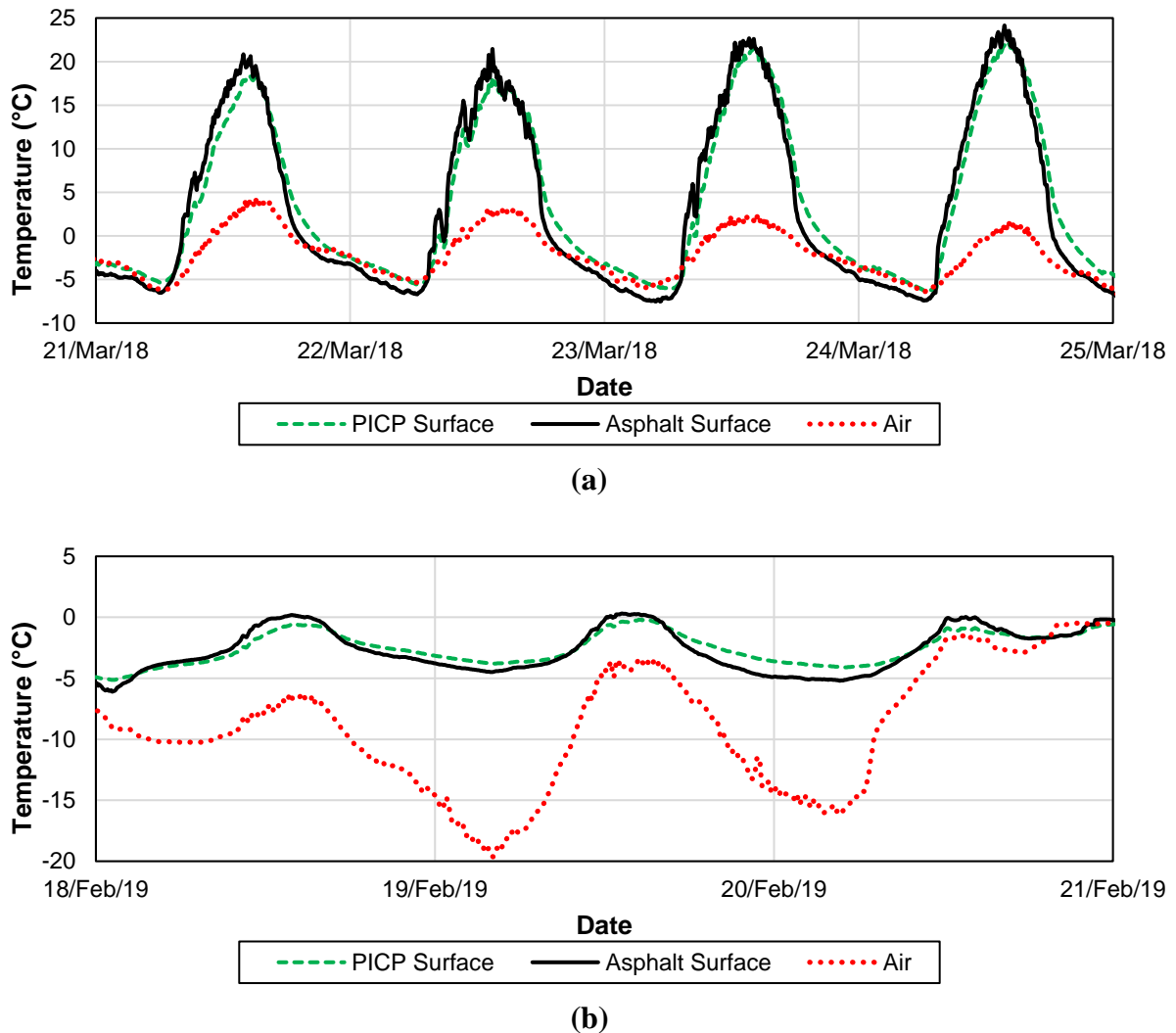


Figure 5: Air and surface temperatures during (a) typical diurnal pattern in March 2018, (b) snow-covered period in February 2019.

While daily minimum surface temperatures of the asphalt were not found to be significantly lower ($p > 0.05$) during the 2018/2019 winter, asphalt surface temperatures were significantly lower ($p < 0.05$) at sunset. As shown in Figure 5, asphalt temperatures dropped more rapidly than PICP temperatures beginning mid-afternoon when air temperatures and solar radiation rapidly decrease. Surface temperatures then remained higher on the PICP cells until the early hours of the following day when air temperatures and solar radiation begin to increase. Box plots of the

daily sunset hour surface temperatures are presented in Figure 6, further illustrating these differences throughout the winter months.

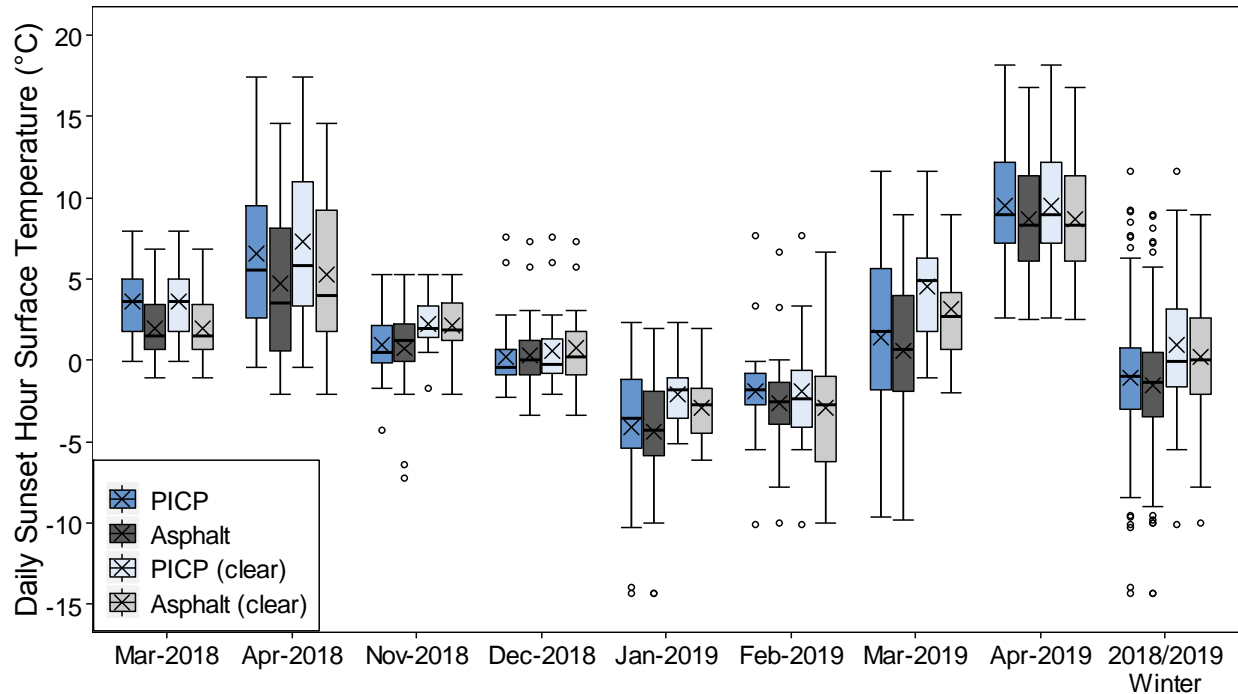


Figure 6: Box plot comparison of daily sunset hour surface temperatures.

Higher sunset temperatures on PICP surfaces may indicate that melted ice and snow has less potential to refreeze at the end of the day on PICP surfaces compared to on asphalt surfaces. More time is also available for the remaining meltwater on PICP surfaces to drain or evaporate before freezing temperatures occur, whereas the more rapid drops in temperatures on asphalt surfaces provide more opportunities for meltwater to refreeze. The slower cooling and higher overnight temperatures of the PICP were likely a result of the concrete pavers having a higher heat capacity than that of the asphalt, as the concrete pavers may have stored more heat than the asphalt during the day. Additional heat provided by the insulated base and subbase layer during the night could have also contributed to the slower cooling, although this interaction between subsurface and surface temperatures of PICP systems during winter conditions has not been researched.

Sunset temperatures on the PICP cells were significantly higher ($p < 0.05$) for all winter months except for December and January, although sunset temperatures were significantly higher ($p <$

0.05) for January when not including days when the sensors were covered in ice or snow. The lack of difference in sunset temperatures in December is likely because daytime hours in the Northern Hemisphere are shortest in December and gradually increase throughout the remaining winter. As a result, less time is available in December for the PICP to warm up and store heat during the day. The potential for PICP systems to reduce meltwater refreeze at sunset based on surface temperatures alone may therefore not be applicable in December.

2.3.2 Melting Processes during Undisturbed Snow Conditions

A total of fifteen melt events occurred throughout the two winters where snow was left undisturbed on the pavement surfaces. Pavement melt times to trace snow cover conditions (between 95% and 99% clear) and fully clear conditions (> 99% clear) are provided in Table 6. During these events, an even melting pattern through the joint spaces was observed on the PICP cells, whereas an uneven and radial melting pattern was usually observed on the asphalt cell. Melting always began in the morning or before peak daytime air temperatures. For all events, melting began first on the asphalt cell. Melting to trace cover conditions also always occurred sooner on the asphalt cell than on the PICP cells, whereas clear conditions occurred sooner on the asphalt cell for only one third of the events. The longer times to achieve fully clear conditions on the asphalt cell was a result of snow remaining at the low point around the catch basin for extended periods. Snow at the catch basin was unable to melt by the end of the day for 47% of the melt events. An example of the melting patterns described above can be observed in Figure A2.

Table 6: Pavement melt times for undisturbed conditions.

Melt Event	Time to Trace Snow Cover (minutes) ^{a,b,c}					Time to Fully Clear (minutes) ^{a,b,c}				
	PICP- RS-M	PICP- RS-L	PICP- BJ-M	PICP- BJ-L	Asph- RS-M	PICP- RS-M	PICP- RS-L	PICP- BJ-M	PICP- BJ-L	Asph- RS-M
13/Mar/2018	165	170	165	160	85	180	195	195	175	175
14/Mar/2018 ^e	250	215	215	235	210	275	215	235	255	1,520
05/Apr/2018	105	105	105	100	55	125	105	115	110	155
24/Nov/2018 ^{d,e}	7,000	7,045	7,045	7,085	6,365	7,105	7,165	7,170	7,260	6,640
28/Nov/2018	60	50	50	50	35	100	80	80	80	125
07/Dec/2018 ^e	-	-	-	-	120	-	-	-	-	-
08/Dec/2018 ^e	-	-	-	1,720	60	-	-	-	3,055	-
12/Dec/2018 ^e	-	-	-	-	105	-	-	-	-	-
14/Dec/2018 ^d	1,380	1,390	1,375	1,350	1,155	1,395	1,405	1,390	1,370	1,505
24/Dec/2018	-	-	-	-	75	-	-	-	-	175
31/Dec/2018 ^d	475	475	475	475	40	480	480	480	480	220
05/Jan/2019 ^e	-	-	-	-	1,285	-	-	-	-	2,225
11/Jan/2019 ^e	720	720	720	720	310	1,925	2,005	1,885	1,730	-
17/Mar/2019	375	375	375	375	325	390	390	390	390	445
31/Mar/2019	-	-	-	-	275	-	-	-	-	295

^aTime from when melting began on the asphalt cell.

^bBold text indicates that the cell had the lowest time for each event.

^cNo data indicates that the respective surface cover conditions were not observed before the next snowfall event.

^dMelting was influenced by rainfall.

^eSnow remained at the catch basin on the asphalt cell at the end of the day.

The delayed melting on the PICP surfaces are likely due to a combination of lower surface temperatures during the morning and due to meltwater draining vertically from the snow through the joint spaces rather than pooling or draining along a path. As shown in Figure A3, snow mounding was observed on the PICP surfaces and on the catch basin due to partial melting that occurred on the surrounding impervious surfaces, whereas any melted snow on the PICP cells and on the catch basin would have rapidly drained through their surfaces and had less influence on additional melting. These observations indicate that while melting processes may be delayed on PICP surfaces, snowmelt may be less likely to refreeze on these surfaces on days where only partial melting occurs, provided that the snow remains uncompacted.

Flooding of the asphalt cell occurred during a rainfall event on 24/Feb/2019 as a result of ice accumulation in the catch basin and outlet pipe (see Figure A4). The ice formed after three days of air temperatures fluctuating above and below 0 °C while snow on the surface was gradually melting. Manual ice removal was carried out on 25/Feb/2019 so that winter observations and experiments could continue. While ice accumulation within the PICP underdrains and within the base and subbase layers could not be assessed, no surface flooding on the PICP cells occurred through the study. Similar to previous studies, these observations demonstrate that PICP systems

can still provide surface drainage even when ice accumulation below the surface is likely present. The PICP cells were shallow installations of less than 400 mm total depth from the PICP surface to the native soil, so ice formation within the aggregate layers was likely to occur during the winter.

2.3.3 Surface Friction during Dry Pavement Conditions

Surface friction measurements were collected during dry pavement conditions on 29/May/2018 and are presented in Figure B6. As a reference, a minimum DCOF of 0.42 measuring using a BOT 3000-E is specified by ANSI A326.3 (ANSI 2017) and a corresponding Pendulum Test Value of 40 specified by BS 8204 (British Standards Institution 2008) is required for pedestrian safety on indoor flooring. Mean DCOF was measured to be 0.74 on the PICP cells and 0.71 on the asphalt cell, whereas mean TCOF was measured to be 0.72 for the PICP and 0.73 for the asphalt. No significant differences in DCOF or TCOF were found between the four PICP cells based on the Kruskal-Wallis H test ($p > 0.05$), and no significant differences in DCOF or TCOF were found between the PICP cells and the asphalt cell based on the Mann-Whitney U test ($p > 0.05$, two-tailed). Similarities in DCOF between the two pavement types were further demonstrated by a maximum DCOF of 0.79 being measured on all five cells.

2.3.4 Shovelled Snow Experiments

Six experiments were carried out where the pavement cells were first shovelled to a thin layer of snow or ice pellets and then treated with de-icing chemicals. Snow compaction carried out prior to two of the experiments (21/Jan/2019 and 30/Jan/2019) had minimal impact on the thin layer of snow that remained after shovelling. Friction measurements were collected during the shovelled snow experiments within 30 minutes after shovelling (Test 1), within 30 minutes after salting (Test 2), and one to two hours after salting (Test 3). Statistical comparisons of DCOF and TCOF for each of the three tests were carried out by combining the data from all experiments. For reasons outlined in Table 7, statistical hypothesis tests only included four, three, and two of the experiments for Test 1, Test 2, and Test 3, respectively. Mean DCOF and TCOF values of each test for each pavement cell are provided in Table 8.

Table 7: List of included and excluded data from shovelled snow experiments.

Experiment Date	Data Included?			Reason for Excluding Data
	Test 1	Test 2	Test 3	
01/Feb/2018				shadows, no salting due to positive temperatures
05/Feb/2018	✓	✓	✓	(all tests included)
08/Feb/2018				de-icers from previous experiment still present
21/Jan/2019	✓	✓	✓	(all tests included)
30/Jan/2019	✓	✓		blowing snow conditions after Test 2
07/Feb/2019	✓			freezing drizzle conditions after Test 1

Table 8: Mean DCOF and TCOF values for shovelled snow experiments.

Pavement Cell	Test 1		Test 2		Test 3	
	Mean DCOF	Mean TCOF	Mean DCOF	Mean TCOF	Mean DCOF	Mean TCOF
PICP-RS-M	0.22	0.23	0.42	0.46	0.52	0.61
PICP-RS-L	0.23	0.23	0.39	0.44	0.51	0.59
PICP-BJ-M	0.24	0.20	0.43	0.49	0.55	0.63
PICP-BJ-L	0.23	0.25	0.42	0.52	0.52	0.63
Asph-RS-M	0.35	0.48	0.37	0.51	0.47	0.68

Statistical comparisons between PICP-RS-M and Asph-RS-M were carried out using the Wilcoxon signed-rank test ($\alpha = 0.05$, two-tailed), as the data was nonparametric and the measurements were paired based on when they were collected. Surface friction soon after shovelling (Test 1) was always lower on the PICP cells than on the asphalt cell, and this difference was found to be significant ($p < 0.05$). Lower friction on the PICP surfaces after shovelling is not surprising, as the PICP surfaces have a monolithic texture that likely caused the thin layer of snow to have a more consistent thickness, whereas the asphalt had a more rugged and irregular texture that allowed for snow to settle into surface depressions (see Figure A5). Surface friction soon after salting (Test 2) and one to two hours after salting (Test 3) was found to be statistically similar between PICP-RS-M and Asph-RS-M ($p > 0.05$). This finding suggests that both pavement types provide similar levels of safety soon after snow begins to melt on shovelled surfaces.

Statistical comparisons between de-icer application rates and types for the four PICP cells during Test 2 and Test 3 were carried out using the two-way repeated measures ANOVA test. This statistical hypothesis test was selected because it could compare two variables simultaneously and because the values were dependent on the time. Normality tests for the Test 2 and Test 3 datasets demonstrated that violations to normality in the data were not sufficiently large enough

to discount the use of the two-way repeated measures ANOVA test (see Appendix C). However, the Friedman test was used to compare friction on the four PICP cells during Test 1, as larger deviations from normality were observed for this test and only one variable (friction) could be evaluated prior to salting. As shown in Table 9, no significant differences in surface friction were found between the four PICP cells during the three tests ($p > 0.05$), and no significant differences were found between application rates and de-icer types during Test 2 and Test 3 ($p > 0.05$). These results suggest that de-icer application rates can be reduced to 5 lb/1000 ft² on shovelled PICP surfaces while providing similar levels of safety, whereas the benefits of pre-wetting road salt with beet juice were not demonstrated for these conditions.

Table 9: Comparison of PICP cell variables for shovelled snow experiments.

Variable	Test 1 (p-value) ^a		Test 2 (p-value) ^b		Test 3 (p-value) ^b	
	DCOF	TCOF	DCOF	TCOF	DCOF	TCOF
Application Rate	-	-	0.42	1.00	0.07	0.61
De-Icer Type	-	-	0.32	0.12	0.54	0.17
Both Variables	0.69	0.22	0.43	0.33	0.61	0.55

^a Calculated using Friedman test.

^b Calculated using two-way repeated measures ANOVA test.

Undissolved salt particles remained on the five pavement cells after the shovelled snow experiments, preventing surface friction values associated with dry pavement conditions from being achieved. However, larger quantities of undissolved salt particles remained on the PICP cells than on the asphalt cell (see Figure A6) due to the wetter conditions of the asphalt surface (see Figure A7 and Figure A8). Salt dissolution on the PICP surfaces was also inhibited by some of the salt particles entering the joint spaces where meltwater drains vertically around the aggregates instead of radially along the pavers. The leftover salt particles on the PICP cells suggest that using smaller and more evenly applied salt particles may provide more benefits on PICP surfaces than on asphalt surfaces. Moreover, salt application rates may be able to be reduced on PICP surfaces since less salt dissolves and runs off in meltwater, although some of the applied salt may be less effective if it enters the joint spaces.

After meltwater had evaporated from the pavement surfaces, a portion of the dissolved salt remained as precipitate. This salt created anti-icing conditions for subsequent snowfall events when there was no rainfall to flush it away (see Figure A6). Precipitated salt particles were more widespread and concentrated on the asphalt cell because of its slope and increased salt

dissolution. Snow accumulation rates were slower on the asphalt surfaces when leftover salt was present, as the precipitated salt coverage on the asphalt cell was more representative of common anti-icing treatment conditions where a liquid brine is applied to the surface. These observations suggest that leftover salt particles provide less benefits on PICP surfaces for preventing accumulation of subsequent snowfall.

Both the undissolved and the precipitated salt particles created isolated patches of ice during temperatures below $-15\text{ }^{\circ}\text{C}$ where blowing snow would adhere to the salt, partially melt, and refreeze (see Figure A9). On 31/Jan/2019, almost the entire asphalt cell was covered in ice and blown snow due to its more widespread coverage of precipitated salt particles that had been applied the previous day, whereas ice and blown snow on the PICP cells were limited to the locations where there was leftover salt. This resulted in approximately 90% ice coverage on cells that received medium application rates and approximately 50% ice coverage on the cells that received low application rates, as reflected in the friction measurements collected after shovelling the blown snow to a thin layer (see Figure B9). Despite surface temperatures on these days being below the operational range for road salt, no reduction in ice or increase in friction occurred on the cells that received road salt pre-wetted with beet juice, as most of the beet juice coating drained off during the 30/Jan/2019 experiment. Observations during these blowing snow conditions exemplify the safety hazards of using road salt when temperatures are below its operational range.

2.3.5 Ice Cover Experiments

Two ice cover experiments were carried out where compacted snow had partially melted and then refroze to form a dense layer of ice on the pavement cells. The first experiment was carried out on 16/Feb/2019 where a dense and even layer of ice had formed on the pavement cells the previous day after air and surface temperatures temporarily rose above $0\text{ }^{\circ}\text{C}$. The pavement cells were salted at 9:30 am on 16/Feb/2019, and friction measurements were collected throughout the day from before salting until after sunset, which occurred at 5:50 pm. DCOF and TCOF measurements collected on 16/Feb/2019 are presented in Figure 7, and percent coverages of ice and snow throughout the experiment calculated from site photos are provided in Figure 8. Statistical comparisons of DCOF and TCOF between individual pavement cells were carried out using the Mann-Whitney U Test ($\alpha = 0.05$, two-tailed) and are presented in Table 10. This test

was selected because sample sizes were small (five samples per measurement set) and nonparametric, and because the slow melting and freezing that occurred on this day allowed for each measurement to be independent of collection time within a given measurement set. As shown in Table 10, statistical comparisons were performed on de-icer application rate, de-icer type, and pavement type.

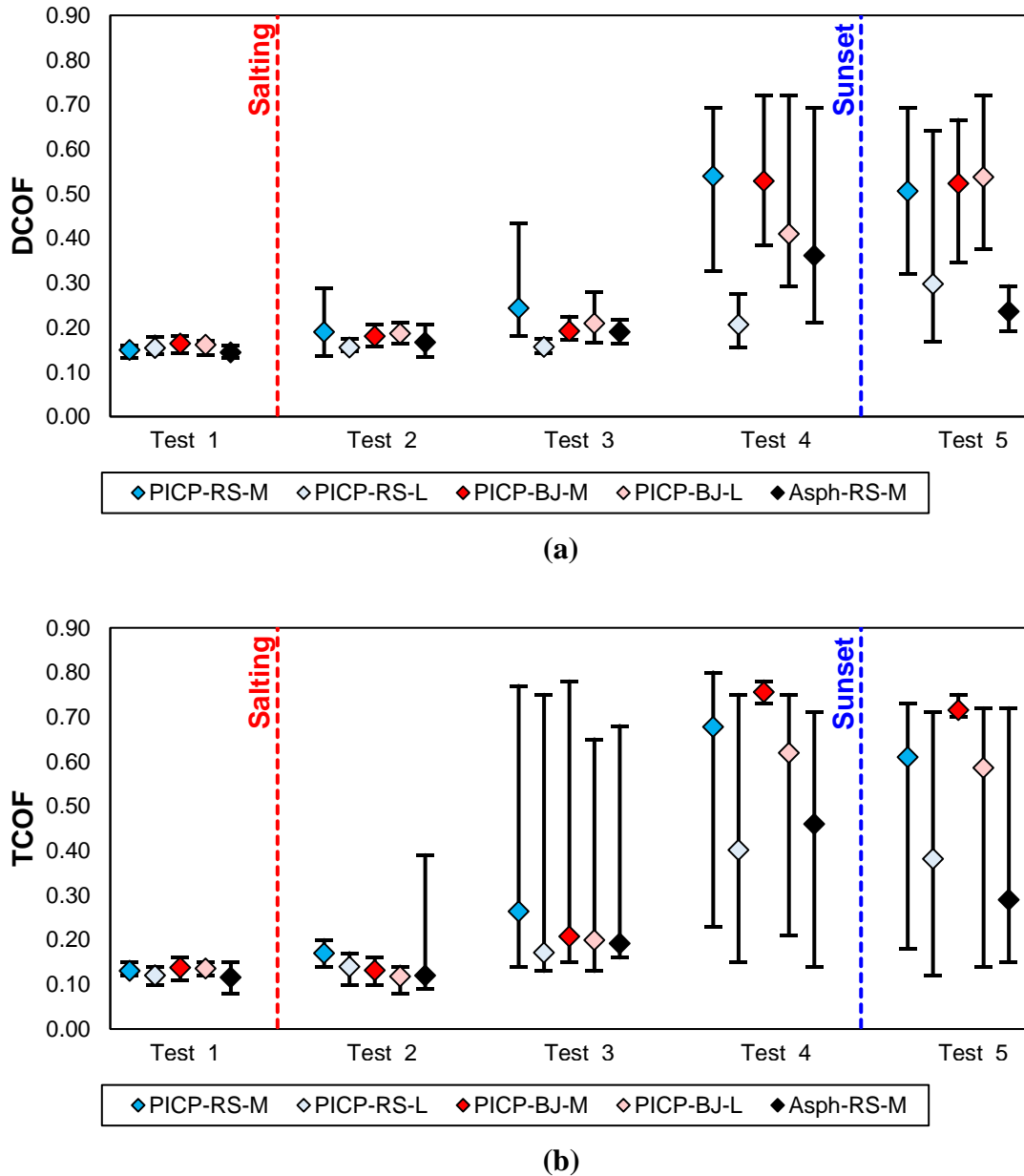


Figure 7: Means and ranges of (a) DCOF and (b) TCOF measurements collected during 16/Feb/2019 experiment.

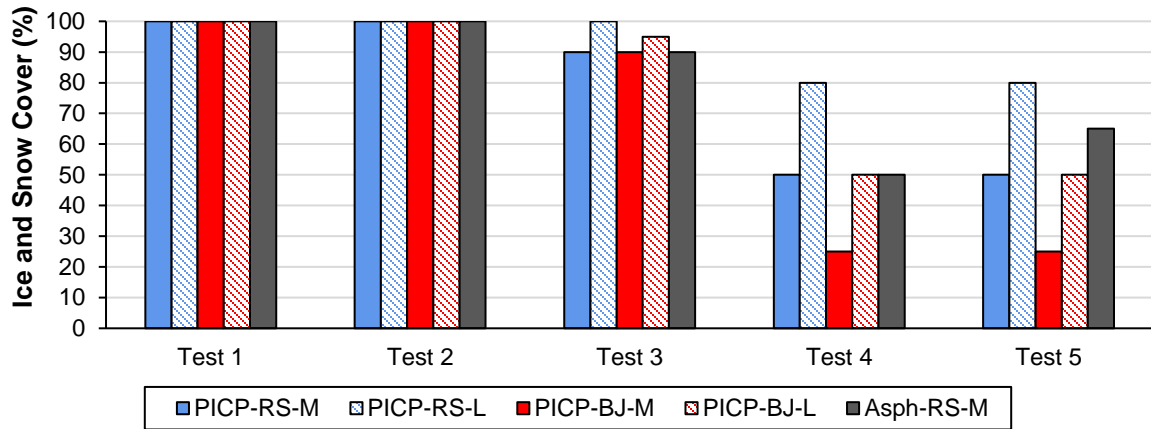


Figure 8: Ice and snow coverage during melting and refreeze on 16/Feb/2019.

Table 10: Comparison of friction between pavement cells for 16/Feb/2019 experiment.

Pavement Cell Comparison	Significant Difference ($p < 0.05$)? ^a									
	Test 1		Test 2		Test 3		Test 4		Test 5	
	DCOF	TCOF	DCOF	TCOF	DCOF	TCOF	DCOF	TCOF	DCOF	TCOF
PICP-RS-M vs. PICP-RS-L					✓		✓			
PICP-BJ-M vs. BJ-M-L								✓		
PICP-RS-M vs. BJ-BJ-M										
PICP-RS-L vs. PICP-BJ-L			✓		✓		✓			
PICP-RS-M vs. Asph-RS-M								✓		✓

^aCalculated using two-tailed Mann-Whitney U Test. A “✓” symbol indicates significant difference ($p < 0.05$).

No significant differences ($p > 0.05$) in surface friction were found prior to salting (Test 1) when comparing the individual pavement cells, reflecting the similar surface cover conditions that were present on all cells. Within 30 minutes after salting (Test 2), significant differences ($p < 0.05$) in surface friction were only found for DCOF between PICP-RS-L and PICP-BJ-L, suggesting that initial melting occurs more rapidly at low application rates when beet juice is used to pre-wet the salt. Surfaces remained ice-covered during Test 2 except for a few small pockets of partially clear pavement on the asphalt cell ($< 1\%$ of cell area) at the top of its slope and near its catch basin where a maximum TCOF of 0.39 was measured.

During Test 3, which was carried out approximately 2 hours after salting, significant differences ($p < 0.05$) in DCOF were found between PICP-RS-M and PICP-RS-L and again between PICP-RS-L and PICP-BJ-L, as the low application rate and absence of beet juice provided slower

melting conditions on PICP-RS-L. While no significant differences ($p > 0.05$) were found for TCOF during Test 3, drastic changes in maximum TCOF occurred on all cells due to various pockets of dry and semi-dry patches. As a result, maximum TCOF ranged from 0.65 to 0.78 for the PICP cells and was 0.68 for the asphalt cell. However, large increases in mean DCOF and TCOF did not occur until six hours after salting (Test 4) when more areas were clear of ice and snow.

During Test 4, DCOF was again significantly higher ($p < 0.05$) on PICP-RS-M than on PICP-RS-L, as reflected by the high ice coverage on PICP-RS-L (80%). Significant difference ($p < 0.05$) was also found between PICP-BJ-M and PICP-BJ-L for TCOF, as ice was no longer present on PICP-BJ-M at locations where TCOF measurements were collected. The impacts of de-icer application rates were therefore evident during Test 4. With regards to de-icer type, significant difference ($p < 0.05$) was only found between PICP-RS-L and PICP-BJ-L for DCOF. However, percent coverage of ice and snow was higher on PICP-RS-L than on PICP-RS-M by a factor of 1.6 and was higher on PICP-BJ-L than on PICP-BJ-M by a factor of 2, indicating that the use of beet juice enhanced melting. Finally, significant difference ($p < 0.05$) in TCOF was found between PICP-RS-M and Asph-RS-M, although DCOF was similar ($p > 0.05$) between the two cells despite PICP-RS-M having a mean DCOF that was higher than Asph-RS-M by a factor of 1.5. While ice and snow coverage on both pavement types were 50%, the higher friction on PICP-RS-M was likely caused by its cleared areas being dry, whereas half of the cleared areas on Asph-RS-M remained wet. Thus, while melt rates were similar between the two pavement types, friction was found to increase on PICP surfaces sooner because its cleared areas dry more rapidly. However, several other factors contributed to the ice melting on this day such as initial ice thickness, melting at the pavement cell boundaries, and climate fluctuations. Leftover salt particles were also observed on cleared areas of the PICP surfaces (see Figure A10), again suggesting that the PICP cells would have benefited from smaller particle sizes.

Increased melting when using the pre-wetted road salt occurred on 16/Feb/2019 despite air temperatures remaining in the operating range for road salt, and despite the benefits of having a tackier product that prevents salt particles from bouncing off the pavement not being applicable to this site. One potential contribution to the improved performance was that the tacky characteristics of the beet juice were observed to create small clumps of salt fines and reduce segregation of fines in the containers holding the salts. While no particle size distribution tests

were carried out, these adhesions likely shifted the percentage of fines towards a higher percentage of small to medium size particles, which are more likely to be picked up when scooping from a container and are more easily spread across pavement surfaces in an even manner. Another observation was that many of the larger salt particles remained on the PICP surfaces once the surrounding pavement area was clear of ice and was dry, as the rapid drainage of melted ice prevented the salt particles from dissolving. PICP surfaces therefore likely benefit more from using smaller and more evenly spread salt particles, as no meltwater path forms that would otherwise continue to dissolve and spread the larger salt particles.

During Test 5, which was carried out within the hour after sunset, 25% of the area on Asph-RS-M that was previously cleared of ice and snow became covered in a thin sheet of ice due to meltwater refreezing (see Figure A10). Refreeze of melted ice and snow along its drainage path is a typical occurrence on impervious sidewalks, as snow residing on properties often melts and drains onto sidewalks during the day and then refreezes during the night (see Figure A11). As a result of the meltwater refreeze on Asph-RS-M, mean DCOF was reduced from 0.34 to 0.22 and mean TCOF was reduced from 0.46 to 0.29. Notably, TCOF near the catch basin was reduced from 0.67 to 0.21 after the meltwater refroze. No refreeze of previously melted ice occurred on the PICP cells, as all remaining wet areas rapidly drained and evaporated. The refrozen ice on the asphalt cell remained on the surface the next morning. At 9:00 am on 17/Feb/2019, TCOF was measured near the catch basin to be 0.14, indicating that the ice was thick enough to not fully sublimate overnight. A thick layer of ice was also observed next to the catch basin on 15/Apr/2019 after a sleet and freezing rain event occurred the previous day, further exemplifying the hazards of pooling or slowly draining meltwater during the winter period (see Figure A12). Other occurrences of ice forming on impervious surfaces while permeable paver surfaces remained clear were observed during the winters, as exemplified in Figure A13.

An attempt was made to repeat the 16/Feb/2019 ice conditions during the first week of March by allowing compacted snow to partially melt during warmer temperature periods and then refreeze, although this was achieved at different times on the PICP cells than on the asphalt cell because peak daytime air temperatures unexpectedly remained below 0 °C on the days following snow compaction. Ice only formed on the asphalt cell during this time, as its surface temperatures temporarily increasing to above 0 °C almost every day. Salting was carried out on 04/Mar/2019 on the compacted snow and ice to expedite melting and to evaluate its impacts. On the days

following salting, clear spots formed along the meltwater path of the asphalt cell near the catch basin and in the middle of the cell that experienced refreeze during the nights (see Figure A14). Friction measurements carried out on 07/Mar/2019 before and after sunset showed that meltwater refreeze on the asphalt surface decreased TCOF at these locations from 0.47 to 0.08 and from 0.46 to 0.19. While refreezing of partially melted compacted snow eventually occurred during the following two days on the PICP surfaces when temperatures rose to above 0 °C, refreezing of wet surfaces from melted snow never occurred on these surfaces because of their rapid drainage and lack of meltwater path.

Further observations were made during the two ice cover experiments where the ice appeared to adhere to the asphalt surface more than the PICP surfaces. As shown in Figure A15 and Figure A16, gaps between ice and PICP surfaces were observed at the perimeter of ice patches, whereas the ice spatially transitioned into liquid state on the asphalt surface without losing contact. These observations were also made on other permeable paver surfaces during the winters, as exemplified in Figure A17. Similar observations were made on 15/Apr/2018 after the sleet and freezing rain event where ice pellets were notably easier to shovel down to a thin layer on the PICP cells compared to the asphalt cell. Ice may therefore be less bonded to PICP due to its rapid drainage of water below any ice and snow cover and due to the air spaces within the joints, potentially allowing for easier removal with shovelling and plowing equipment.

2.4 Conclusions and Recommendations

Winter monitoring of four PICP cells and an asphalt pavement cell at an outdoor test site in Vaughan, Ontario demonstrated that PICP provides enhanced winter safety benefits and opportunities to reduce the application of winter de-icing materials such as road salts. The PICP cells did not allow for conditions where runoff from melted ice and snow could refreeze unless road salt was applied during temperatures below its operational range and blowing snow conditions were present. Ice otherwise only formed on PICP surfaces following freezing rain events or compacted snow conditions where the snow had trapped liquid water during partial melting processes or rainfall events. This ice appeared to be less bonded to the PICP surfaces, as gaps were frequently observed between the ice layer and the pavement, and ice pellets following a sleet and freezing rain event were more easily shovelled from the PICP surfaces than the asphalt surface. Surface temperature trends on PICP surfaces may also reduce the risk meltwater

refreeze, as less drastic decreases in surface temperatures occurred at sunset on the PICP cells, allowing more time for meltwater to drain and evaporate. Conversely, meltwater draining from compacted snow or ice along the asphalt surface towards its catch basin refroze on multiple occasions, and ice cover was always observed to be highly bonded to the asphalt surface.

Prolonged melting was frequently observed near the catch basin when the asphalt cell was left undisturbed, demonstrating how low areas on impervious pavements can create an increased risk of ice formation. These low areas with catch basins are also at higher risk of flooding during the winter due to the possibility of ice accumulating in the catch basin. However, even if ice were to accumulate within the PICP underdrain or within the base and subbase layers, the large storage volume and infiltration area may lower the risk of surface flooding during winter rainfall events.

Experiments carried out throughout the two winters on surfaces that were shovelled to thin layers of snow and then salted showed that surface friction prior to salting is always lower on PICP surfaces than on asphalt surfaces, whereas both pavement types experienced similar friction after salting and several hours later. Differences in de-icing application rates and de-icer types did not impact melting on PICP surfaces after the snow was shovelled to a thin layer, indicating that the low application rate of 5 lb/1000 ft² may have been too high for these conditions. This is further demonstrated by the large amount of salt particles that remained on the PICP surfaces after all snow had melted. Pre-wetting road salts with beet juice may, however, provide improved performance when melting ice cover.

While no notable differences in snowmelt were consistently observed during the shovelled snow experiments, asphalt surfaces always remained wet for longer periods after melting. The drier conditions of PICP surfaces therefore decrease the risk of meltwater refreeze at sunset, and they also prevent additional salt from dissolving after ice and snow have melted. However, the drier and faster drainage conditions of PICP surfaces also reduce both the quantity and the surface coverage of dissolved salt that can precipitate out onto the surface and provide anti-icing conditions for subsequent snowfall events. Future research is therefore needed on anti-icing practices for PICP surfaces, as liquid anti-icing applications may benefit PICP surfaces more than impervious surfaces in achieving widespread coverage. Further research is also needed on PICP surfaces that receive regular but controlled pedestrian and vehicular traffic during melting periods, as continuous compaction and introduction of snow, slush, water, and salt from outside

sources would have notable impacts on surface conditions. Additional research should be carried out on nighttime de-icing practices for PICP surfaces, as surface conditions are not impacted by solar radiation and peak midday temperatures during the night. Finally, this study was conducted on a new PICP installation with extremely high surface infiltration rates of $> 10,000$ mm/hr, whereas the behaviour of partially clogged PICP could substantially differ.

Based on the findings from this research, recommendations for winter maintenance of PICP (and possibly for other PP technologies) are as follows:

1. Unlike impervious pavement surfaces, de-icers are not needed on PICP surfaces to prevent melted ice and snow from refreezing. De-icers should also not be used on compacted snow, regardless of pavement material. De-icing on PICP surfaces should therefore be limited to when surfaces are covered in ice formed by freezing rain or rapid freezing of wet compacted snow. De-icers can, however, also be used as needed to melt remaining snow after PICP surfaces are plowed or shovelled if surface temperatures are below 0°C , although application rates of 5 lb/ 1000 ft² or lower are recommended.
2. Smaller de-icer particle sizes are recommended for PICP surfaces because the drier surface conditions can cause larger particles to remain after ice and snow have melted, and leftover de-icing particles are not needed to prevent meltwater from refreezing. Using smaller particle sizes may also provide opportunities for reducing application rates.
3. De-icing treatments need to evenly cover PICP surfaces because their flat slopes and rapid drainage characteristics prevent de-icing chemicals from spreading with the melted ice and snow. Unlike impervious surfaces that experience meltwater drainage paths and refreeze, no benefits are gained from treating cleared surfaces within a partially cleared pavement installation.
4. Shovelling and plowing of icy PICP surfaces should be attempted before applying de-icers, as the ice may be less bonded to the surface and easily removed. If ice can only be removed in some areas, this may limit the areas where de-icers are needed.

Chapter 3

3 Additional Data and Observations

Chapter 3 provides an evaluation of additional data and observations that were collected at the research site but were not included in the manuscript from Chapter 2. These additional data and observations include:

- 1) Conductivity and chloride data collected in the PICP underdrains and asphalt runoff during the 2018/2019 winter;
- 2) Additional surface temperature data collected using infrared sensors on the PICP and asphalt cells that received medium road salt application rates; and,
- 3) Additional observations on the applicability of SlipAlert and Mark IIIB to measuring surface friction on PICP test cells during winter conditions.

3.1 Evaluation of Chloride Concentrations in PICP Outflows

While PP systems are not able to reduce the total mass of chlorides released to the environment from winter salting activities, they have been shown to attenuate peak winter chloride concentrations and delay their release to downstream drainage systems (Borst and Brown 2014; Drake et al. 2014; Zhu 2017). Chloride monitoring was carried out to examine the timing and concentration of chlorides in runoff and discharge from the asphalt and PICP systems. This section presents a summary and evaluation of the conductivity and chloride data that was collected in the PICP underdrains and asphalt runoff during the 2018/2019 winter.

3.1.1 Methodology

Conductivity, which can be used as an indicator for the concentration of chloride, was continuously monitored in the outflow from the four PICP underdrains (installed at the bottom each cell) and from the outlet pipe of the catch basin on the asphalt cell. The PICP cells were constructed as partial infiltration systems where outflows from the PICP underdrains consist of stormwater and meltwater that has percolated through the aggregate layers but has not infiltrated into the native clay soil below. Outflows from the asphalt cell consist of all stormwater and meltwater runoff that has drained from its impervious surface into the catch basin.

Conductivity was measured using CT2X sensors, which have an accuracy of $\pm 0.5\%$ for conductivity values up to $100,000 \mu\text{S}/\text{cm}$. Two-point calibration was performed on each sensor using conductivity solutions of $1,413$ and $12,880 \mu\text{S}/\text{cm}$. The sensors were installed within U-shaped rubber pipe traps connected to the PICP underdrains and catch basin outlet pipe. Rubber traps with clamp connections were used such that the traps could withstand soil expansions and contractions throughout the winter period without leaking, and monitoring wells were connected to the traps such that the sensors could be installed and accessed. The traps were bedded in a 400 mm deep layer of High Performance Bedding (3 to 8 mm washed aggregates) to further minimize movement of the traps, and the bedding layer was covered with 2 inches of foam insulation to minimize frost penetration. Native soil was backfilled above the insulation. Trap installation was completed on 31/Oct/2019, and a photo of the traps during installation prior to being covered and backfilled is provided in Figure 9.



Figure 9: Installation of traps for housing conductivity sensors.

Within the traps, the conductivity sensors were submerged within a permanent pool of water that was approximately 300 mm deep and stored approximately 1.2 L of water, and conductivity was measured approximately 110 mm from the bottom. Measurements were collected every five minutes throughout the 2018/2019 winter beginning on November 8, 2018. While flows were not monitored, the sensors also measured water depth and temperature. Changes in these data were used to identify the presence of flows. Water depth varied throughout the monitoring period as a result of periodic water sampling but were always kept at above 200 mm to maintain submergence of the sensors.

Water samples were collected in each trap using a 15 mL bottle attached to a swing sampler. For each sample, the 15 mL bottle was dipped into the bottom of the trap next to the conductivity sensor, removed, and then poured into a larger 250 mL sampling bottle. This process was repeated a minimum of five times for each well such that sample volumes of 75 mL or greater were collected. A new 15 mL bottle was used for each trap to prevent contamination. Between samples, the swing sampler was washed with reverse osmosis water and then quickly dried using a space heater to prevent ice from forming on the sampler during the frigid outdoor temperatures. The collected water samples were then sent to AGAT Laboratories where they were tested for chloride concentrations within 28 days of sampling. Water samples were first collected on 14/Jan/2019 to identify background chloride concentrations in each trap prior to the first application of de-icing treatments. Sampling was then carried out whenever changes in conductivity were observed after rainfall events or melting periods.

3.1.2 Results and Discussion

3.1.2.1 Conductivity Measurements

Conductivity measurements collected from the middle of January to the end of May are presented in Figure 10, and background and peak winter conductivities are presented in Table 11. Conductivity spikes were found to be more closely associated with rainfall rather than snowfall, as larger flows occurred during rainfall events. The daily rainfall data presented in Figure 10 was obtained from Environment Canada for the Toronto North York station, which is located approximately 11 km from the research site and therefore only provides a general estimation of rainfall amounts. Moreover, some of the observed rainfall at the airport may have occurred as snowfall at the research site, and some of the rainfall that occurred at the research site may have

been observed at snowfall at the airport. The background conductivities presented in Table 11 are the mean values from the 08/Nov/2018 to 22/Jan/2019 period, which was prior to the traps receiving runoff from the first de-icing treatment. While minimal changes in conductivity occurred during this period, conductivity in the asphalt outflow would temporarily spike to zero during rainfall events and then gradually increase and eventually equalize.

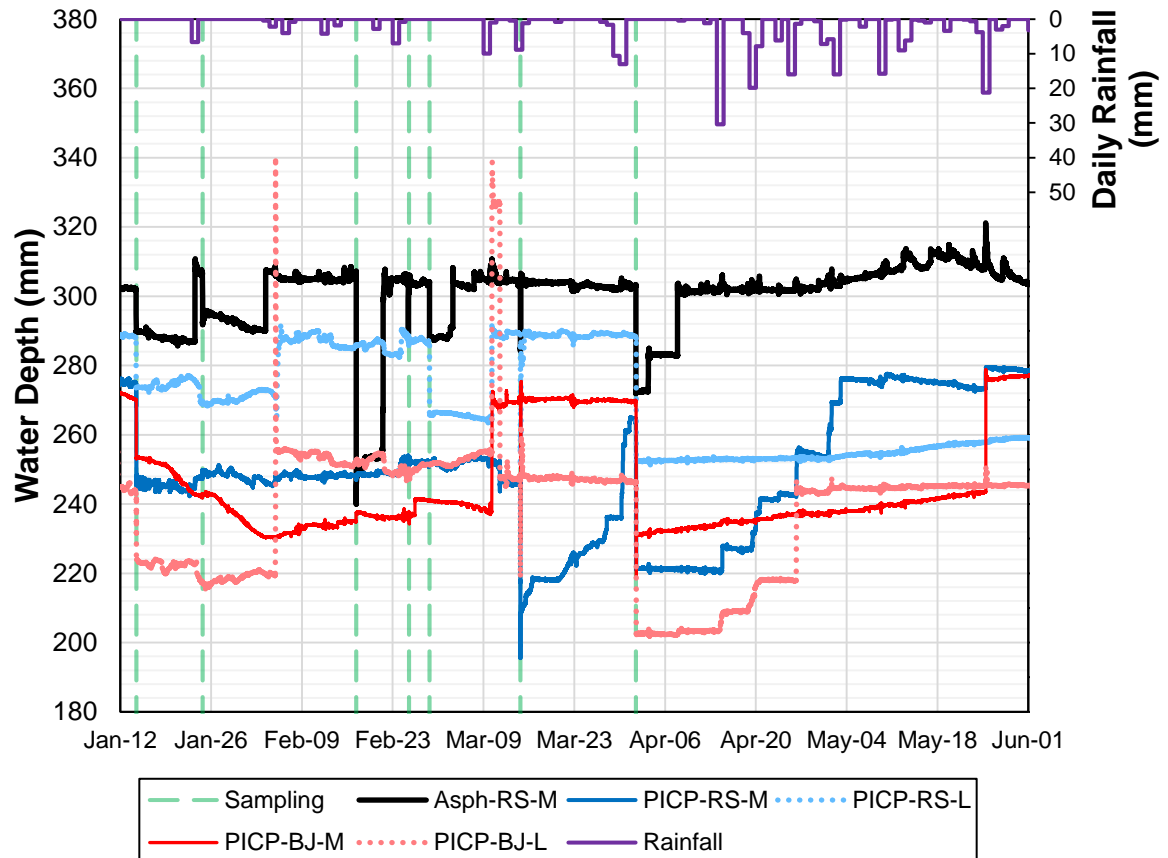


Figure 10: Conductivity measurements collected during the 2019 winter and spring.

Table 11: Background and peak winter conductivities in pavement cell outflows.

Test Cell	Background Conductivity ($\mu\text{S}/\text{cm}$)	Peak Conductivity ($\mu\text{S}/\text{cm}$)	Peak Conductivity Reduction ^a	Peak Measurement Date
PICP-RS-M	908	1,090	96%	09/Mar/2019
PICP-RS-L	649	3,450	88%	14/Mar/2019
PICP-BJ-M	774	1,240	96%	11/Mar/2019
PICP-BJ-L	383	3,450	88%	14/Mar/2019
Asph-RS-M	155	29,400	-	23/Jan/2019

^a Percentage of peak conductivity in the respective PICP cell to that of the asphalt cell.

As shown in Figure 10 and Table 11, the peak winter conductivity in the asphalt cell outflow was measured at 29,400 $\mu\text{S}/\text{cm}$ and occurred after the first rainfall event that followed the first de-icing treatment. Similar conductivity levels were then observed in the asphalt cell outflow until after the last de-icing treatment was carried out on 04/Mar/2019. Beginning on 10/Mar/2019, rainfall events began to result in peak minima conductivity values rather than peak maxima conductivity values, indicating that very little road salt was left either on the pavement surface or in the catch basin. Conductivity levels would rapidly increase at the end of each rainfall event and gradually increase during the following dry periods, indicating that low quantities of the salt may be remaining in the system, or denser water that contains elevated levels of dissolved salt may not be fully flushing out of the trap during periods of flow. This pattern continued until the end of May, including multiple rainfall events where conductivity temporarily dropped to near zero. Overall, the total chloride masses discharged from the asphalt cell were likely minimal during the spring compared to the winter when peak maxima conductivity values were observed during rainfall events.

For the two PICP cells that received medium de-icer application rates, peak winter conductivities in the underdrain outflows were 4% of those in the asphalt cell outflow. For the two PICP cells that received low de-icer application rates, peak winter conductivities in the underdrain outflows were 12% of those in the asphalt cell outflows. While similarities in conductivity peaks for PICP cells that received the same application rate were expected, the PICP cells that received low application rates had peaks that were three times higher than those that received high application rates. This conflicting result may have been caused by ice accumulation within the cells influencing the outflows and infiltration rates, as the amount of salt applied to each cell may have impacted the amount of ice accumulation below the surface. Ice in the subbase layer can create preferential flow paths to the underdrain, or it can increase infiltration by blocking flows to the underdrain. Additionally, having more salt in the system can either inhibit or promote ice accumulation below the surface depending on temperatures in the subbase and in the native soil, and depending on its dilution within the stored water. These processes can, however, only be speculated, as ice accumulation below the PICP surfaces was not able to be monitored.

While peak winter conductivities in the asphalt outflows occurred immediately after the first de-icing treatment, peak winter conductivities in the PICP outflows occurred in March after rainfall events became more frequent and temperatures began to rise. The PICP cells were therefore

found to both reduce and delay the peak winter conductivity spikes. From 14/Mar/2019 onward, peak minima conductivities were observed in the PICP outflows whenever the traps received flows. Similar to the asphalt cell, this likely occurred as a result of low quantities of the salt remaining in the system, or the denser water containing dissolved salts not fully flushing out of the traps.

3.1.2.2 Discharge Observations

Conductivity levels measured in the PICP traps were likely impacted by the low percentage of rainfall discharged to the traps throughout the monitoring period. This is evident from the temperature data where 30 temporary spikes occurred in the asphalt outflow from 23/Jan/2019 to 31/May/2019 following rainfall or melt events, whereas the number of temperature spikes in the PICP outflows only ranged from 4 to 11. During January and February, most rainfall that landed on the PICP surfaces likely infiltrated into the ground or accumulated as ice within the cells, as minimal flows were observed in the PICP underdrains during this period based on changes in conductivity, water depth, and water temperatures. However, larger flow responses to rainfall events were observed in the PICP traps in March. After sampling on 14/Mar/2019 lowered the water levels in the traps, three of the four PICP traps rapidly filled back up to their maximum water levels during a 9 mm rainfall event that occurred later that evening. For PICP-RS-M, the trap slowly filled up during the month of March after 40 mm of cumulative rainfall occurred. Water depths and water temperatures measured during the monitoring period data are presented in Figure 11 and Figure 12, respectively.

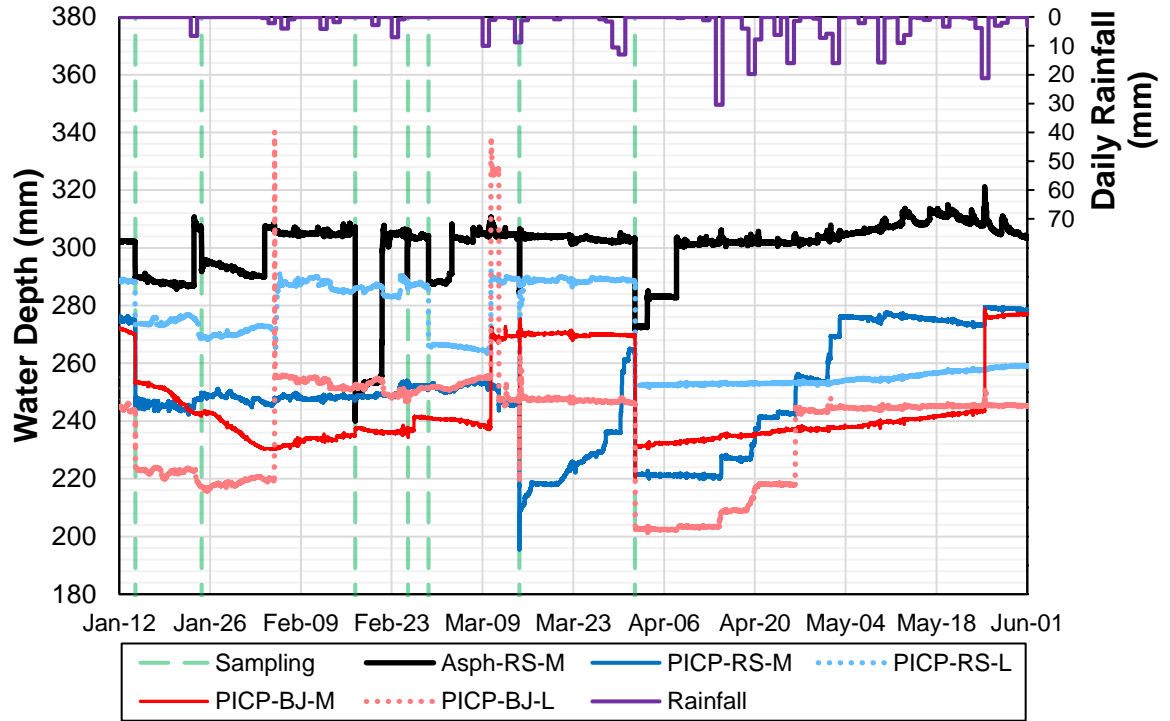


Figure 11: Water depth measurements collected during the 2019 winter and spring.

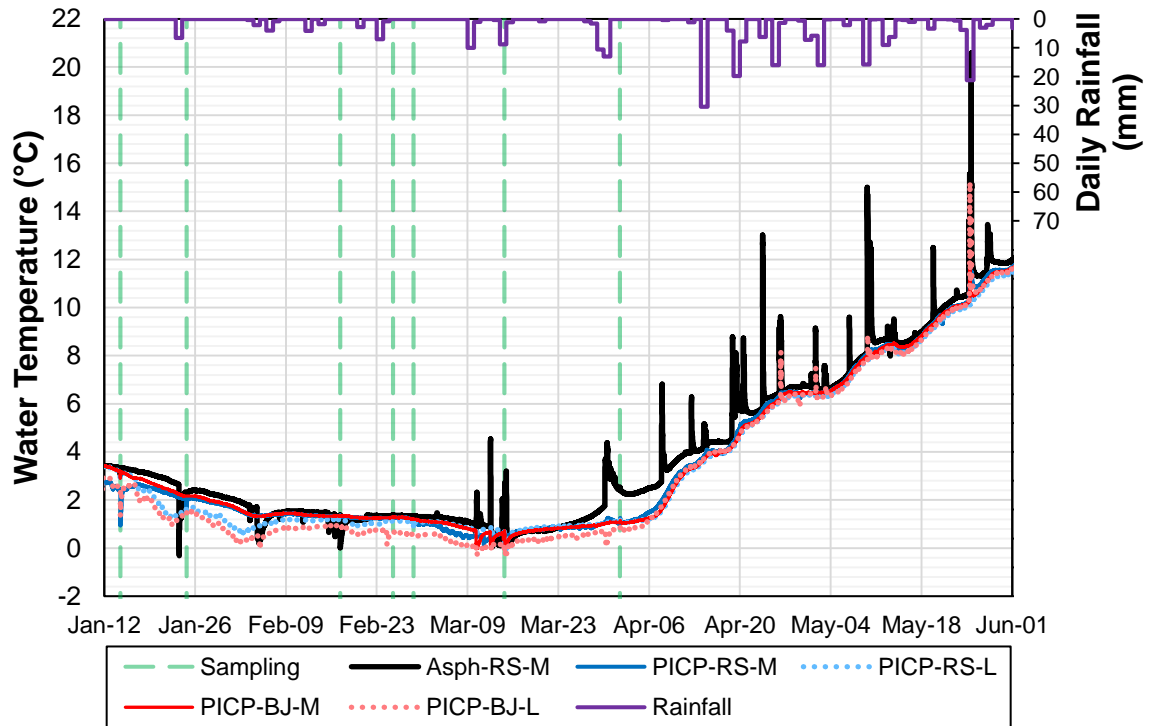


Figure 12: Water temperature measurements collected during the 2019 winter and spring.

While frost penetration depths were not monitored, it is likely that native soil infiltration rates were reduced in March, or preferential flow paths to the PICP underdrains formed from ice accumulation within the cells. This is evident when looking at the PICP underdrain flow responses in April in May, which were substantially reduced compared to in March. After sampling on 01/Apr/2019 lowered the water levels in the traps, none of the PICP traps fully filled back up until at least 90 mm of cumulative rainfall occurred. Moreover, almost all rainfall that fell on the PICP cells in April and May was estimated to infiltrate or evaporate based on the measured water volumes in the traps. Thus, despite having clayey soils, high infiltration rates occurred below the PICP cells in April and May, whereas increased flow responses occurred in March.

3.1.2.3 Measured Chloride Concentrations

Chloride concentrations measured in the collected water samples are presented in Table 12. As a reference, the United States Environmental Protection Agency (USEPA) currently recommends a chronic chloride concentration limit of 230 mg/L and an acute chloride concentration limit of 860 mg/L to sustain aquatic life (USEPA 2019). As shown in Table 12, samples were collected for all pavement cells on the following three days: (1) 14/Jan/2019, which was prior to the first de-icing treatment, (2) 14/Mar/2019, which was after conductivity spikes were first observed in all PICP outflows, and (3) 01/Apr/2019, which was after the remaining March rainfalls events occurred. An additional sample was collected for PICP-RS-L on 28/Feb/2019 after rainfall events during February were observed to increase conductivity in the trap. For the asphalt cell, additional samples were collected on 24/Jan/2019, 17/Feb/2019, and 28/Feb/2019 after conductivity spikes were observed in the asphalt outflow.

Table 12: Chloride concentrations measured in water samples.

Test Cell	Sample Number	Sample Date	Chloride Concentration (mg/L)	Conductivity Measurement (µS/cm)
PICP-RS-M	1	14/Jan/2019	43.9	978
	2	14/Mar/2019	29.9	1,040
	3	01/Apr/2019	32.9	936
PICP-RS-L	1	14/Jan/2019	16.1	671
	2	28/Feb/2019	786	1,500
	3	14/Mar/2019	766	3,213
	4	01/Apr/2019	413	2,195
PICP-BJ-M	1	14/Jan/2019	30.6	779
	2	14/Mar/2019	44.9	496
	3	01/Apr/2019	26.2	520
PICP-BJ-L	1	14/Jan/2019	28.7	427
	2	14/Mar/2019	674	3,169
	3	01/Apr/2019	143	722
Asph-RS-M	1	14/Jan/2019	1.62	151
	2	24/Jan/2019	610	26,411
	3	17/Feb/2019	2,910	21,375
	4	28/Feb/2019	3,390	20,699
	5	14/Mar/2019	110	6,881
	6	01/Apr/2019	185	4,393

Baseline chloride concentrations prior to any de-icing activities were found to be substantially higher in the PICP outflows (30 mg/L on average) compared to the asphalt outflows (1.6 mg/L). These chloride concentrations are, however, much lower than the current USEPA chronic limits. While no chloride sources were identified in the PICP cells, low levels of chlorides were likely leaching from the aggregates or pavers into the underdrains.

For the asphalt cell, the chloride concentration measured on 24/Jan/2019 after the first de-icing treatment and subsequent rainfall event was 610 mg/L. However, large amounts of suspended sediment were observed in the sample, which may have impacted its chloride content. Turbidity of the asphalt outflows was visually observed to decrease as the winter progressed. The source of the turbidity was likely sediment leftover from construction activities during installation of the traps and from atmospheric deposition before the winter season. For the two samples collected on 17/Feb/2018 and 28/Feb/2018 after additional de-icing treatments and rainfall events, chloride concentrations were substantially higher at 2,910 and 3,390 mg/L despite slightly lower conductivity readings of 21,375 and 20,699 mg/L, respectively. Partially frozen water was also

observed in the 17/Feb/2018 sample, which may have contributed to its lower chloride content than in the 28/Feb/2018 sample. These chloride concentrations were therefore several magnitudes higher than both USEPA chronic and acute limits. Chlorides concentrations were then reduced to 110 and 185 mg/L in the 14/Mar/2019 and 01/Apr/2019 samples, which were collected after the cells were no longer receiving de-icing treatments and peak minima conductivities began to occur.

For the two PICP cells that received medium de-icer application rates, the water samples provided no evidence that chloride levels had increased during the conductivity monitoring period. The absence of increased chloride levels on 14/Mar/2019 also indicates that most chlorides were rapidly flushed out of the system during the previous rainfall events associated with the peak winter conductivity observations. Additional sampling on 01/Apr/2019 and sustained conductivity values into May further confirmed that no increased chloride concentrations were likely discharged from the two cells during the spring.

For the two PICP cells that received low de-icer application rates, increased chloride concentrations were measured on 14/Mar/2019 after the peak winter conductivity observations. On this day, similar chloride concentrations of 766 mg/L and 674 mg/L, and similar corresponding conductivities of 3,213 and 3,169 $\mu\text{S}/\text{cm}$, were measured in the PICP-RS-L and PICP-BJ-L outflows, respectively. However, slush was observed in both water samples, indicating that partially frozen conditions in the traps may have impacted the conductivity readings and chloride concentrations in the water samples. These impacts can be observed when comparing the measurements collected on 28/Feb/2019 and 14/Mar/2019 in the PICP-RS-L outflows. Between these two days, conductivity more than doubled from 1,500 to 3,213 $\mu\text{S}/\text{cm}$ while chloride concentrations remained relatively unchanged from 786 to 766 mg/L, respectively. The presence of frozen water in the traps also indicates that ice may have accumulated in the PICP underdrains and aggregate layers. On 01/Apr/2019, conductivities and chloride concentrations had decreased in both cells but were still elevated when compared to baseline values. However, this could again be attributed to low quantities of salt remaining in the system or water containing higher quantities of dissolved salts not fully flushing out of the traps.

3.1.2.4 Estimated Chloride Concentrations

Relationships between the measured conductivities and chloride concentrations were developed such that chloride concentrations could be continuously estimated for the entire monitoring period. These relationships were developed by first transforming the data onto a log-log scale. Linear regressions were then computed for the transformed data, as shown in Figure 13. A single regression was applied for the two PICP cells that received conventional road salt and for the two PICP cells that received road salt pre-wetted with beet juice since individual regressions were unable to be computed for each cell. Data from the four PICP cells could not be combined because the chemical properties of beet juice may have impacted the conductivity readings. The 24/Jan/2019 sample was omitted from the asphalt regression due to the chloride concentration being an extreme outlier that could have been caused by the large quantity of particulate matter that was collected on that day. However, it should be noted that there is a large uncertainty associated with the use of these regressions, as the regressions were developed using a small dataset, and the dataset included samples where the water was partially frozen at the time. Moreover, the R^2 value of the regression was low (0.48) for the PICP cells that received conventional road salt.

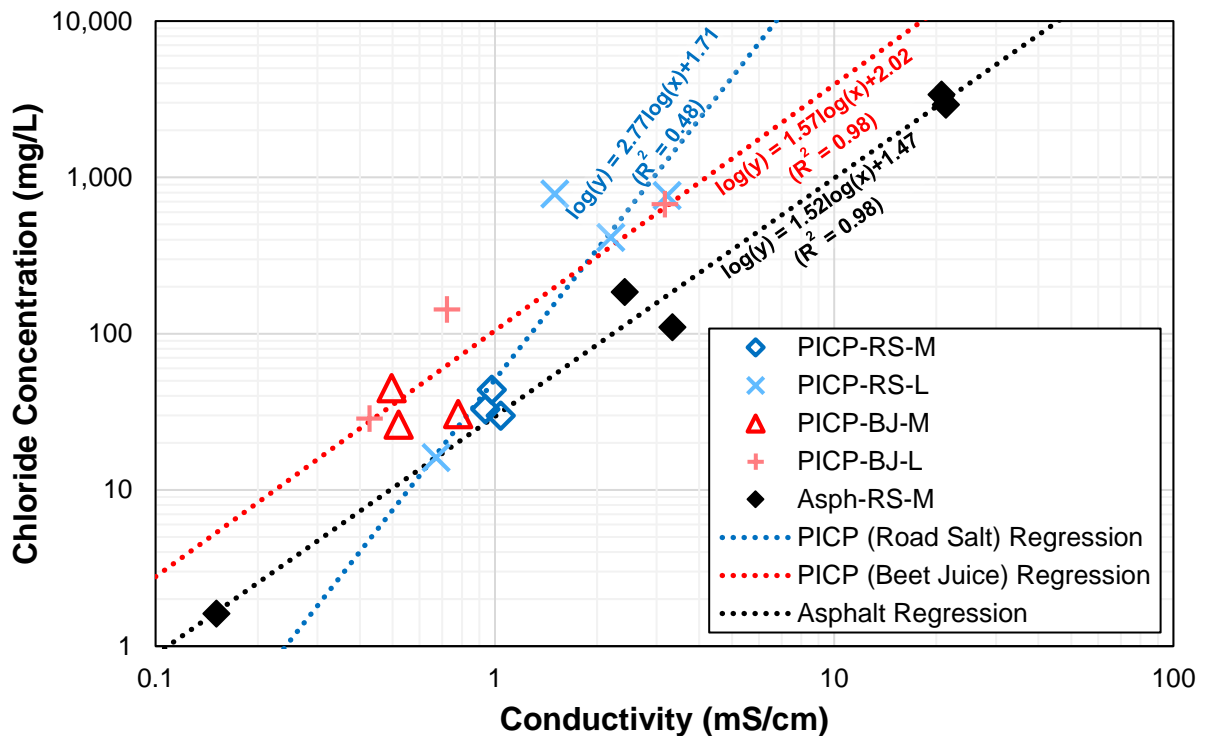


Figure 13: Linear regressions of conductivity and chloride data.

The two regression curves were then used to estimate chloride concentrations during the monitoring period from the conductivity data. Continuous estimations of chloride concentrations are presented in Figure 14, and the associated peak winter chloride concentrations are summarized in Table 13. Using the regression curves, the peak winter chloride concentration for the asphalt cell was estimated to be 5,100 mg/L, whereas peak winter chloride concentrations were estimated to be between 1% and 31% of this value for the four PICP cells. Chloride concentrations for the two PICP cells that received medium de-icer application rates were estimated to never exceed the USEPA chronic limit of 230 mg/L, and only PICP-RS-L was estimated to exceed the USEPA acute limit of 860 mg/L.

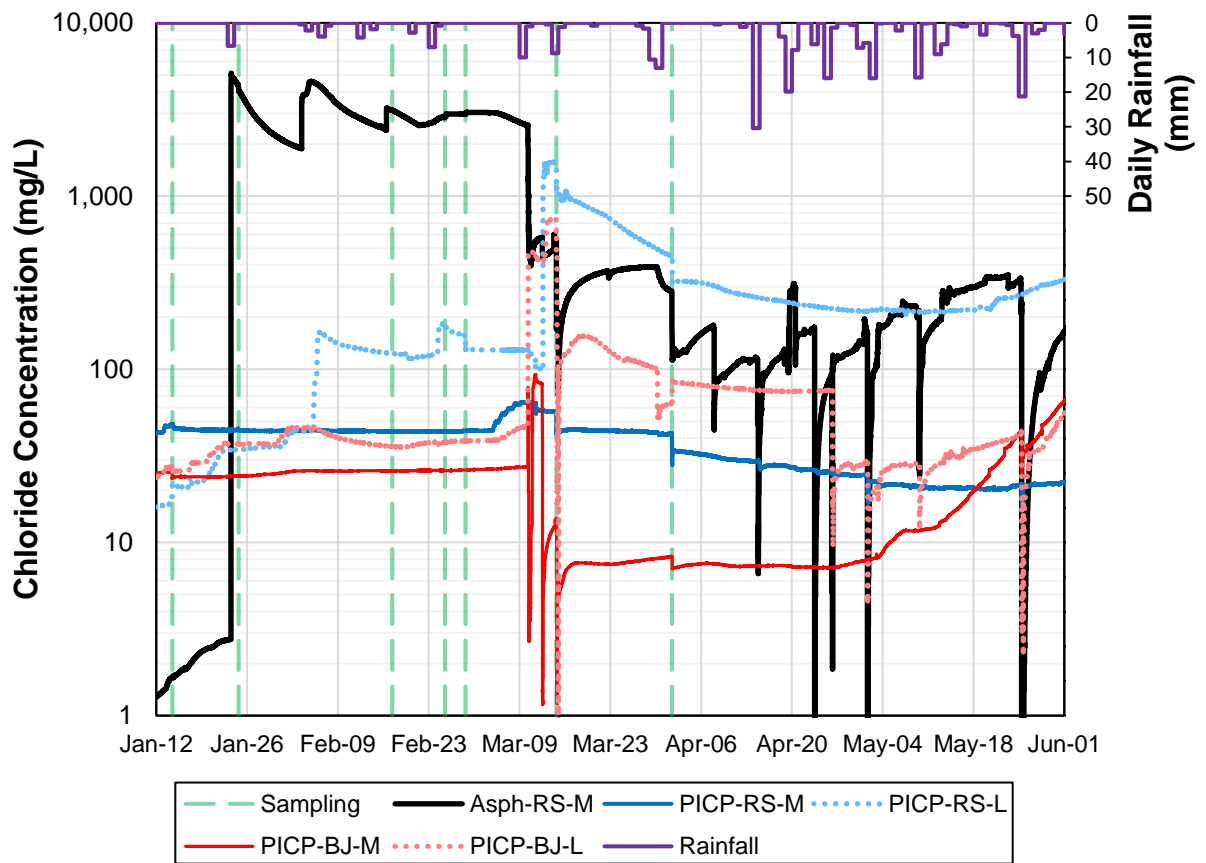


Figure 14: Estimated chloride concentrations during the 2019 winter and spring.

Table 13: Estimations of peak winter chlorides in pavement cell outflows.

Test Cell	Peak Chloride Concentration (mg/L)	Peak Chloride Concentration Reduction¹	Measurement Date
PICP-RS-M	65	99%	09/Mar/2019
PICP-RS-L	1,560	69%	14/Mar/2019
PICP-BJ-M	90	98%	11/Mar/2019
PICP-BJ-L	730	86%	14/Mar/2019
Asph-RS-M	5,100	-	23/Jan/2019

¹Percentage of peak chloride concentration in the respective PICP cell to that of the asphalt cell.

3.1.3 Conclusions and Recommendations

Conductivity and chloride monitoring showed that PICP systems with partial infiltration on clayey soils can reduce peak winter chloride concentrations in stormwater runoff by up to 99%. However, most precipitation during the winter period may still infiltrate into the native soil in the absence of extreme rainfall events. The total mass of chlorides discharged to both downstream surface waters and groundwater are therefore likely not reduced by PICP systems, and road salt reduction strategies remain the most viable solutions to reducing chloride pollutants in cold climate locations.

PICP systems delay the release of chlorides, whereas high chloride concentration spikes are immediately observed during rainfall events that follow de-icing treatments on conventional asphalt pavements. While these delays could be partially attributed to the precipitation of dissolved road salts onto aggregates below the surface, they can also occur if PICP systems produce minimal outflows during the winter period as a result of lower intensity rainfall events or ice accumulation within the systems. More research is needed on these processes, as native soil infiltration rates and temperatures below the surface were not monitored at this research site.

Multiple data collection challenges can occur when measuring conductivity from test cells with small surface areas, as underdrain flow rates are substantially reduced in this setting than in a typical parking lot or walkway installation. Thus, the use of traps for housing conductivity sensors may not result in complete flushing during flow events, and chlorides may remain at the bottom of the traps throughout the monitoring period. Alternatively, if conductivity sensors were instead placed along the bottom of a pipe or a conduit with a narrow geometry, the low flows would result in flow depths that are insufficient to submerge most sensors. The use of traps also

results in water levels to be reduced when sampling, and prolonged periods may occur before the traps fill back up. Improved methods are therefore needed for monitoring conductivity and collecting water samples from PICP installations with small surface areas.

In addition to the issues associated with small surface areas, the use of shallow depths for the base and subbase layer increases the risk of freezing within these layers and within the native soil. This can influence infiltration rates during the winter period, which impacts the amount of outflows discharged from the PICP systems. To eliminate the potential impacts of freezing in future research projects, deeper installations are recommended such that temperatures at the bottom of test cells and within the native soil below remain above freezing. Alternatively, heat trace cables could be installed, although the heat introduced by such devices may increase melt rates, which would not be representative of typical winter conditions for PICP installations.

3.2 Evaluation of Non-Contact Infrared Sensors for Measuring PICP Surface Temperatures

In addition to the use of thermistors to monitor surface temperatures on the five pavement cells, non-contact infrared temperature sensors were also installed above PICP-RS-M and Asph-RS-M to monitor the overall surface temperature of the two cells above any ice or snow accumulation. However, due to several data quality and equipment malfunction issues associated with the infrared sensors, only the thermistor measurements were included in the manuscript presented in Chapter 2. This section provides an evaluation of the infrared sensor data and its correlation to the contact sensor data, including a discussion on the issues that were encountered at the research site with the infrared sensors.

3.2.1 Methodology

Two non-contact infrared sensors were installed at the research site to measure surface temperatures on PICP-RS-M and Asph-RS-M. These two cells were selected to provide a comparison of surface temperatures between PICP and asphalt pavements that receive the same de-icing treatment. The infrared sensors used for this study were Surface Sentinel Model 5439-00, which have an accuracy of $\pm 1^\circ\text{C}$ for surface temperatures collected in the -40 to 85°C range. Unlike the contact sensors installed on all cells that are only capable of measuring surface temperatures at a single location, the infrared sensors measure surface temperatures based on the

area captured within their field of view (FOV). For the Surface Sentinel, objects within its 12° FOV contribute to 75% of each measurement, whereas objects within its 90° FOV contribute to the remaining 25% of each measurement.

The infrared sensors were installed immediately outside the corners of the two pavement cells at a height of 2.5 m above the ground. Sensors were placed on the northern side of the cells to avoid shadows. This configuration resulted in a sensor angle of 65° from the horizon after the sensors were pointed towards the centre of the cells. At this angle and location, the 12° FOV was estimated to measure a surface area of 0.3 m² on each cell and the 90° FOV was estimated to measure a surface area of 35 m², assuming a flat terrain beyond the cells. Since each pavement cell has a surface area of 4 m², 75% of each surface temperature measurement was collected on 8% of the pavement cell, whereas 25% of each measurement was collected on the remaining 78% of the pavement cell plus an additional area outside of the cells that was in the order of 8 times the area of each cell. The contribution of area outside of the pavement cells could not be accurately estimated beyond knowing that it would be less than 25%. A photo showing the infrared sensor configuration and approximated extend of the 12° FOV projection onto the pavement surfaces is presented in Figure 15.

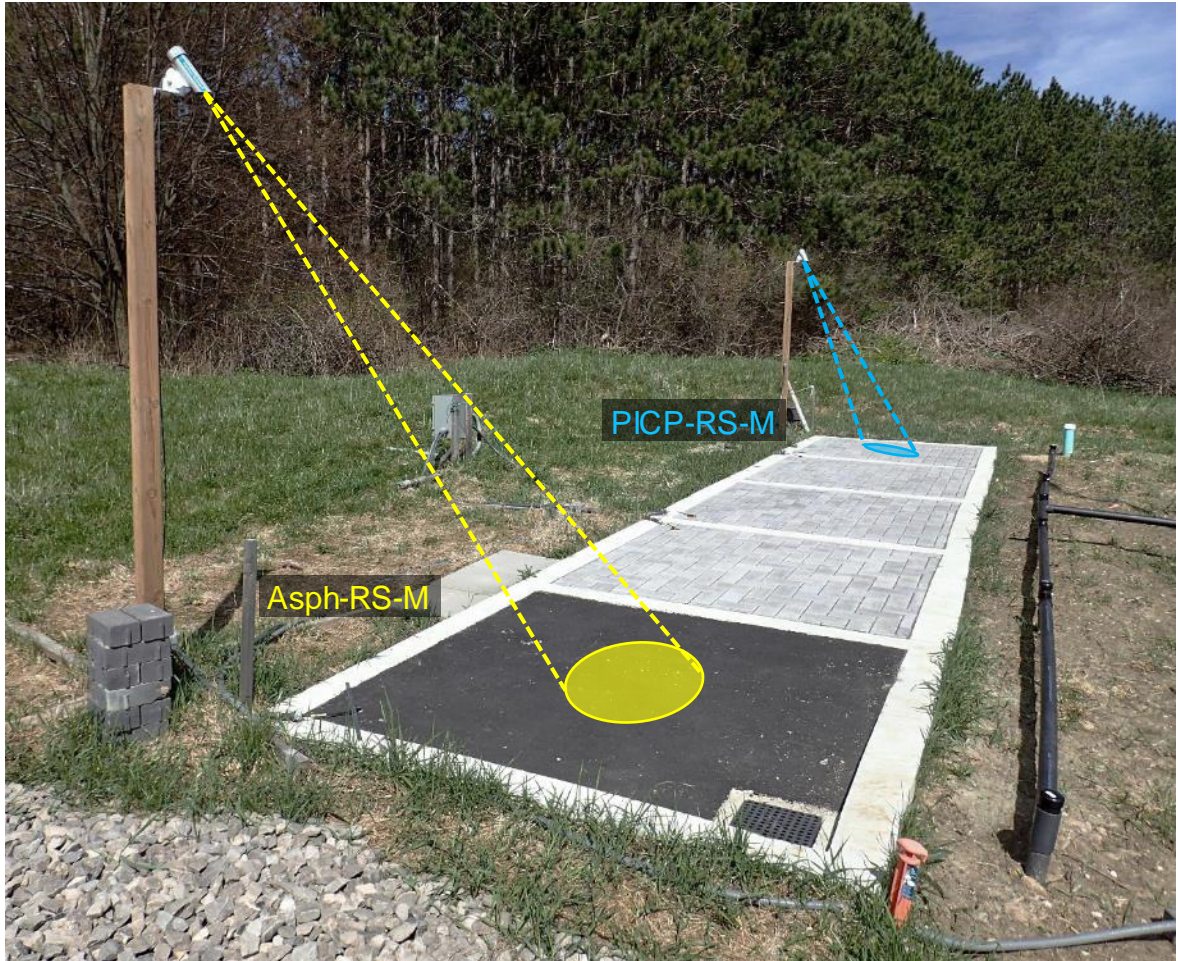


Figure 15: Infrared sensor installation showing approximate extent of 75% data capture on PICP-RS-M and Asph-RS-M.

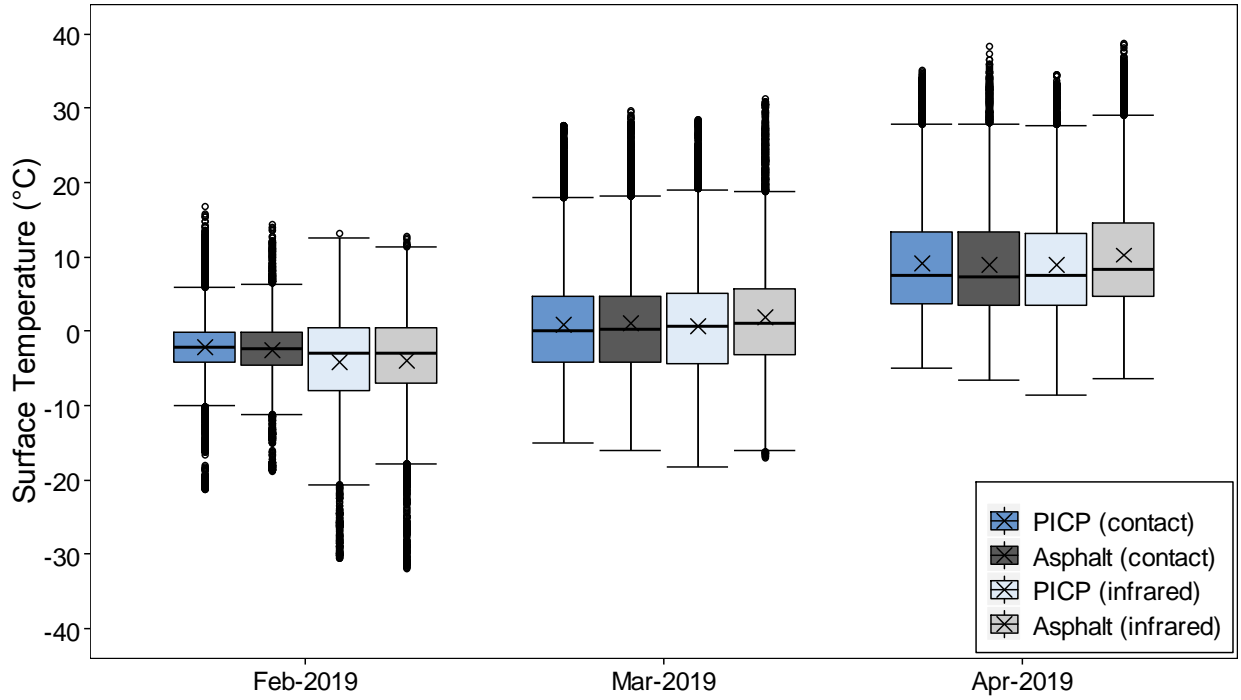
Surface temperature measurements were collected throughout the 2017/2018 winter beginning 27/Feb/2018 and throughout the 2018/2019 winter beginning 08/Nov/2018. However, an equipment malfunction issue related to the interaction of the infrared sensors with the data logger resulted in one of the sensors frequently powering down when air temperatures dropped below 0 °C. This issue was not able to be fixed until 24/Jan/2019. Thus, simultaneous data for both cells was mostly not available prior to this date.

The surface temperature data collected from the infrared sensors were then processed following the same methodology as described in Chapter 2 for the contact sensors. Monthly means of daily mean, maximum, minimum, and sunset hour temperatures were calculated for February, March, and April. Data collected during the last week of January were omitted from the monthly summaries due to the minimal number of days with data collected at the end of the month.

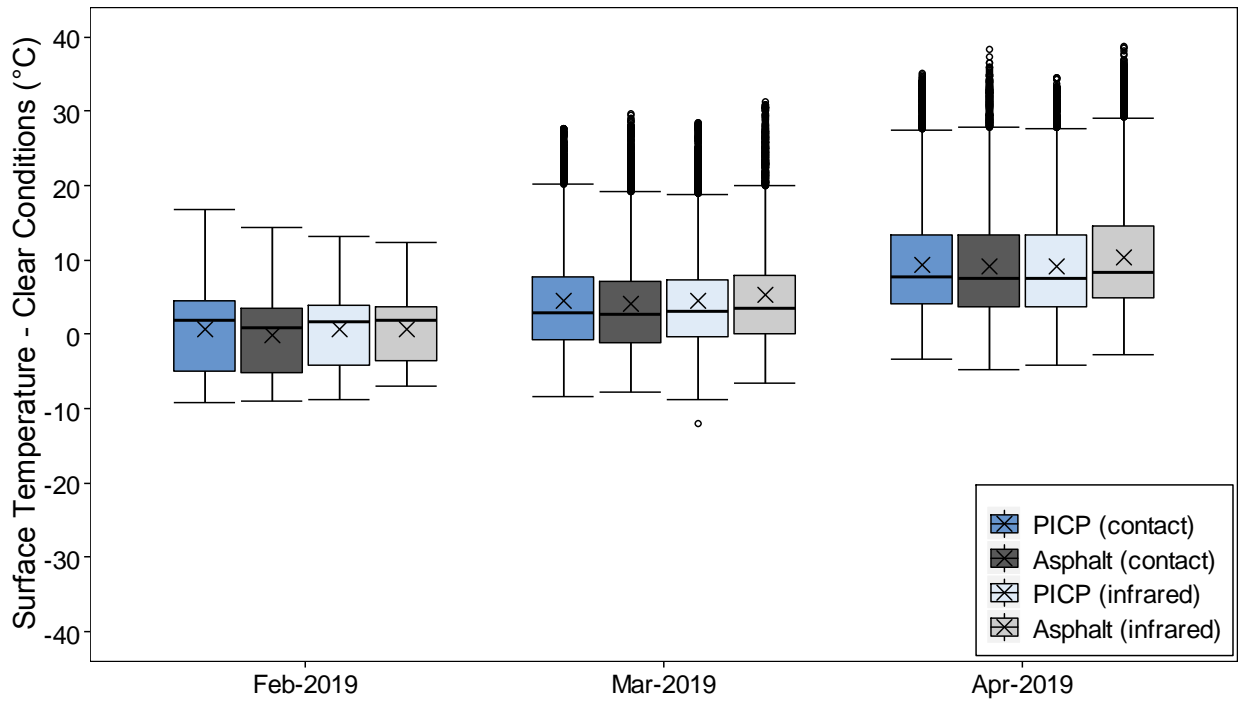
Monthly means were also calculated for clear conditions by omitting time steps where one of the two cells were impacted by surface cover. Statistical hypothesis testing was carried out to compare the differences between temperature measurements from the contact sensors and from the infrared sensors for the respective cells, and differences in surface temperatures between the PICP cell and the asphalt cell. The Wilcoxon signed-rank test ($\alpha = 0.05$, two-tailed) was selected because the daily measurements were paired and the monthly datasets were nonparametric.

3.2.2 Results and Discussion

A box plot comparison between the contact sensor data and infrared sensor data is presented in Figure 16, and monthly averages of the daily mean, maximum, minimum, and sunset hour surface temperatures for the two sensors are presented in Table 14. Differences between contact and infrared sensor measurements were expected during 26 days in February, 15 days in March, and one day in April as a result of measurements being collected above and below surface cover conditions such as ice and snow. An example data collection period illustrating these differences is provided in Figure 17. As shown in the figure, insulation provided by snow after a snowfall event on 27/Feb/2019 maintained nighttime surface temperatures below the snow between -2 and -4 °C, whereas peak low nighttime temperatures on the surface of the snow were between -30 and -32 °C. While air temperatures only dropped to -21 °C during the night, the reason for the lower temperatures on the surface of the snow could not be determined. Similar differences were, however, observed on multiple occasions when the cells were covered in snow. Differences between nighttime lows above and below the snow were substantially less extreme the following night (less than 4 °C differences) after the snow was compacted during the day on 28/Feb/2019, although air temperatures were also slightly higher that night with a peak low of -18 °C. Increased surface temperatures on the asphalt cell measured by the infrared sensors were then observed on 01/Mar/2019 when partial melting began to occur on the cell.



(a)



(b)

Figure 16: Box plot comparison of surface temperatures measured by contact sensors and infrared sensors for (a) all surface cover conditions and (b) clear conditions.

Table 14: Monthly averages of contact and infrared sensor data.

Month	Item ^a	Surface Temperature (°C)							
		Daily Mean		Daily Maximum		Daily Minimum		Daily Sunset Hour	
		All Days	Clear Days	All Days	Clear Days	All Days	Clear Days	All Days	Clear Days
Feb-2019	PICP (C)	-2.2	3.8	4.6	11.7	-5.7	-1.4	-2.2	-0.9
	PICP (IR)	-4.1	4.0	4.9	9.9	-9.6	-0.6	-4.1	-0.6
	Asph (C)	-2.5	2.8	3.6	9.7	-5.7	-1.8	-2.6	-1.8
	Asph (IR)	-3.9	3.1	4.8	9.8	-9.3	-1.1	-4.1	-1.0
Mar-2019	PICP (C)	0.9	4.7	11.5	16.9	-5.4	-2.9	1.4	4.4
	PICP (IR)	0.7	4.8	13.2	16.6	-6.7	-2.8	1.0	4.7
	Asph (C)	1.1	4.3	13.2	16.3	-5.8	-3.0	0.5	3.1
	Asph (IR)	1.5	5.5	13.8	17.8	-5.6	-2.0	1.3	4.8
Apr-2019	PICP (C)	9.4	9.5	21.0	21.0	2.3	2.6	9.7	9.7
	PICP (IR)	9.2	9.3	21.5	21.5	1.7	2.1	9.3	9.3
	Asph (C)	9.3	9.3	22.1	22.1	1.8	2.1	8.6	8.6
	Asph (IR)	10.6	10.6	23.7	23.7	2.9	3.2	10.1	10.1

^aC = contact sensor, IR = infrared sensor

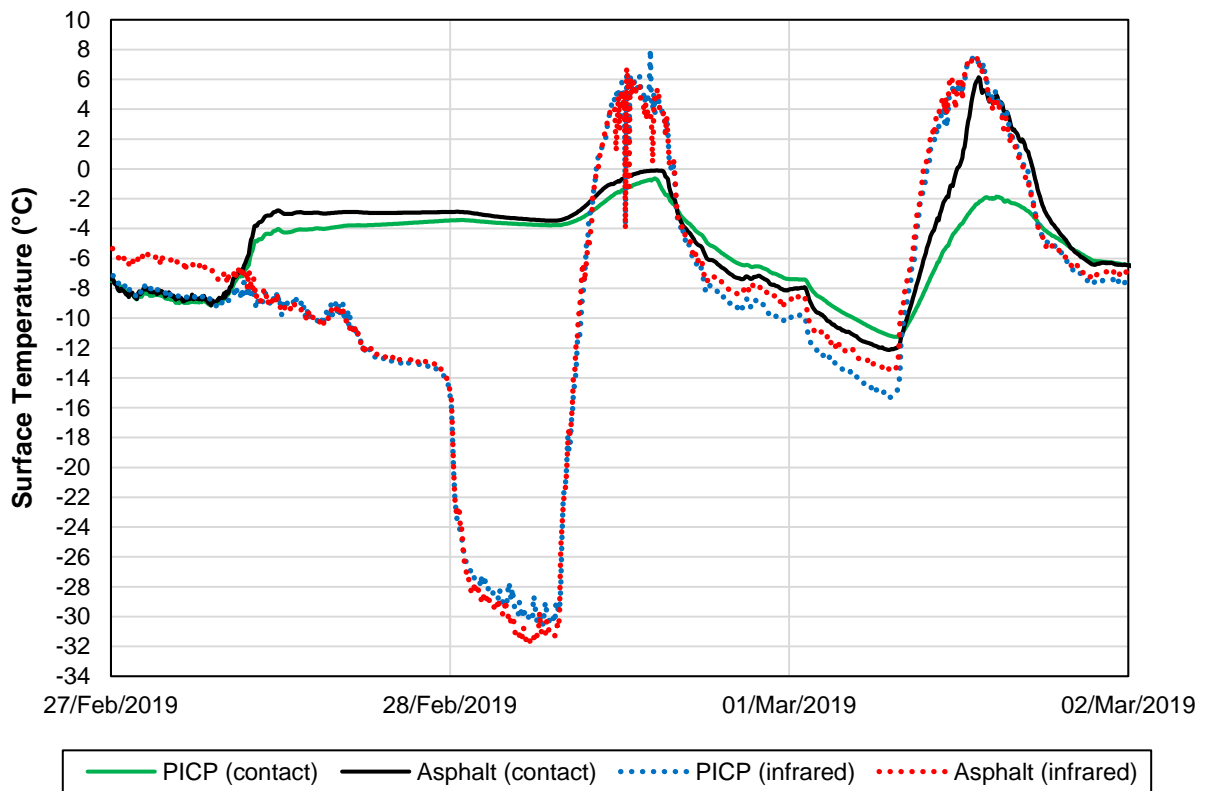


Figure 17: Surface temperature measurements collected from contact sensors and infrared sensors after a snowfall event on 27/Feb/2019, subsequent snow compaction on 28/Feb/2019, and partial melting of the asphalt cell on 01/Mar/2019.

An example of surface temperature data collected by both the contact sensors and infrared sensors during clear conditions on 24/Mar/2019 is presented in Figure 18. During clear conditions, surface temperatures on the asphalt cell were typically higher when measured using the infrared sensors than when using the contact sensors. Asphalt surface temperatures were found to be significantly higher ($p < 0.05$) when measured using the infrared sensors than when measured using the contact sensors for the daily mean, maximum, minimum, and sunset hour values collected between 24/Jan/2019 and 30/Apr/2019 during clear conditions. For the PICP cell, daily mean, maximum, and sunset hour values were similar between the two sensor types ($p > 0.05$), whereas daily minimum temperatures were significantly lower ($p < 0.05$) when measured using the infrared sensors than when measured using the contact sensors.

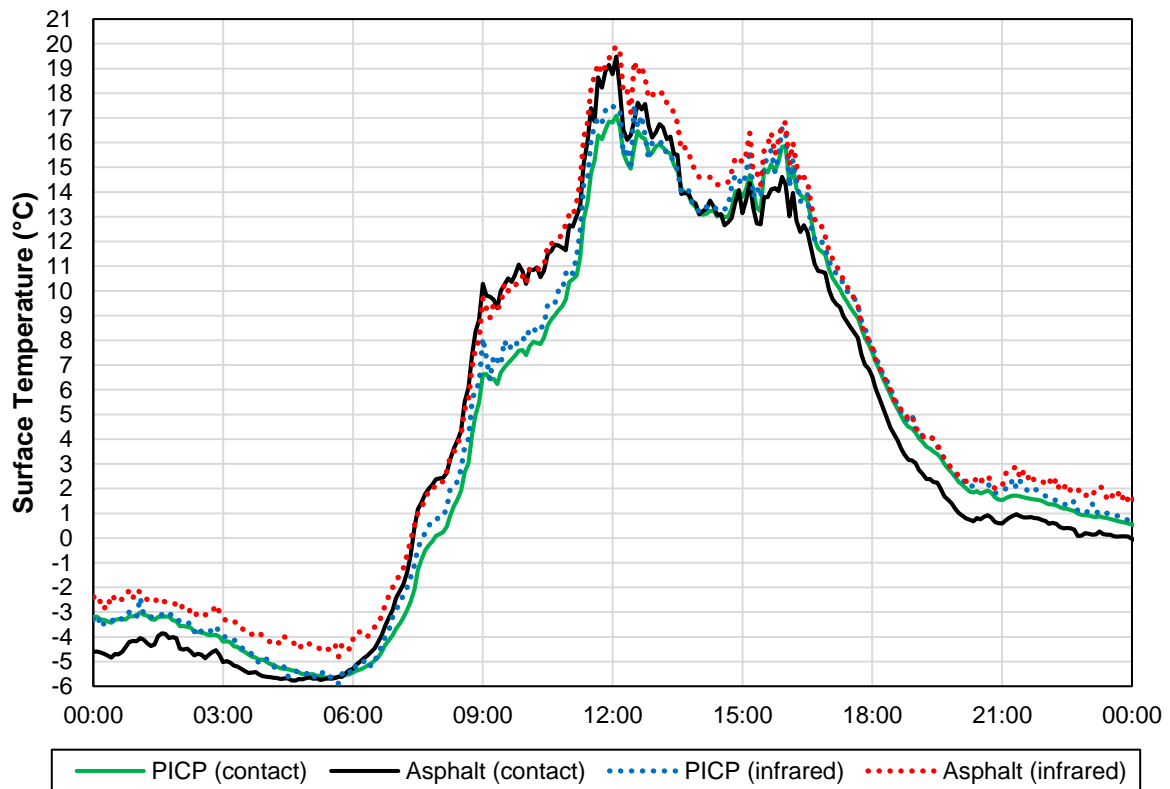


Figure 18: Surface temperature measurements collected from contact sensors and infrared sensors during clear conditions on 24/Mar/2019.

Differences between the two types of sensors could have been from the accuracy of the contact and infrared sensors being ± 0.2 °C and ± 1 °C, respectively. Mean differences in temperatures during clear conditions were 0.4 and 1.2 °C for the PICP and asphalt cells, respectively, and

therefore fell within the combined accuracy range of the two sensor types. Other reasons for these differences include surfaces beyond the cells contributing to the infrared surface temperature measurements, and localized temperature differences between the corner of the cells and the centre of the cells. While the infrared sensors were pointed towards the southern hemisphere and therefore sometimes received direct sunlight and reflections that could have impacted the readings, this would not account for the differences in temperatures that were observed during the night.

As a result of the above accuracy concerns associated with the infrared sensors and their limited data collection period, an evaluation of surface temperature trends between the PICP and asphalt cells was not carried out. However, discrepancies observed between the two sensor types warrant the need for additional surface temperature research on PICP surfaces. For example, the sunset hour temperatures were significantly higher ($p < 0.05$) on the PICP cell than on the asphalt cell when using the contact sensor data, whereas these differences were not significant ($p > 0.05$) when using the infrared sensor data.

3.2.3 Conclusions and Recommendations

An evaluation of the PICP and asphalt surface temperature data collected using Surface Sentinel Model 5439-00 infrared sensors was carried out for the 24/Jan/2019 to 30/Apr/2019 period when simultaneous data was available on PICP-RS-M and Asph-RS-M. Higher surface temperatures were measured on the asphalt cell by the infrared sensors than by the contact sensors, whereas temperature differences between the two sensor types were not significant on the PICP cell with the exception of the daily minimum values. These differences were likely related to the infrared sensors having a lower accuracy and being influenced by direct sunlight, reflections, and surfaces outside of the cell. The potential impacts of sunlight and reflections could have been mitigated by placing the sensors at a higher elevation to increase its angle with the horizon, although this would have resulted in additional contributions from surfaces outside of the cells. Non-contact sensors that are less influenced from surfaces within a 90° FOV are therefore recommended for future research on small pavement cells, although the extent this impact was not able to be quantified for this study. More importantly, non-contact sensors with higher accuracy are recommended for future research on differences between PICP and asphalt surface temperatures, as these differences are often less than 1°C .

3.3 Evaluation of Surface Friction Measuring Devices for PICP under Winter Conditions

Winter conditions present unique challenges for quantifying pedestrian and vehicle safety on pavement surfaces, as most friction measuring devices are not designed to be operated on snowy and icy surfaces. This section evaluates the applicability of the two friction measuring devices used at the research site, SlipAlert and Mark IIIB, to PICP surfaces when subject to snow, ice, slush, and road salt in a controlled outdoor environment. The purpose of this evaluation is to provide information on the winter usability and challenges of these two devices to help guide future friction measurement practices for PICP under winter conditions. The content presented in this section is mostly taken from a conference proceeding that was previously published for and presented at the 12th International Conference on Concrete Block Pavement held from October 16th to 19th, 2018 in Seoul, South Korea (Marvin and Drake 2018). The original conference proceeding has been updated in this section to reflect additional findings from the 2018/2019 winter and to follow the layout of this thesis.

3.3.1 Methodology

A description of the two friction measuring devices, the reasons why they were selected for this research site, and the data collection methodology is provided in Chapter 2. In general, SlipAlert and Mark IIIB were selected because the research required the use of devices that are capable of rapidly collecting repeatable measurements within a small area, and that could provide measures of both DCOF and TCOF to simulate pedestrian slipping and vehicle skidding. Measurement sets were collected after shovelling, after salting, at various time intervals until the pavements were dry or experienced no further changes in surface cover, and before and after sunset if refreezing conditions occurred. For each measurement set, five DCOF (SlipAlert) and five TCOF (Mark IIIB) measurements were collected on each cell at spatially representative locations to estimate mean values, and additional measurements were collected as needed to estimate maximum and minimum values.

3.3.2 Results and Discussion

The presence of salt on the pavement surfaces was found to more unevenly affect the Mark IIIB measurements than the SlipAlert measurements. Mark IIIB requires an iterative procedure to estimate the launch angle of the test foot that causes a slip to occur, and this procedure caused

the test foot to repeatedly crush the salt particles every time it was launched. The test foot then slid along the resulting thin layer of crushed salt particles whenever a slip occurred. The thin layer of crushed salt was observed to impact TCOF measured on the PICP surfaces more than on the asphalt surface, as small depressions between the asphalt aggregates were observed where the crushed salt particles would fall into and avoid contact with the test foot, and the wetter conditions of the asphalt were observed to dissolve more of the salt particles. The paver joints had no impact on TCOF measurements, as all Mark IIIB measurements for the PICP cells were collected on the paver surfaces rather than over the joint spaces.

Snow on the PICP surfaces generally melted evenly through the paver joints, whereas melting on the asphalt surface would first occur within the steepest area of its slope, which was then followed by melting at the bottom of the slope next to the catch basin (see Figure A2). Because of this, isolated patches of ice or snow would frequently be present on the asphalt surface and were sometimes missed by the locations selected for friction measurements. These locations were more commonly missed while using Mark IIIB since the device collects spot measurements. Additional TCOF measurements were therefore collected on the asphalt cell using Mark IIIB to quantify the hazard of isolated patches of ice and snow when present, as these areas represent locations where pedestrians could slip on a surface that is otherwise clear of winter hazards. However, some isolated patches of ice and snow on the asphalt cell could not be accurately measured using Mark IIIB due to unevenness. A tool is provided with Mark IIIB to test whether the surface is adequately flat and even to collect an accurate measurement, and TCOF measurements were only collected when the tool indicated these conditions were present. Additional TCOF measurements were also collected on the PICP cells during the ice cover salting experiments, as melting during these conditions would typically occur radially from any areas that were fully melted, resulting in both fully cleared areas and ice covered areas being present on the cells at the same time (see Figure A10).

Both friction devices were visually observed to disturb the surface conditions of the pavement when snow and slush were present. This was particularly problematic with Mark IIIB, as the test procedure requires launching the test foot at estimated angles until a slip occurs. Compaction and heat transfer were therefore provided to the surface each time the test foot was launched. When the test foot slipped, it sometimes pushed ice, snow, or slush away from the point of impact. Because of these disturbances, a good initial estimation of the angle that causes the test foot to

slip was needed to minimize the number of launches and acquire a more representative friction measurement. Once a slip occurred, the test location was considered unusable for future measurements. With SlipAlert, the friction measurement is collected by a single launch of the car, causing less disturbance to the surface conditions. However, the area disturbed by SlipAlert is much larger than the area disturbed by Mark IIIB due to the long sliding path needed for the SlipAlert car. The compaction, displacement, and heating of surface conditions by SlipAlert along its path was therefore more widespread on the test cells. Thus, Mark IIIB has the potential to highly disturb surface conditions at single points on the surface, whereas SlipAlert has the potential to disturb surface conditions to a lesser degree but over a larger area.

Friction measurements collected on icy, snowy, slushy, and wet surface conditions ensured that the rubber test foot or slider remained wet for subsequent measurements, providing conditions that were somewhat representative of footwear and tires during these conditions. However, the rubber test foot/slider had to be lightly wiped with a cloth to remove collected ice, snow, slush, and salt to prevent contamination of subsequent measurements. If a measurement was collected on a dry surface after being used on a wet surface, the test foot/slider had to be fully dried between the two measurements. Thus, the test foot/slider sometimes needs to be cleared of ice, snow, slush, salt and water between measurements to ensure that the measurements are accurate and that the devices provide minimal disturbance to surface conditions.

3.3.3 Conclusions and Recommendations

Friction measurements collected at the test site using SlipAlert and Mark IIIB friction measurements demonstrated how these devices can be applied to winter surface conditions on PICP and asphalt surfaces. Mark IIIB allows for the less common measurement of TCOF to be estimated, but its measurements take longer to execute, can disturb winter surface conditions, and are highly impacted by the presence of salt particles. The device can, however, be successfully applied to winter surface conditions if the initial estimate of TCOF is slightly higher than the final measured value, and if salt particles can be avoided during measurements. Mark IIIB also has the advantage of being able to collect spot measurements on isolated patches of ice and snow, as these locations pose safety concerns for pedestrians and vehicles on pavements that may otherwise have less hazardous surface conditions.

Unlike Mark IIIB, SlipAlert does not require iterative measurements and can therefore be used rapidly with less disturbance to surface conditions, and SlipAlert measurements are less impacted by the presence of salt particles. SlipAlert can also be used to quantify skidding distances on a sloped surface in addition to measuring dynamic friction, as sloped surfaces are known to increase sliding hazards. Overall, the two devices can successfully provide measurements of DCOF and TCOF on winter surface conditions for PICP when used in the context of the limitations described above.

Chapter 4

4 Conclusions

This study evaluated the winter safety and environmental benefits of PICP in comparison to conventional asphalt pavement using an outdoor test site located in Vaughan, Ontario. Findings from the two winters of data collection and observations demonstrated that multiple opportunities exist for reducing winter de-icing quantities on PICP surfaces without reducing slip and skid resistances. These findings are summarized as follows:

1. Unlike the impervious asphalt surface, the PICP surfaces did not provide conditions where runoff from melted ice and snow could refreeze. This suggests that de-icers are not needed on PICP surfaces for the purpose of preventing melted ice and snow from refreezing. De-icers are, however, still needed to melt ice that has formed from freezing rain or partially melted compacted snow.
2. PICP has less surface friction than asphalt immediately after surfaces are shovelled or plowed because of differences in texture that impact the remaining thin layer of snow. However, the two pavement types exhibit similar surface friction soon after the remaining thin layer of snow begins to melt, and melted areas become dry on PICP surfaces sooner than on asphalt surfaces. De-icers can therefore be used as needed to melt the remaining snow after shovelling or plowing, although de-icing is only recommended for when surface temperatures are below 0 °C, and application rates of 5 lb/1000 ft² or lower should be used for such conditions.
3. The drier conditions of PICP surfaces prevent road salts from dissolving after they have been used to melt ice or snow, and leftover salt particles are not needed on PICP surfaces to prevent previously melted ice and snow from refreezing. As a result, smaller and more evenly distributed salt particles may allow for application rates to be reduced without also reducing surface friction. The potential for smaller particle sizes to reduce road salt application rates on PICP surfaces should therefore be evaluated in future research.
4. The rapid drainage characteristics of PICP reduces the bond between ice and pavement when partially melted compacted snow refreezes. This potentially allows for easier removal with shovelling and plowing equipment, reducing the areas where de-icers are needed.

Future research is therefore needed on how conventional ice and snow removal equipment removal equipment can break up ice on PICP surfaces that forms under realistic conditions.

5. Pre-wetting road salt with beet juice can enhance the melting of ice on PICP surfaces. The use of beet juice may therefore allow for application rates to be reduced for such conditions. However, no enhanced melting benefits were found when applying road salt pre-wetted with beet juice to shovelled surfaces.
6. Compared to conventional asphalt, surface temperatures of PICP during the winter are typically lower from sunrise until mid-afternoon and higher from late-afternoon until sunrise of the following day. The lower surface temperatures early in the day therefore cause melting of undisturbed snow to occur sooner and faster on asphalt surfaces, although the higher temperatures at sunset and during the night reduces the risk of ice formation. While these differences are likely attributed to thermal properties of the pavement materials, the impact of subsurface temperatures on surface temperatures should be evaluated for PICP systems, as the insulated subsurface layers may provide some heat transfer to the paving stones during the night.

Key limitations of this study were that the pavements did not receive any pedestrian or vehicular traffic during the melt experiments, de-icers were only applied to the pavements during the day, and the pavements did not receive any anti-icing treatments. Future research should therefore be carried out on PICP surfaces that receive regular but controlled pedestrian and vehicular traffic during melting periods, as continuous compaction and introduction of snow, slush, water, and salt from outside sources could impact ice formation. Research should also be carried out on de-icing practices for PICP surfaces during the night when the risk of refreeze is substantially higher. Finally, anti-icing practices should be evaluated for PICP surfaces, as liquid anti-icing applications may benefit PICP surfaces more than impervious surfaces due to their more widespread coverage.

Conductivity and chloride monitoring of the PICP and asphalt outflows further confirmed the findings from previous research on PICP and other PP surfaces that chloride concentrations from winter salting practices are attenuated and delayed. The PICP cells were not, however, expected to reduce the total mass of chlorides discharged to the environment, although chloride masses were not monitored. High runoff volume reductions throughout the winter period in the PICP

cells also delayed the release of peak winter chloride concentrations until mid-March, indicating that a large percentage of the chlorides may infiltrate during the smaller winter rainfall events when using partial infiltration systems. Ultimately, road salt reduction strategies remain the most viable solutions to reducing chloride pollutants in cold climate locations.

The findings from this study further demonstrate the applicability of PICP to cold climate regions such as Southern Ontario, as no surface flooding occurred on the PICP cells during the two winters, and multiple opportunities were identified for using lower quantities of de-icing materials. While concerns remain that full and partial infiltration PICP systems may concentrate chloride pollutants from winter salting activities into groundwater systems, the salt reduction opportunities identified by this study may allow for these groundwater impacts to be reduced. For groundwater systems that require higher protection against chloride contamination, zero infiltration PICP systems that include impermeable barriers below the underdrain and subbase layer are still applicable, or alternative winter safety strategies such as applying PICP joint material aggregates on the surface to improve traction may be a viable option.

This research provides information and recommendations that can help guide the development of best practices for PICP maintenance in cold climate regions, which may help to eliminate implementation barriers that have been inhibiting the use of PICP in these areas. This is important because PP systems such as PICP are commonly used for managing stormwater in highly urbanized areas where less space is available for other types of LID and stormwater management technologies that do not double as paved surfaces. Moreover, the use of PICP and other PP systems in cold climate regions helps reduce flooding and improve surface water quality downstream of urban areas, and these benefits are observed throughout all seasons.

References

- Al-Rubaei, A. M., Stenglein, A. L., Viklander, M., and Blecken, G.-T. (2013). “Long-term hydraulic performance of porous asphalt pavements in northern Sweden.” *J. Irrig. Drain. Eng.* 139(6), 499–505.
- American National Standards Institute (ANSI). (2017). *American national standard test method for measuring dynamic coefficient of friction of hard surface flooring materials (ANSI A326.3)*.
- American Society of Civil Engineers (ASCE). (2018). *Permeable interlocking concrete pavement, ASCE/T&DI/ICPI 68-18*. Reston, VA.
- ASTM International. (2014). *Standard practice for validation, calibration, and certification of walkway tribometers using reference surfaces (ASTM F2508)*.
- Bäckström, M. (2000). “Ground temperature in porous pavement during freezing and thawing.” *J. Transp. Eng.* 126(5), 375–381.
- Borst, M., and Brown, R. A. (2014). “Chloride released from three permeable pavement surfaces after winter salt application.” *J. Am. Water Resour. Assoc.* 50(1), 29–41.
- British Standards Institution. (2003). *Screeds, bases and in situ floorings (BS 8204)*.
- Dietz, M. E., Angel, D. R., Robbins, G. A., and McNaboe, L. A. (2017). “Permeable asphalt: A new tool to reduce road salt contamination of groundwater in urban areas.” *Groundwater*, 55(2), 237–243.
- Drake, J., Bradford, A., and Van Seters, T. (2014). “Winter effluent quality from partial-infiltration permeable pavement systems.” *J. Environ. Eng.* 140(11), 04014036.
- Drake, J., Bradford, A., and Van Seters, T. (2013). “Hydrologic performance of three partial-infiltration permeable pavements in a cold climate over low permeability soil.” *J. Hydrol. Eng.* 19(9), 04014016.
- Eisenberg, B., Lindow, K. C., and Smith, D. R. (2013). *Permeable pavements*. Reston, VA: American Society of Civil Engineers.
- Henderson, V., and Tighe, S. (2012). “Evaluation of pervious concrete pavement performance in cold weather climates.” *Int. J. Pavement Eng.* 13(3), 197–208.
- Horst, M., Welker, A. L., and Traver, R. G. (2010). “Multiyear performance of a pervious concrete infiltration basin BMP.” *J. Irrig. Drain. Eng.* 137(6), 352–358.
- Huang, J., Valeo, C., He, J., and Chu, A. (2012). “Winter performance of inter-locking pavers—stormwater quantity and quality.” *Water*, 4(4), 995–1008.

- Huang, J., Valeo, C., He, J., and Chu, A. (2016). "Three types of permeable pavements in cold climates: Hydraulic and environmental performance." *J. Environ. Eng.* 142(6), 04016025.
- Kevern, J. T., King, G. W., and Bruetsch, A. P. (2012). "Pervious concrete surface characterization to reduce slip-related falls." *J. Perform. Constr. Facil.* 26(4), 526–531.
- Kevern, J. T., Schaefer, V. R., and Wang, K. (2009). "Temperature behavior of pervious concrete systems." *Transp. Res. Rec.* 2098(1), 94–101.
- Kottek, M., Grieser, J., Beck, C., Rudolf, B., & Rubel, F. (2006). "World map of the Köppen-Geiger climate classification updated." *Meteorol. Z.* 15(3), 259–263.
- Li, H. (2015). *Pavement materials for heat island mitigation: Design and management strategies*. Butterworth-Heinemann.
- Marvin, J., and Drake, J. (2018). "Evaluation of methods used for measuring the slip and skid resistance of permeable interlocking concrete pavement under winter conditions." *Proc., International Conference on Concrete Block Pavement 2018*, Korean Block Association, Seoul, South Korea.
- Ministry of Transportation of Ontario. (2010). *Foundation frost penetration depths for southern Ontario, Ontario Provincial Standard Drawing (OPSD) 3090.101, Ontario provincial standards for roads & public works, Vol. 3: Drawings for roads, barriers, drainage, sanitary sewers, watermains, and structures*.
- Rohne, R. J., and Lebens, M. A. (2009). "Subgrade temperature and freezing cycles in pervious pavements." *Proc., Conference on Cold Regions Engineering 2009: Cold Regions Impact on Research, Design, and Construction*, American Society of Civil Engineers, Duluth, MN, 429–437.
- Roseen, R. M., Ballesterro, T. P., Houle, J. J., Briggs, J. F., and Houle, K. M. (2012). "Water quality and hydrologic performance of a porous asphalt pavement as a storm-water treatment strategy in a cold climate." *J. Environ. Eng.* 138(1), 81–89.
- Roseen, R. M., Ballesterro, T. P., Houle, K. M., Heath, D., and Houle, J. J. (2014). "Assessment of winter maintenance of porous asphalt and its function for chloride source control." *J. Transp. Eng.* 140(2), 04013007.
- Smith, D. R. (2017). *Permeable interlocking concrete pavements: Design, specifications, construction, maintenance, 5th Ed.* Chantilly, VA: Interlocking Concrete Pavement Institute.
- Tyner, J. S., Wright, W. C., and Dobbs, P. A. (2009). "Increasing exfiltration from pervious concrete and temperature monitoring." *J. Environ. Manage.* 90(8), 2636–2641.

- USEPA. (2019). *National recommended water quality criteria: aquatic life criteria table*. Retrieved June 17, 2019, from: <https://www.epa.gov/wqc/national-recommended-water-quality-criteria-aquatic-life-criteria-table>. United States Environmental Protection Agency.
- Zhu, H. (2017). *Winter road salting in parking lots: Permeable pavements vs. conventional asphalt pavements (thesis)*. University of Toronto.

Appendices

Appendix A: Site Photos



(a)



(b)



(c)

Figure A1: Impacts of shadows on snowmelt processes on (a) overall test site in December 2018 when the sun was at its lowest declination, (b) PICP cell in the morning of 01/Feb/2018, and (c) asphalt cell in the morning of 01/Feb/2018.

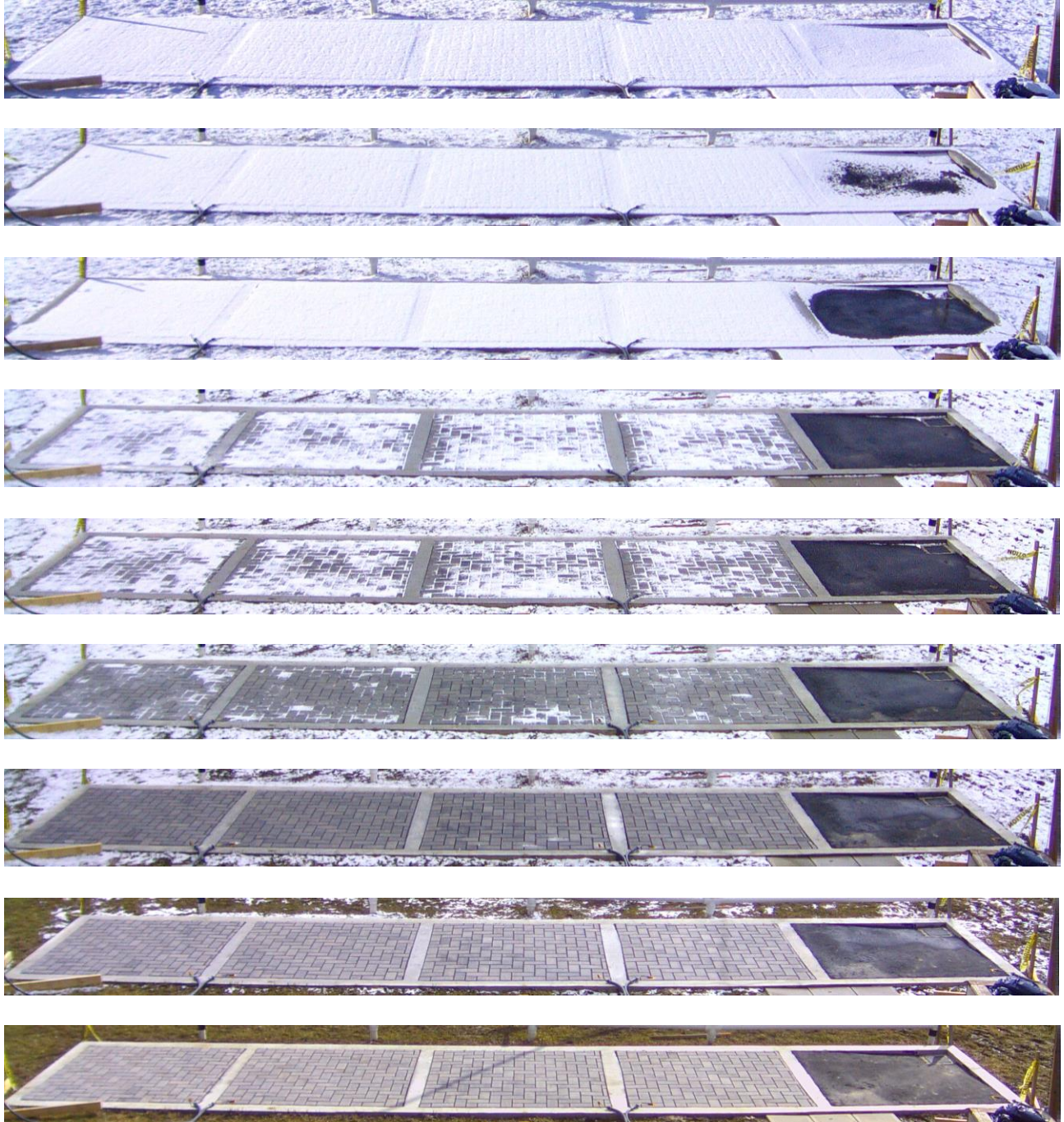


Figure A2: Snowmelt over time on 13/Mar/2018 under undisturbed site conditions. Melting occurs on the asphalt cell prior to the PICP cells. Melting on the asphalt cell begins along its slope, whereas melting on the PICP cells is evenly distributed.



Figure A3: Snow cover conditions on 17/Nov/2018 where mounds formed on pervious surfaces (PICP cells and catch basin) after snow structures collapsed during slow melting processes on the surrounding impervious surfaces (asphalt cell and concrete barriers).



(a)



(b)



(c)

Figure A4: Flooding of asphalt cell on 24/Feb/2019 caused by frozen catch basin: (a) flooded asphalt cell and partially wet PICP cells on 24/Feb/2019 after rainfall event, (b) ice in catch basin during clean-out, and (c) ice in catch basin outlet pipe during clean-out.



(a)



(b)

Figure A5: Comparison of pavement textures between (a) PICP and (b) asphalt. The more rugged asphalt texture allows for snow and small salt particles to fall into depressions whereas the more monolithic PICP texture only allows for snow and salt particles to fall into the joint spaces.



(a)



(b)



(c)

Figure A6: Impacts of leftover salt particles from 08/Feb/2018 de-icing treatment after snow had melted and meltwater had drained and evaporated: (a) larger salt particles remained on PICP surfaces, (b) most salt particles dissolved and precipitated on the asphalt surface, (c) snow accumulation rates the next day were impacted by the leftover salt particles.



(a)



(b)

Figure A7: Impacts of freezing drizzle on surface conditions 30 minutes after salting cells to a thin layer of ice pellets on 07/Feb/2019: (a) thin freezing drizzle particles accumulated on slightly damp PICP surface while ice pellets continued to melt, (b) thin freezing drizzle particles rapidly melted into wet asphalt surface while ice pellets continued to melt.

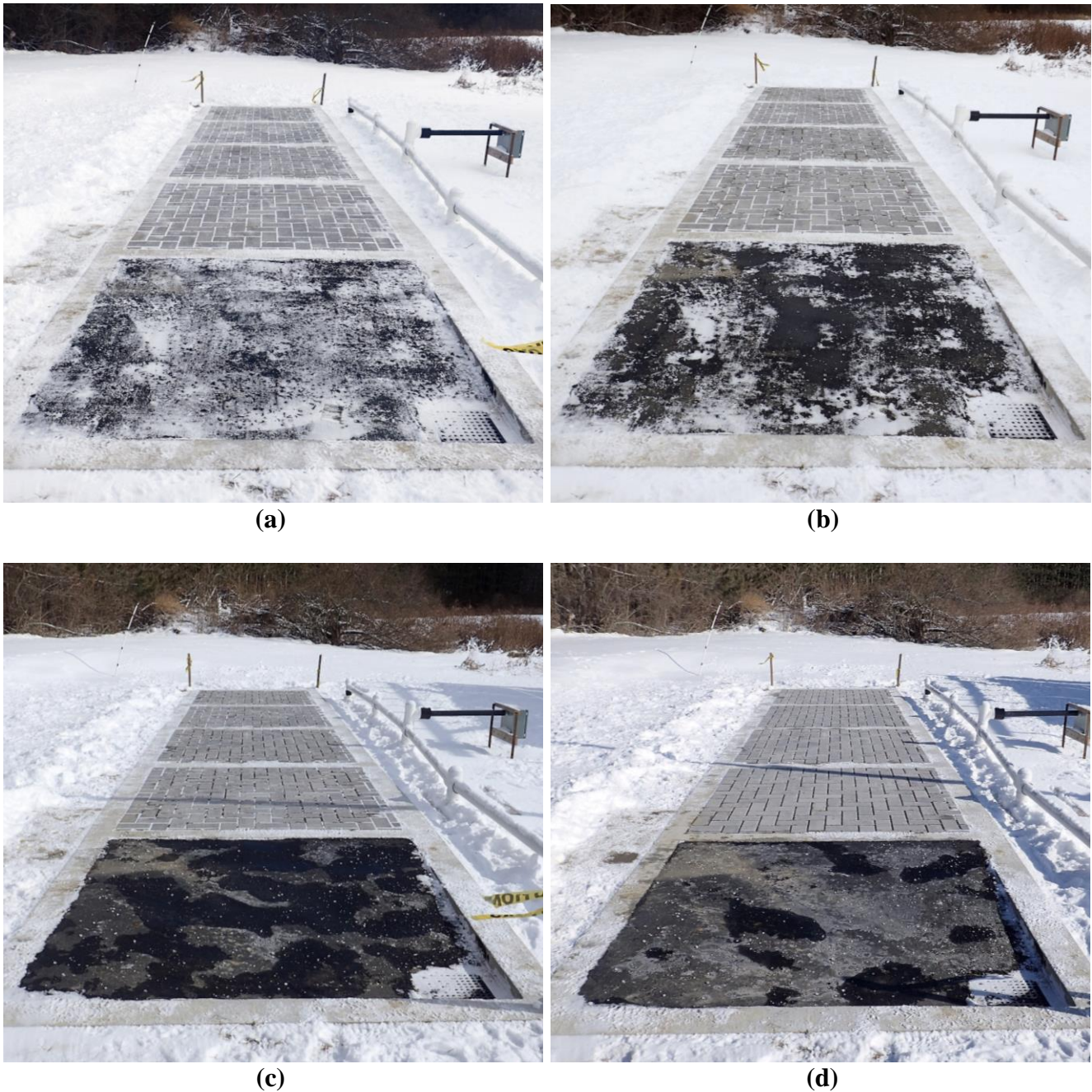


Figure A8: Snow cover during 05/Feb/2018 salting event: (a) 10 minute after salting when a thin layer of snow was present on all surfaces, (b) 50 minutes after salting when the PICP surfaces were mostly dry but with snow in the joint spaces while the asphalt surface was partially covered, (c) 100 minutes after salting when less snow was present in the PICP joint spaces while the asphalt surface was partially wet with snow at the catch basin, and (d) 150 minutes after salting when PICP surfaces and joint spaces were completely clear of snow while asphalt surface remained partially wet with snow near the catch basin.



(a)



(b)



(c)

Figure A9: Impacts of blowing snow on 31/Jan/2019 after salt particles remained on pavement surfaces: (a) comparison of blown snow quantities based on spatial coverage of salt particles and pavement topography, (b) blown snow on PICP, (c) ice patches on PICP where blown snow was shovelled.



(a)



(b)



(c)

Figure A10: Surface conditions after ice cover melting on 16/Feb/2019: (a) prior to sunset when PICP surfaces were slightly damp at locations where ice had just melted while the meltwater path along the asphalt surface remained wet, (b) after sunset when damp areas on the PICP surfaces were reduced while meltwater had refrozen on the asphalt surface, (c) the next morning when all previously damp area on PICP surfaces were dry while refrozen meltwater remained on the asphalt surface at locations where the ice was thickest.



Figure A11: Example of frozen meltwater on Toronto sidewalk on the morning of 17/Feb/2019.

The ice was formed by snowmelt draining from residential properties during the day on 16/Feb/2019 then refreezing during the night, illustrating the processes that were concurrently occurring on the asphalt cell during this period.

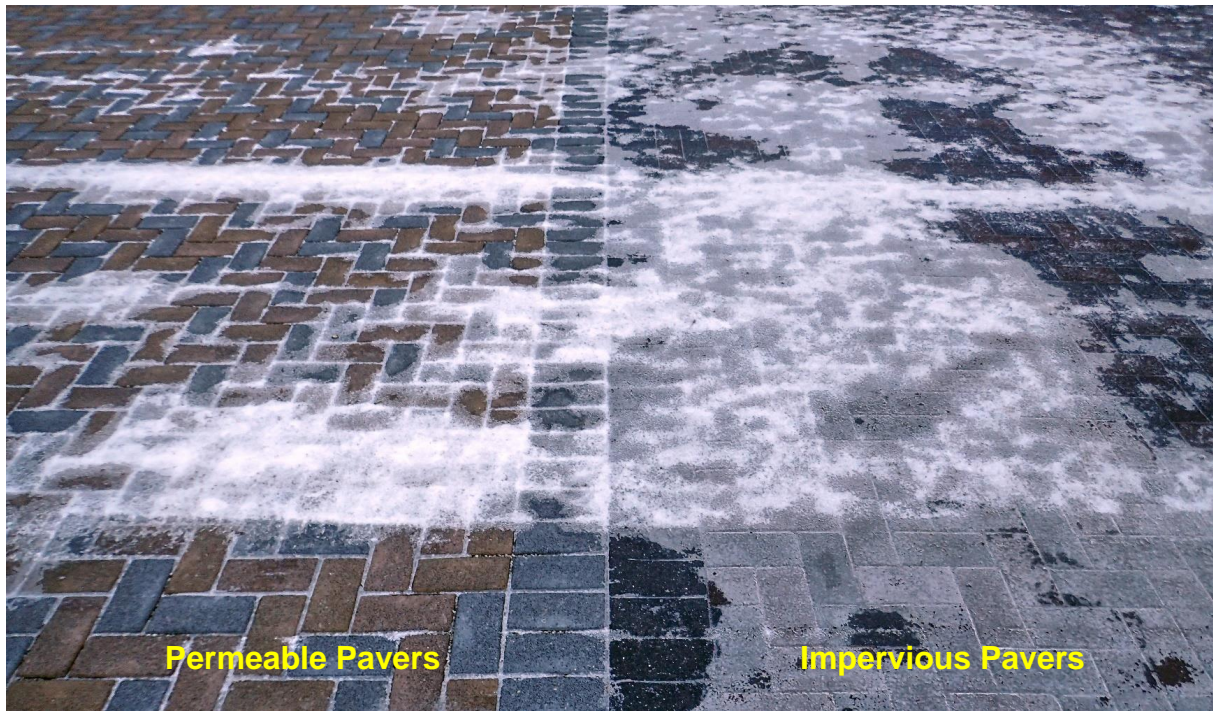


(a)



(b)

Figure A12: Surface conditions on asphalt cell during sleet and freezing rain event on 15/Apr/2018: (a) thick ice accumulation next to catch basin, (b) meltwater paths from individual salt particles buried by ice pellets and freezing rain.



(a)



(b)



(c)

Figure A13: Ice cover at the interlocking rubber paver parking lot at the Kortright Centre for Conservation on 24/Jan/2019: (a) differences in ice cover between permeable pavers and impervious pavers at pavement divide, (b) partial ice cover on permeable paver zone, (c) full ice cover on impervious paver zone. Parking lot traffic and winter maintenance are uncontrolled at this location.



(a)



(b)

Figure A14: Surface cover conditions on 07/Mar/2019 at sunset where (a) PICP surfaces remained clear of ice below compacted snow cover while (b) ice formed on asphalt surface from previous melting of compacted snow during the day.



(a)



(b)

Figure A15: Ice cover characteristics on 16/Feb/2019: (a) partially detached ice cover on PICP, (b) ice transition into wet pavement on asphalt



(a)



(b)

Figure A16: Refreeze of partially melted compacted snow at sunset on 09/Mar/2019 following rapid melting during the afternoon: (a) ice formation on PICP surface where snow had not fully melted while damp but unfrozen areas were present where snow had fully melted, (b) ice extents on PICP surface showing partially detached ice cover and unfrozen damp spots.



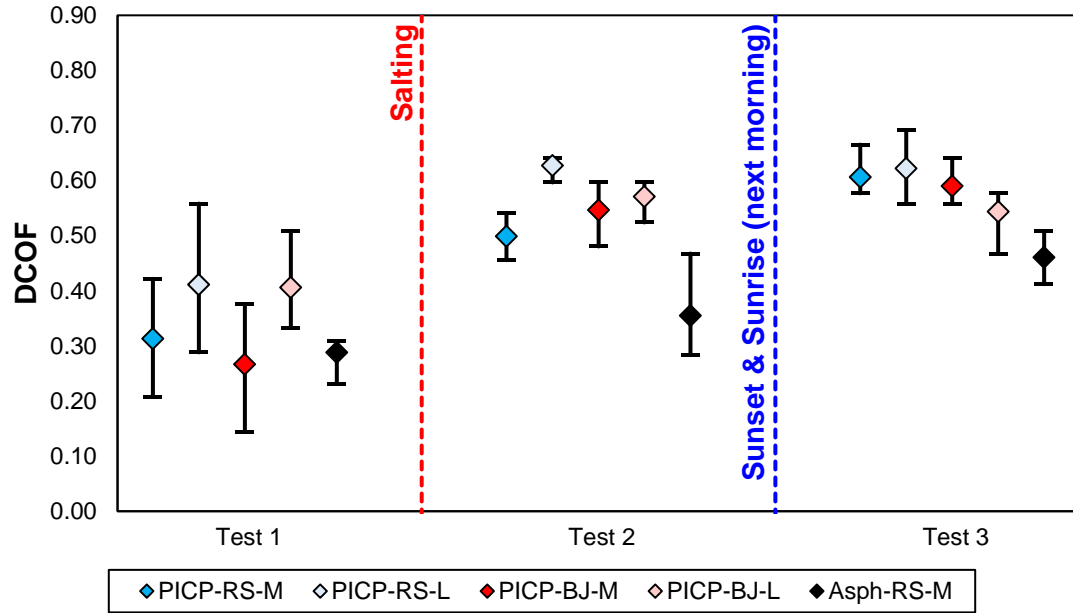
(a)



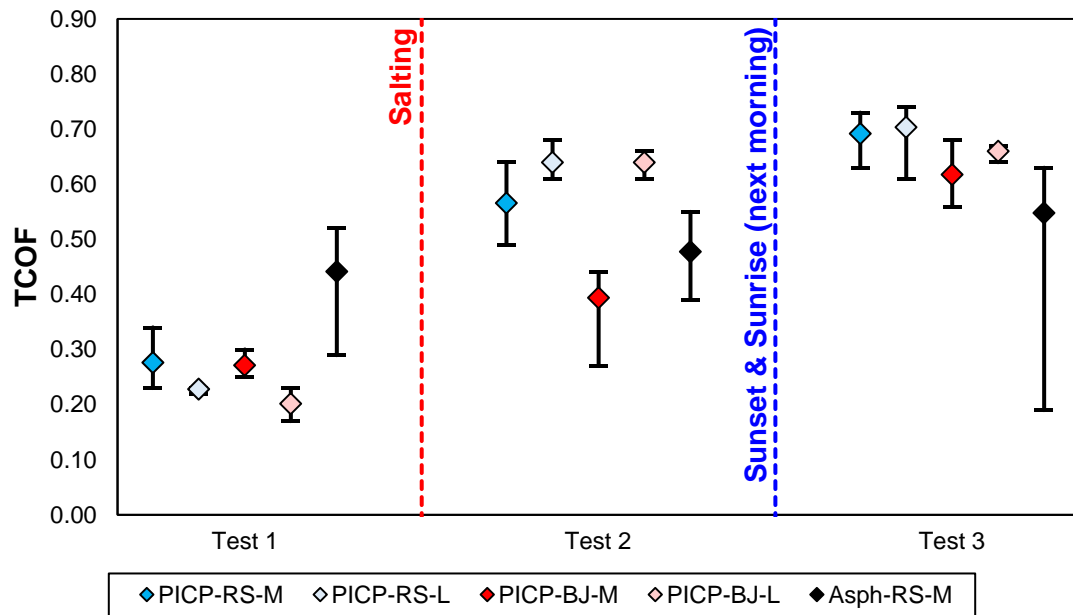
(b)

Figure A17: Ice cover at the interlocking rubber paver parking lot at the Kortright Centre for Conservation observations on 21/Feb/2019: (a) partially detached ice cover on permeable paver zone and (b) ice transition into wet pavement on impervious paver zone. Parking lot traffic and winter maintenance are uncontrolled at this location.

Appendix B: Surface Friction Data

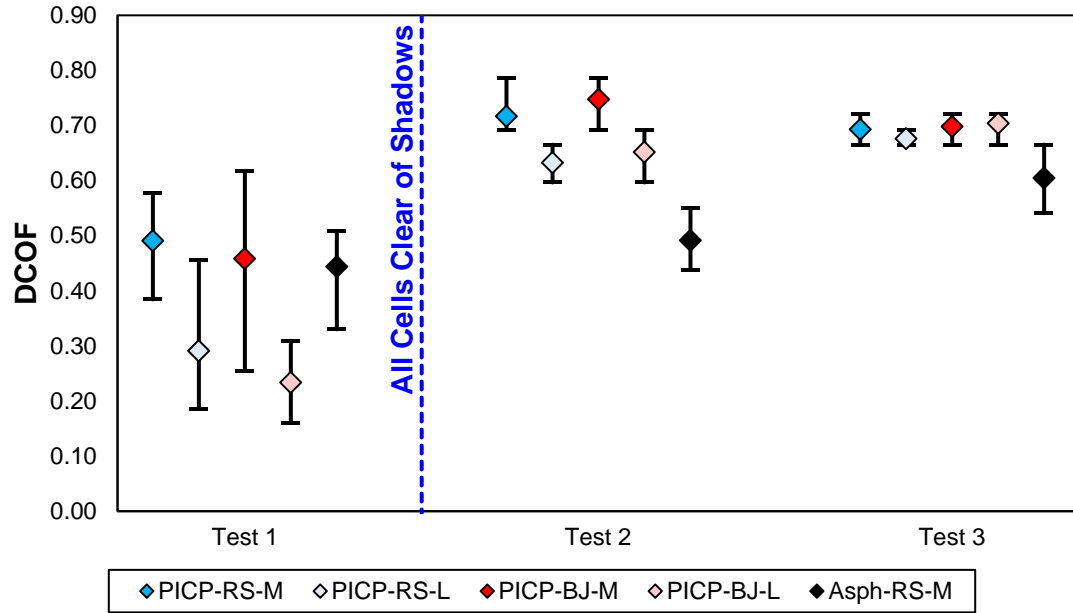


(a)

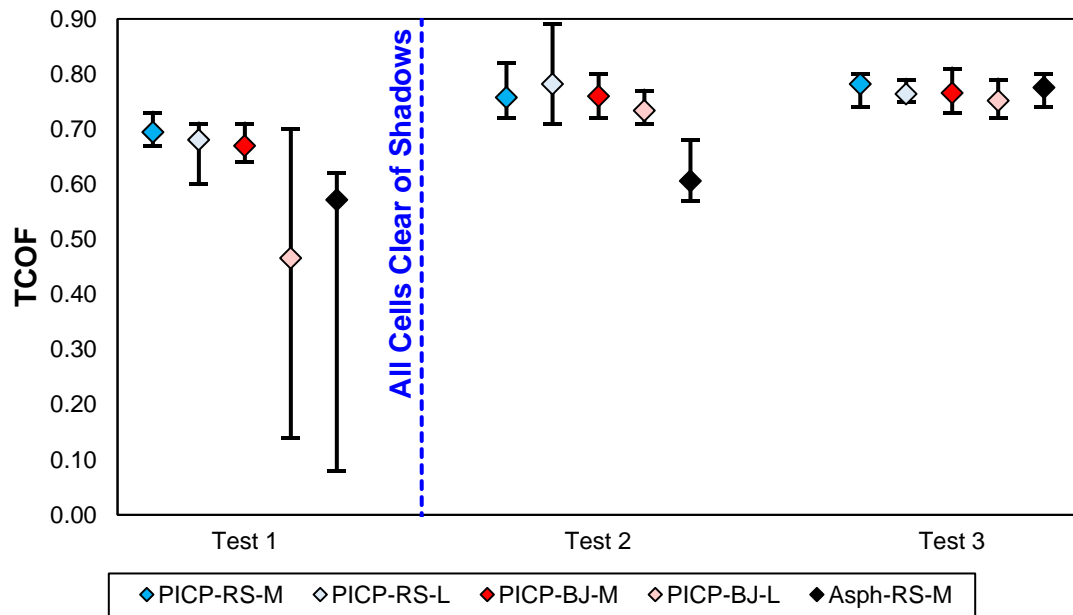


(b)

Figure B1: (a) DCOF and (b) TCOF measurements collected on 17/Jan/2018 and 18/Jan/2018 after cells were shovelled to a thin layer of snow. For this friction data set only, TCOF measurements were collected prior to DCOF measurements, and measurements were not collected simultaneously between cells. Measurements were instead collected in the following order: PICP-BJ-M, PICP-RS-M, PICP-RS-L, PICP-BJ-L, Asph-RS-M.

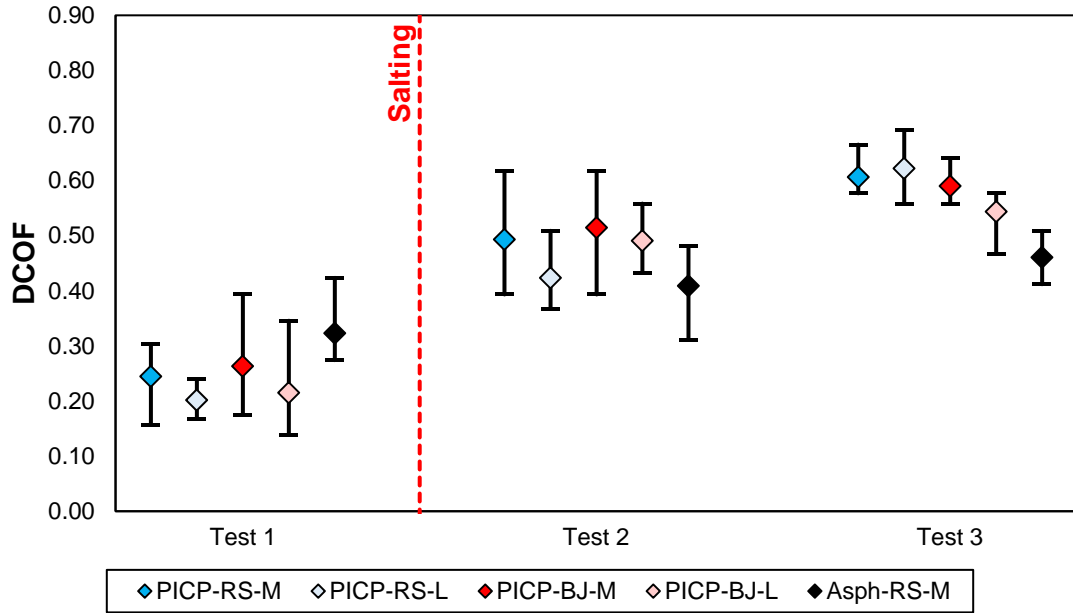


(a)

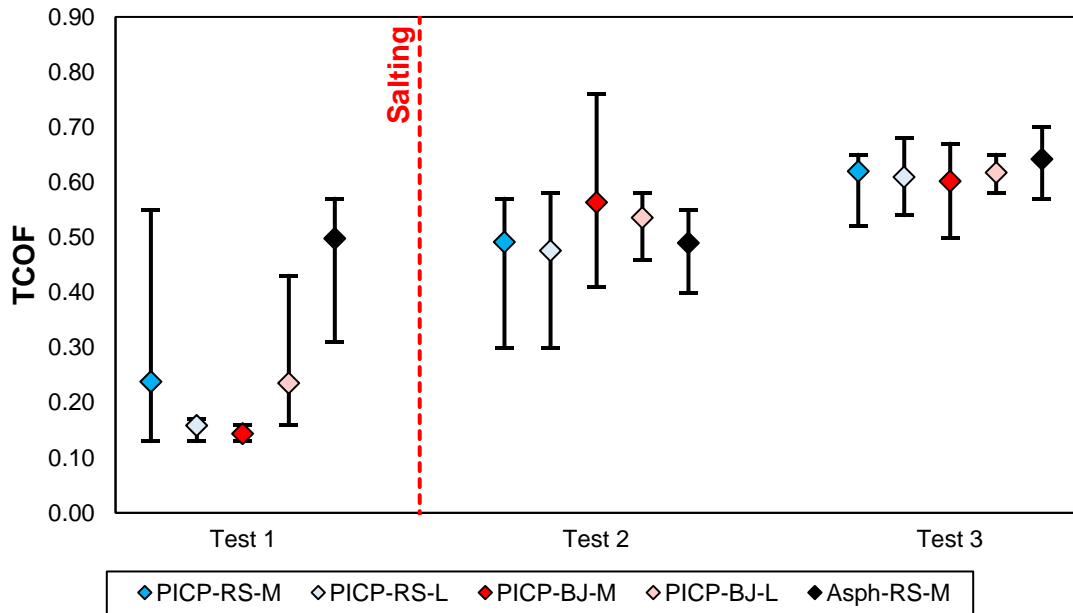


(b)

Figure B2: (a) DCOF and (b) TCOF measurements collected on 01/Feb/2018 after cells were shovelled to a thin layer of snow. No salting was carried out due to positive air temperatures sustained throughout the day. Shadows were temporarily present on the south side of cells PICP-BJ-L and Asph-RS-M until Test 2.

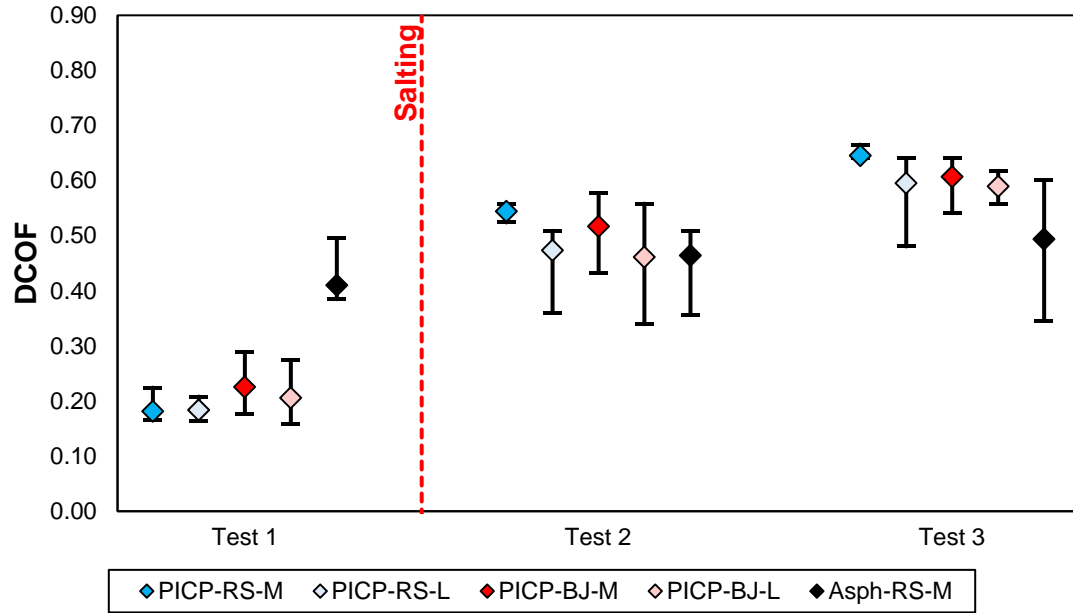


(a)

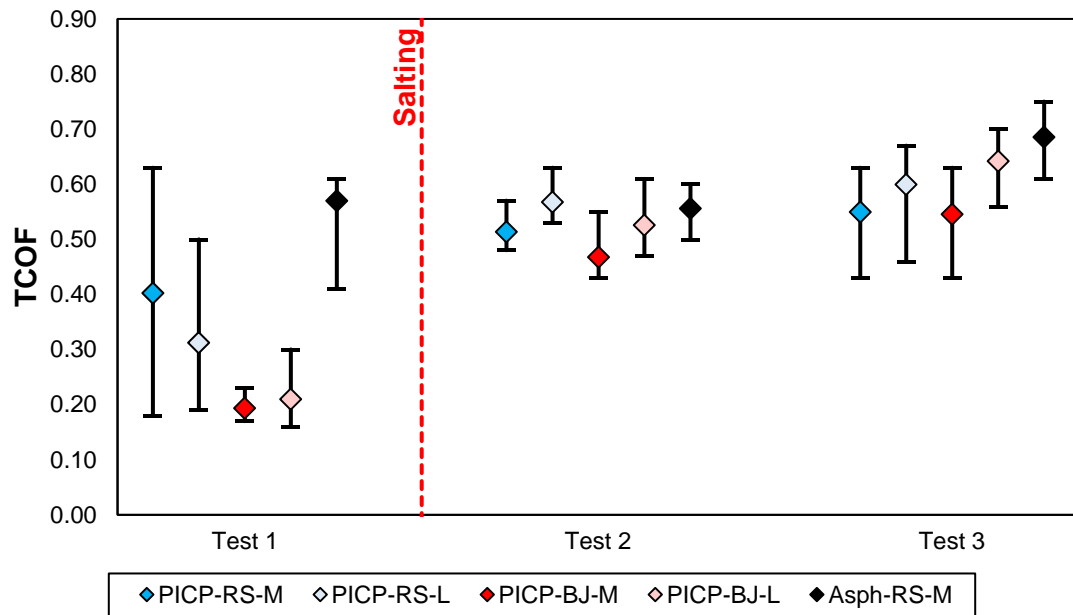


(b)

Figure B3: (a) DCOF and (b) TCOF measurements collected on 05/Feb/2018 after cells were shovelled to a thin layer of snow.



(a)



(b)

Figure B4: (a) DCOF and (b) TCOF measurements collected on 08/Feb/2018 after cells were shovelled to a thin layer of snow. Brine remains from salting on 05/Feb/2018 were still present after shovelling.

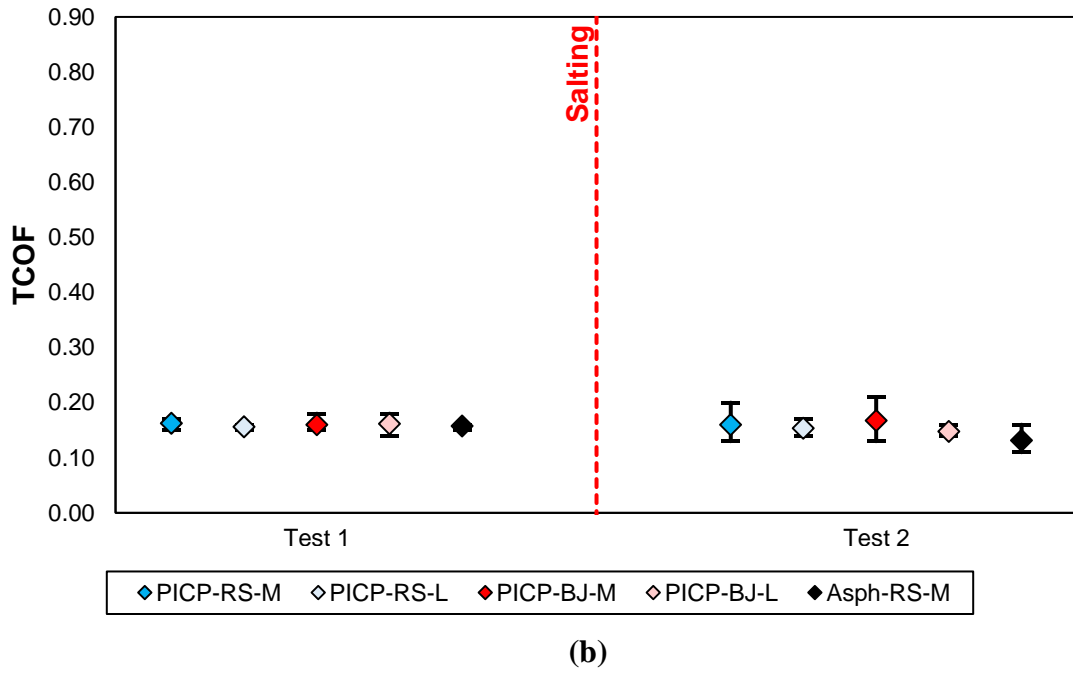
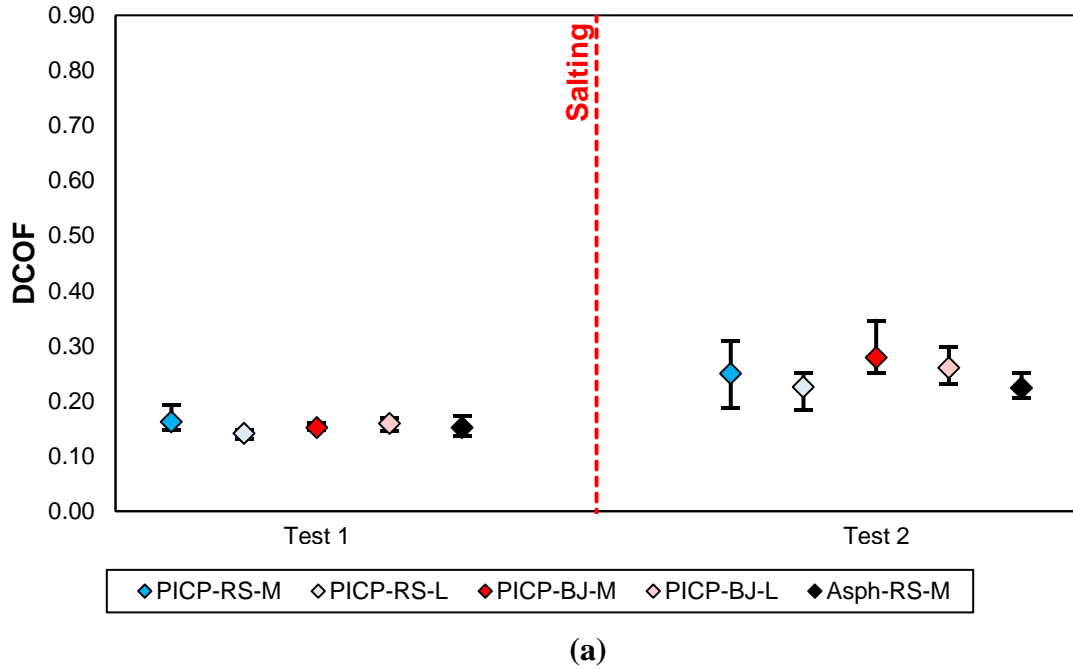
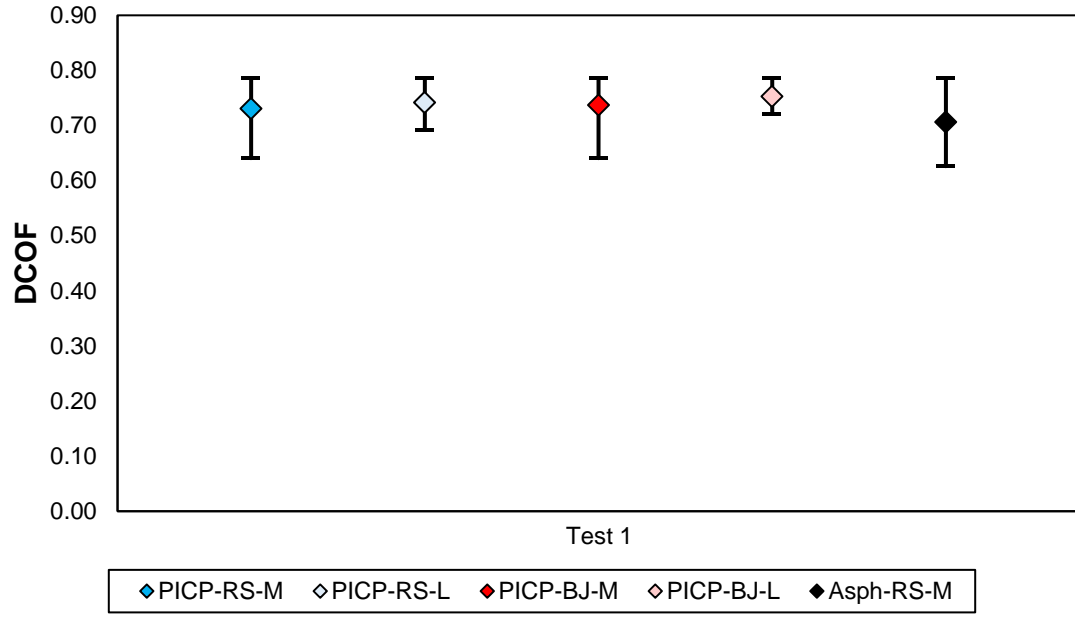
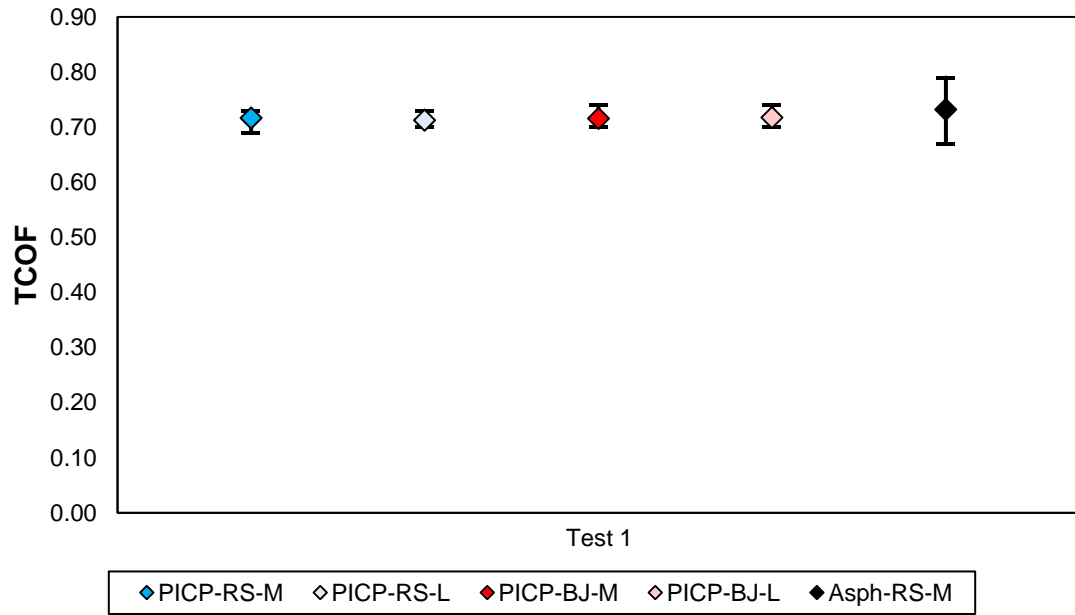


Figure B5: (a) DCOF and (b) TCOF data collected on 15/Apr/2019 after shovelling to a thin layer of ice following a freezing rain and sleet event. Freezing rain occurred throughout tests and higher intensity freezing rain began after Test 2.



(a)



(b)

Figure B6: (a) DCOF and (b) TCOF data collected on 29/May/2018 during dry pavement conditions.

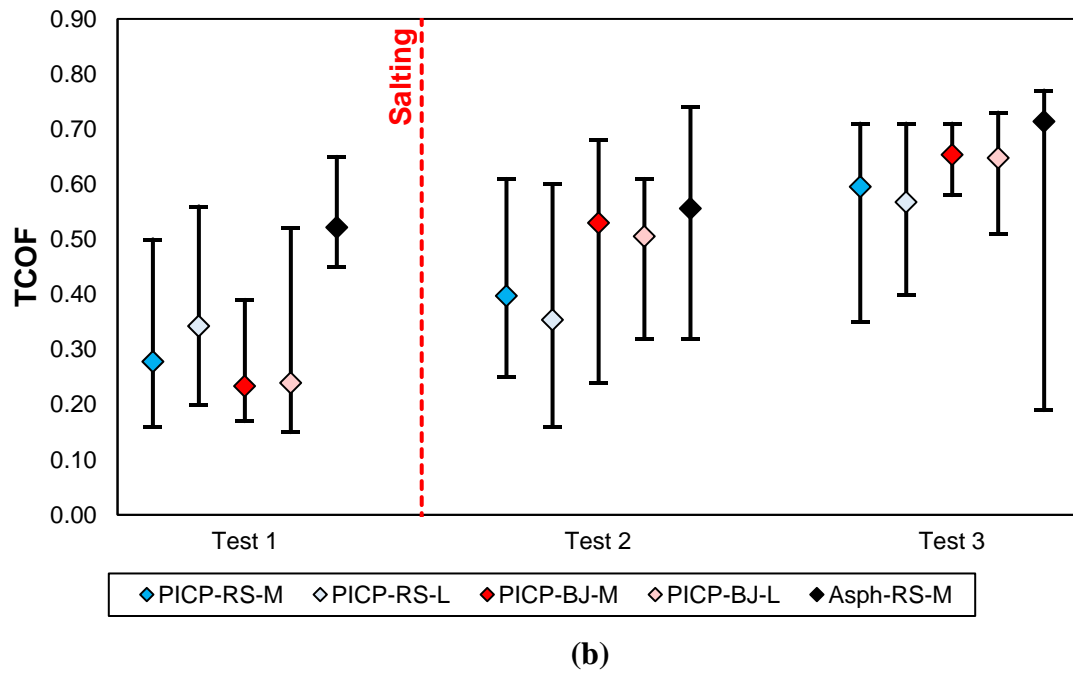
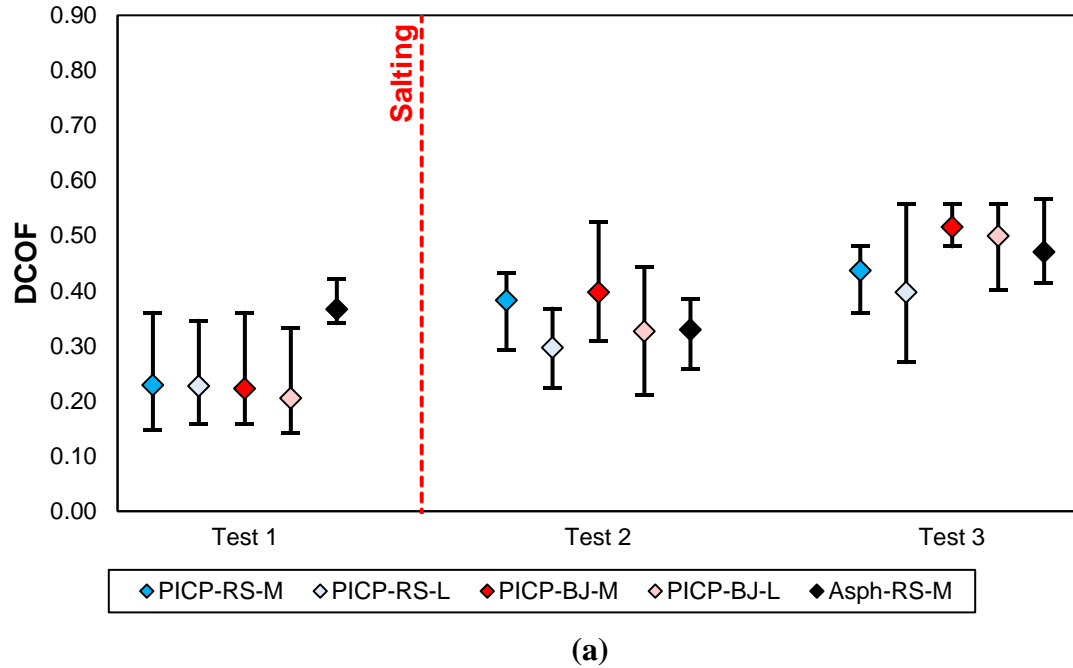


Figure B7: (a) DCOF and (b) TCOF data collected on 21/Jan/2019 after cells were shovelled to a thin layer of snow. No changes in surface conditioned were observed between Test 3 and sunset.

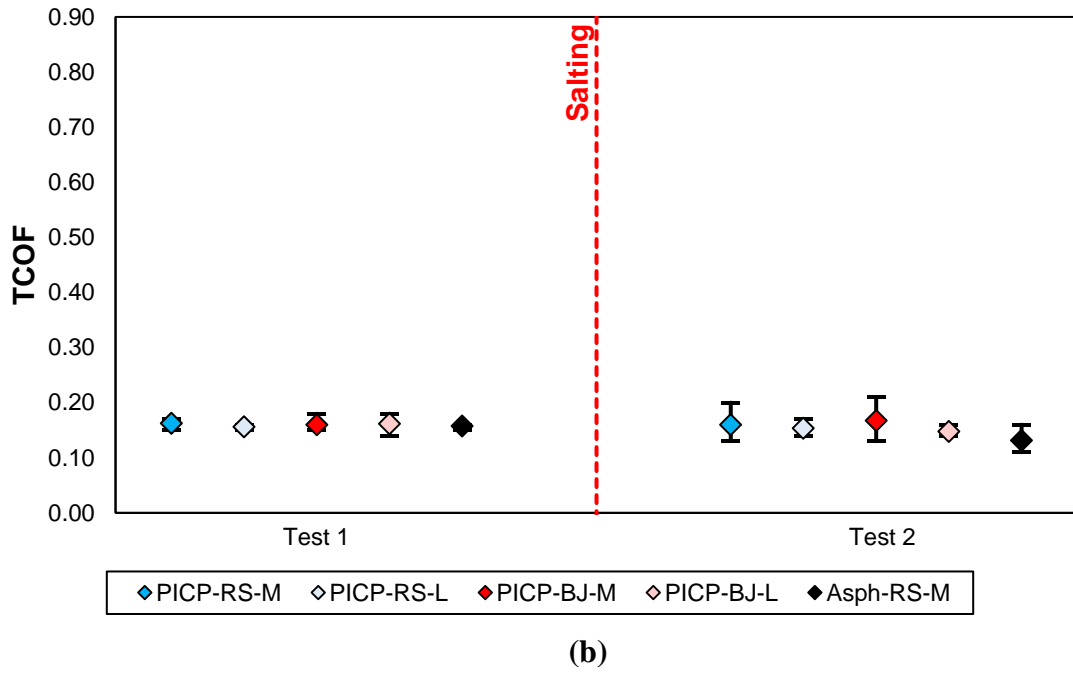
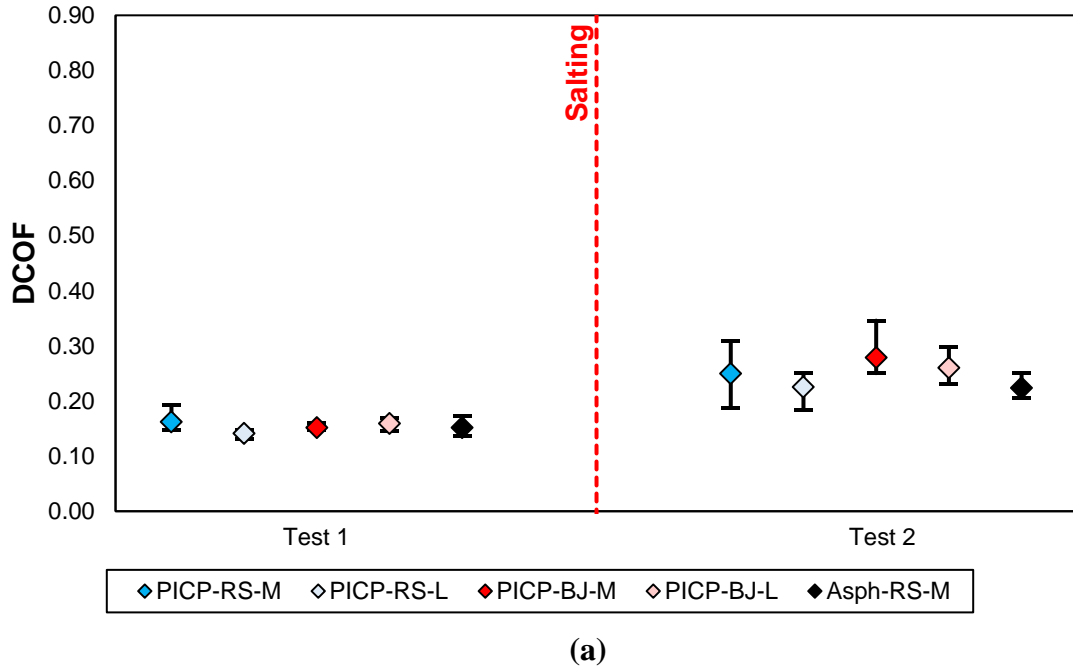


Figure B8: (a) DCOF and (b) TCOF data collected on 29/Jan/2019 on compacted snow where minimal melting occurred after salting.

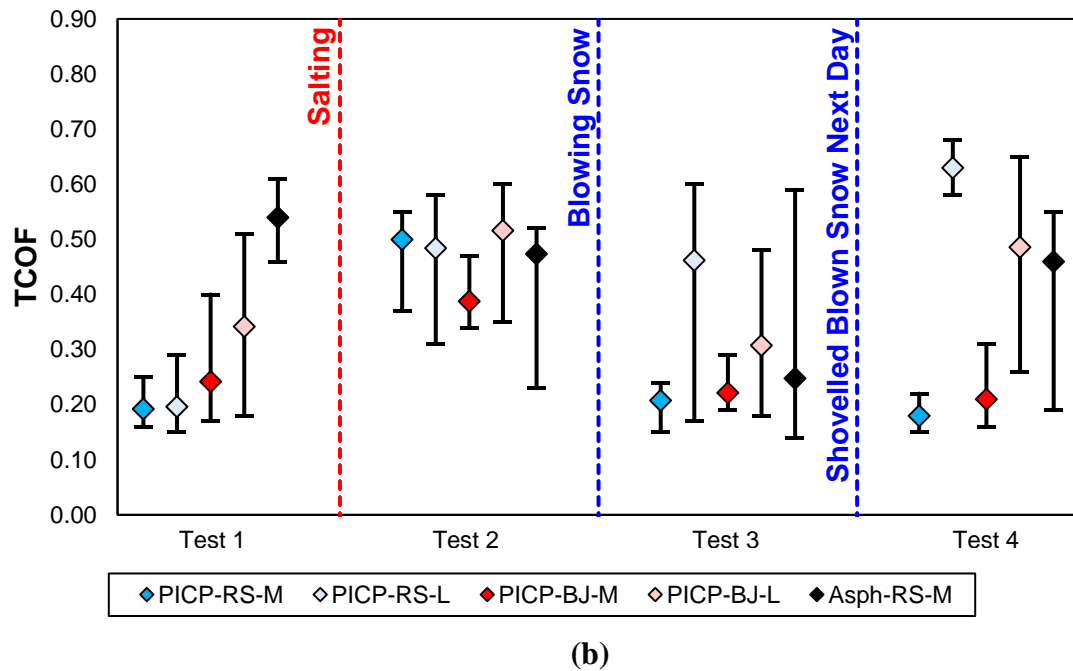
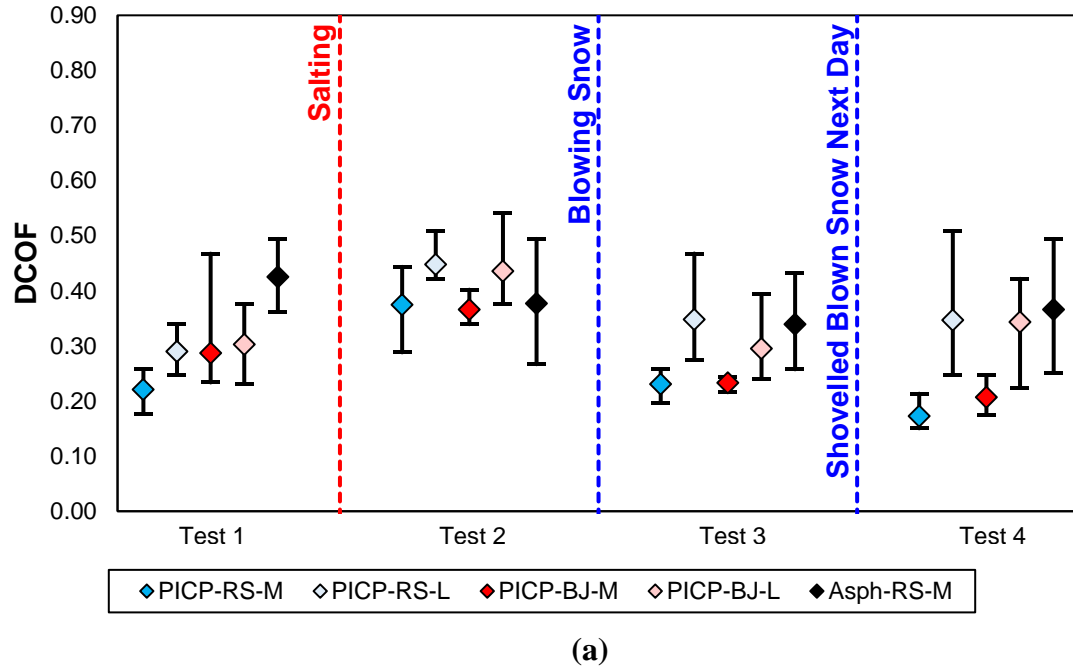
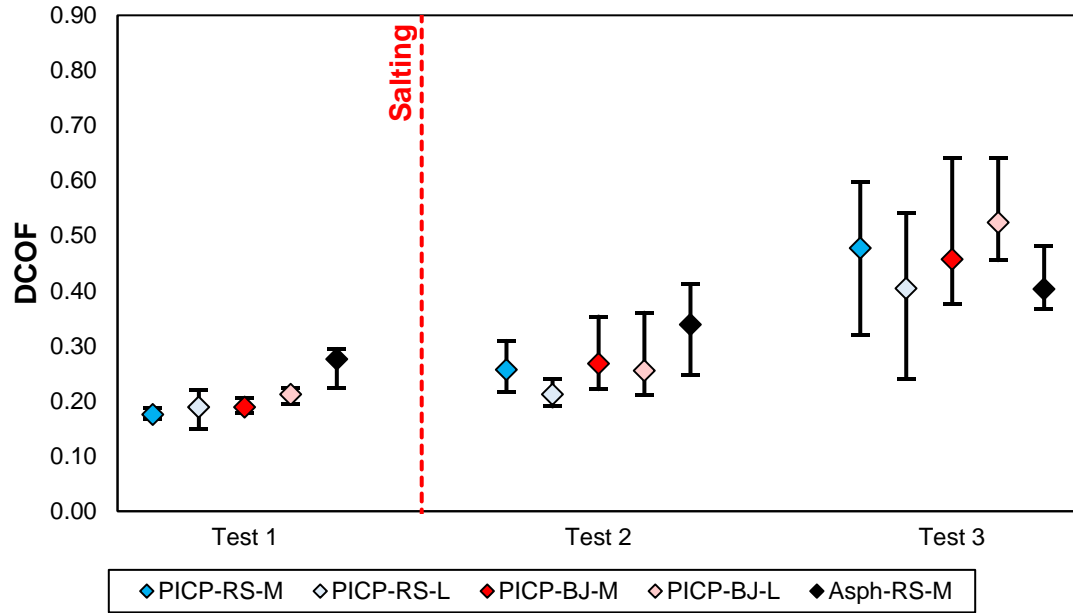
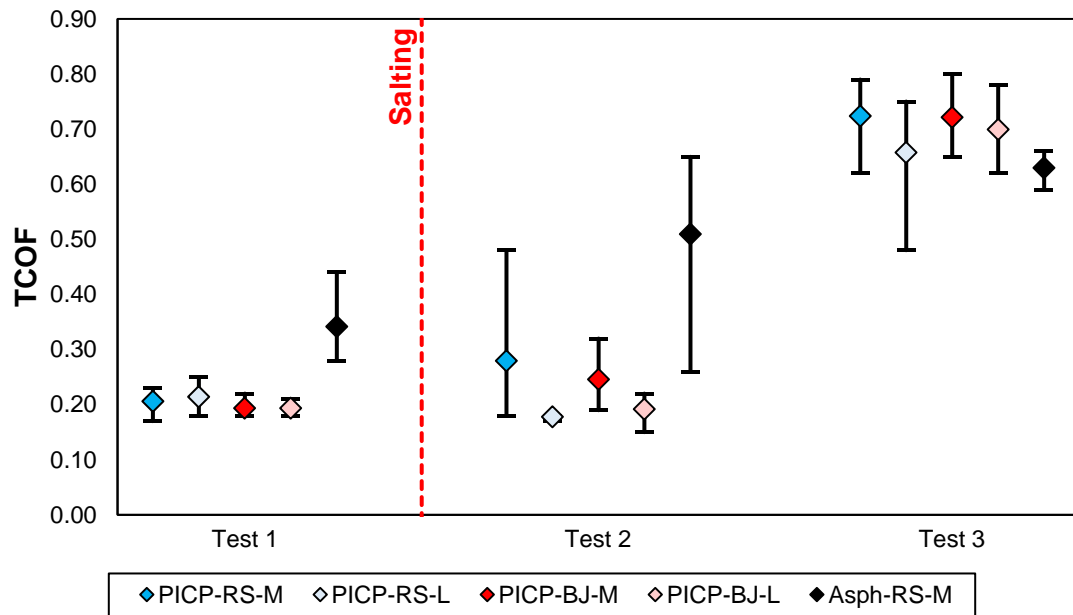


Figure B9: (a) DCOF and (b) TCOF data collected on 30/Jan/2019 and 31/Jan/2019 after cells were shovelled to a thin layer of snow. Blowing snow partially covered cells after Test 2 and again after Test 3. Blown snow was shovelled on 31/Jan/2019 to thin patches of ice that formed where the blown snow had previously melted by salt particles and then refroze. Shovelling on 31/Jan/2019 created thin layers of snow that partially covered PICP-RS-L and PICP-BJ-L, and that fully covered PICP-RS-M, PICP-BJ-M, and Asph-RS-M.

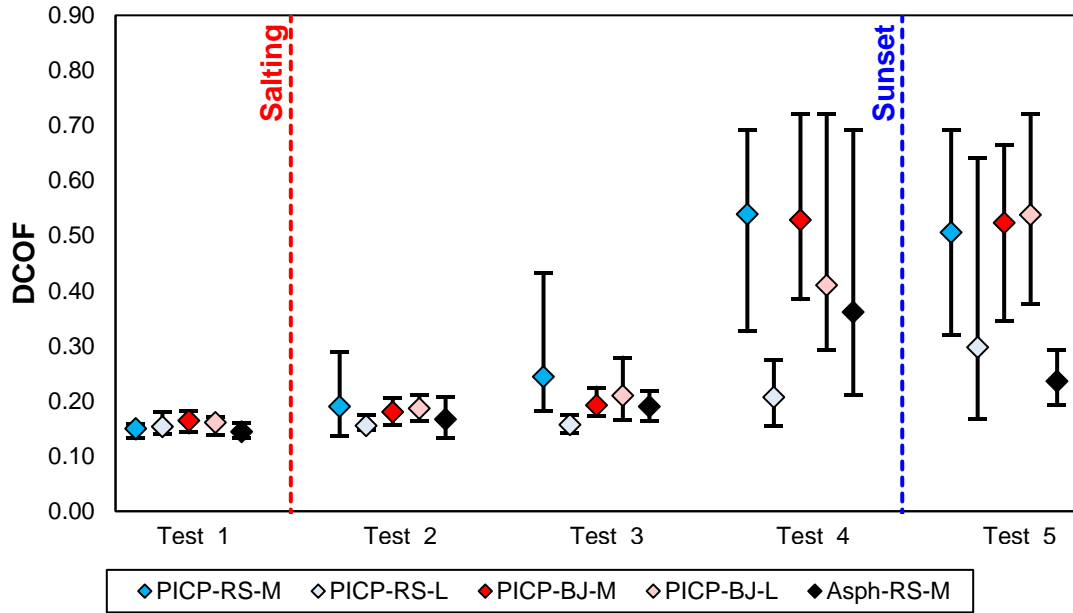


(a)

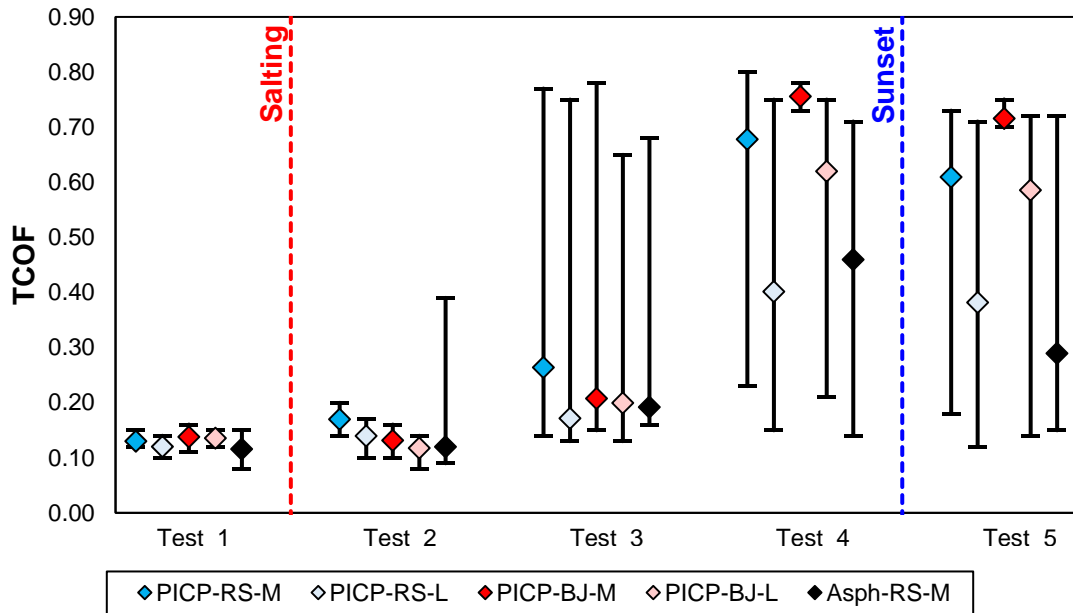


(b)

Figure B10: (a) DCOF and (b) TCOF data collected on 07/Feb/2019 after cells were shovelled to a thin layer of ice pellets following a sleet event. Freezing drizzle occurred throughout all tests and snowfall began after Test 3.

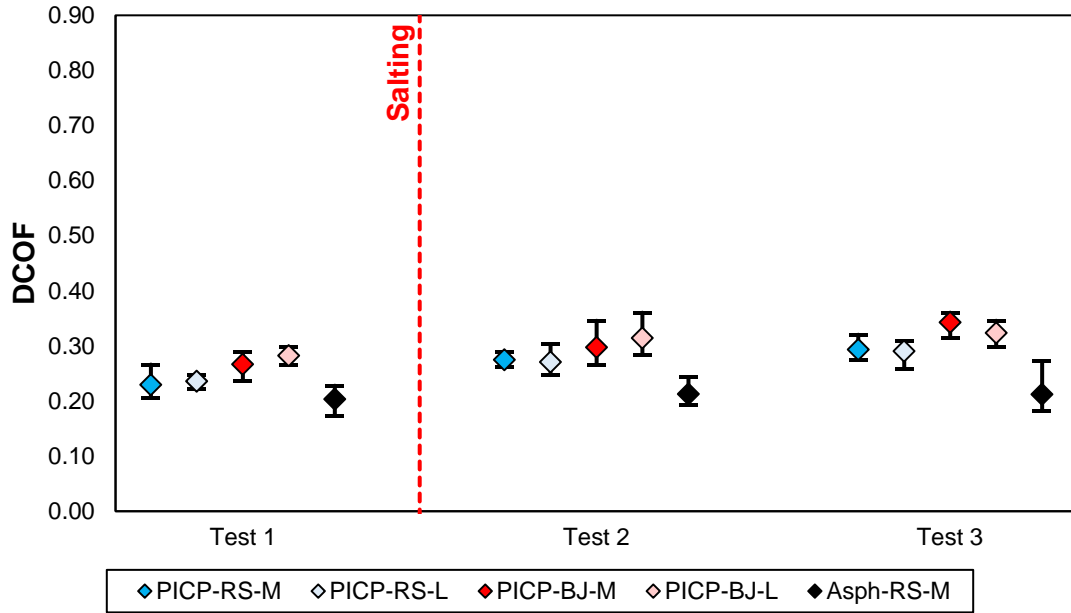


(a)

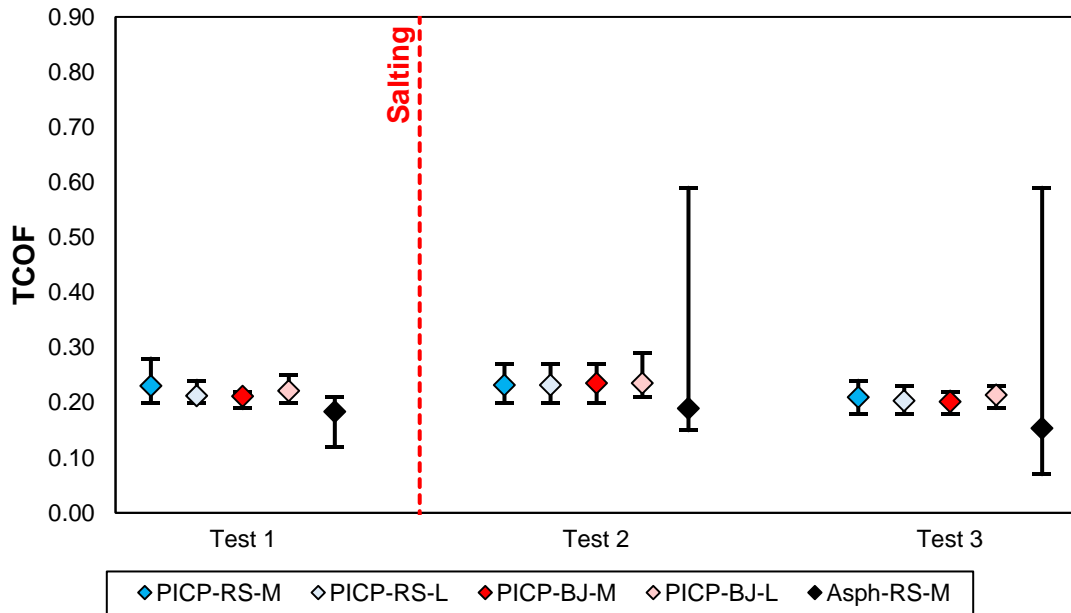


(b)

Figure B11: (a) DCOF and (b) TCOF data collected on 16/Feb/2019 after cells were shovelled to a layer of dense ice formed from compacted snow that partially melted and refroze.

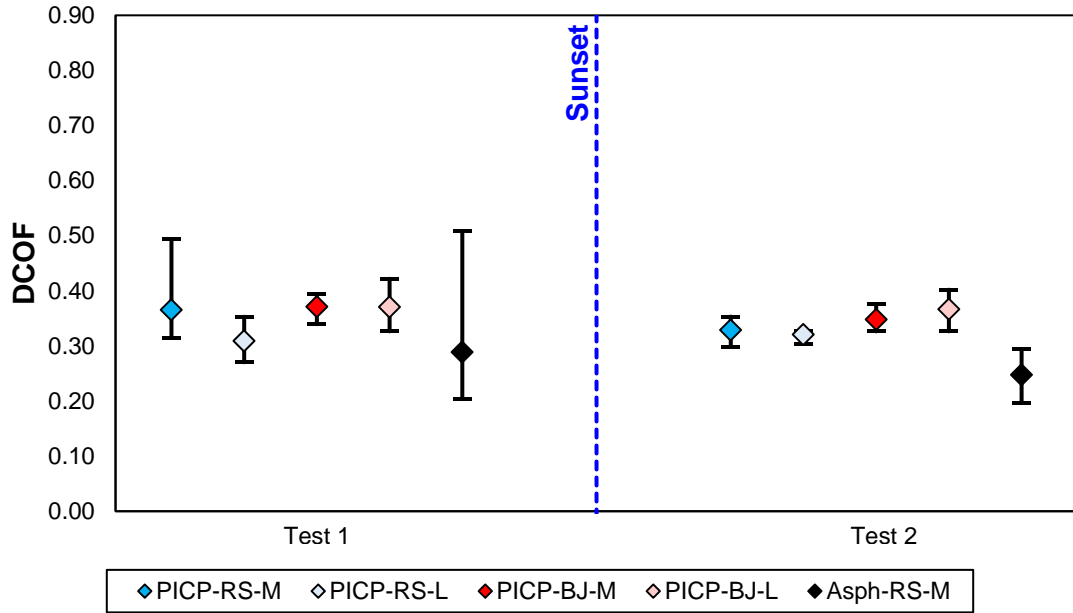


(a)

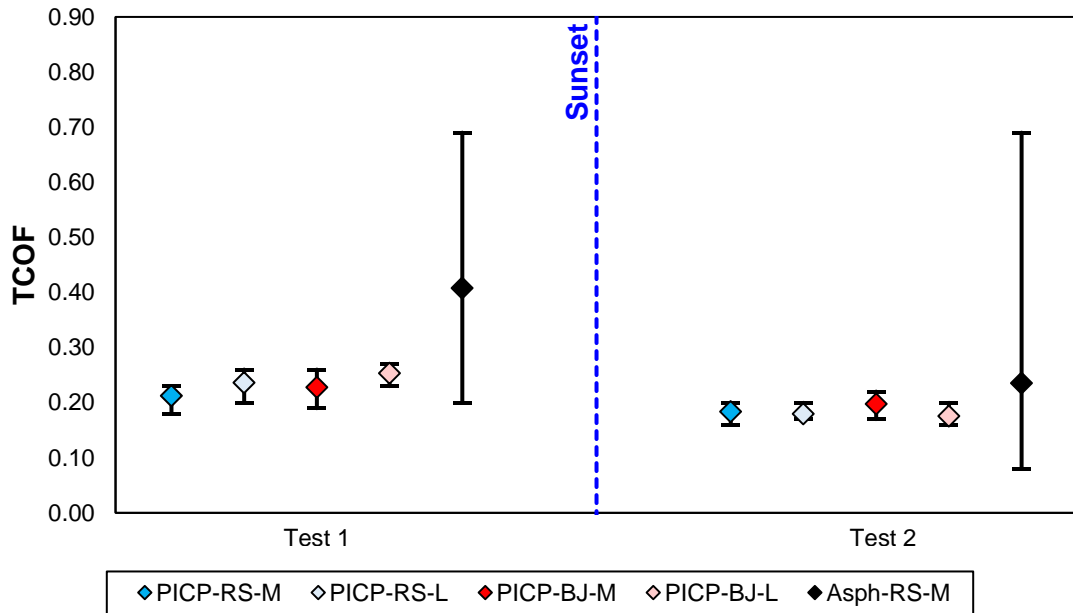


(b)

Figure B12: (a) DCOF and (b) TCOF data collected on 04/Mar/2019 after cells were shovelled to a layer of compacted snow on the PICP cells and to a mixed layer of compacted snow and ice formed from compacted snow that partially melted and refroze on the asphalt cell. Meltwater began to freeze before Test 3.



(a)



(b)

Figure B13: (a) DCOF and (b) TCOF data collected on 07/Mar/2019 before and after sunset when PICP cells were covered in compacted snow and asphalt cell was partially covered in ice formed from compacted snow that partially melted and refroze.

**Appendix C: Normality Testing of Friction Data on PICP Cells for Shovelled Snow
Experiments**

Normality tests were carried out on the DCOF and TCOF data collected from the four shovelled snow experiments (05/Feb/2018, 21/Jan/2019, 30/Jan/2019, and 07/Feb/2019) on the four PICP cells to determine whether the assumption of approximate normality on the data residuals was valid for carrying out two-way repeated measures ANOVA tests. The normality tests consisted of evaluating quantile-quantile (q-q) plots (Figure C1), histograms (Figure C2), kurtosis, skewness, and Shapiro-Wilk p-values (Table C1) of the DCOF and TCOF residuals for each friction measurement set period (Test 1, Test 2, and Test 3). ANOVA tests can still be robust when normality violations are present in the data, and this has been demonstrated for when datasets kurtosis and skewness values between -1 and 1 (Blanca et al. 2017 and references therein). Thus, each dataset was considered to have approximate normality provided its kurtosis and skewness were between -1 and 1, and if some degree of normality was observed from either the Shapiro-Wilk test, q-q plots, or the histograms.

As shown in Table C1, both the DCOF and TCOF datasets failed the Shapiro Wilk test ($p < 0.05$) for Test 1. Moreover, kurtosis and skewness of the TCOF values were both larger than 1 for Test 1. Rapid snowmelt on the PICP cells following shovelling may have contributed to the lack of normality observed during these periods. In particular, TCOF measurements were typically collected during 20 minute periods that began more than 10 minutes after shovelling, and partial melting of the cells may have occurred by this time. The q-q plots and histogram for DCOF and TCOF during Test 1 illustrate how these melted areas cause the datasets to skew to the right. For these reasons, approximate normality was not assumed to be valid for the DCOF and TCOF datasets. However, 2-way ANOVA tests were not needed for DCOF and TCOF measurements collected on the four PICP cells during Test 1 because the datasets were collected prior to applying de-icers. Statistical comparisons of DCOF and TCOF for Test 1 were therefore limited to one-way nonparametric tests.

All kurtosis and skewness values were between -1 and 1 for Test 2 and Test 3. As shown in the q-q plots and histogram, the right skew observed in Test 1 begins to shift back towards centre and to the right during Test 2 and Test 3. Skews towards the right are expected over time as the snow melts because most of the surfaces during later periods are typically clear of snow but with pockets of snow remaining at some locations. Based on Shapiro-Wilk test, less normality was observed for the TCOF datasets than for the DCOF datasets. This was likely due to the TCOF values being point measurements whereas the DCOF values were measured over larger areas.

Overall, violations to normality during Test 2 and Test 3 were not found to be sufficiently large to discount the use of two-way repeated measures ANOVA tests for the four PICP cells.

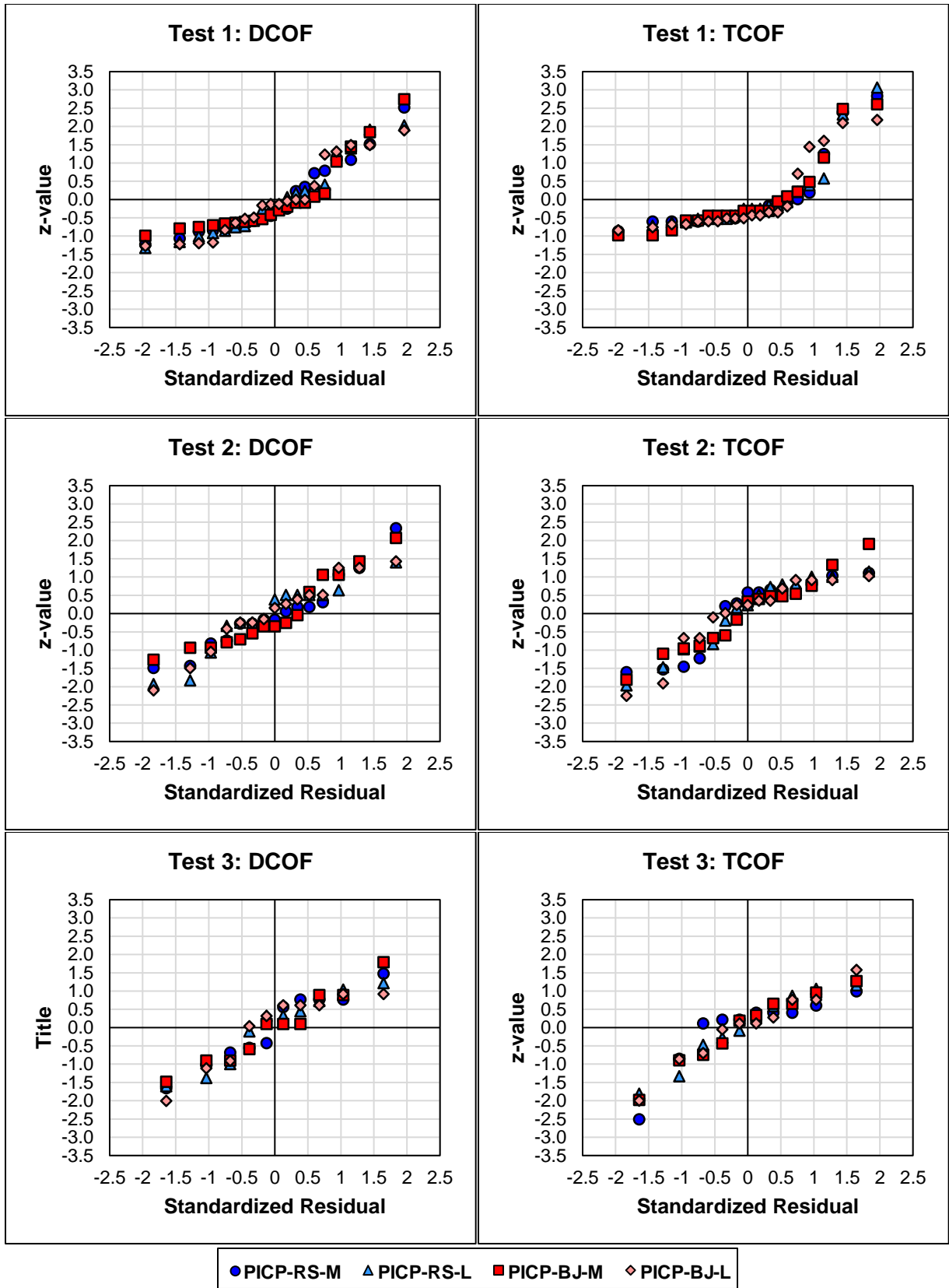


Figure C1: Quantile-Quantile plots of friction data for shovelled snow experiments.

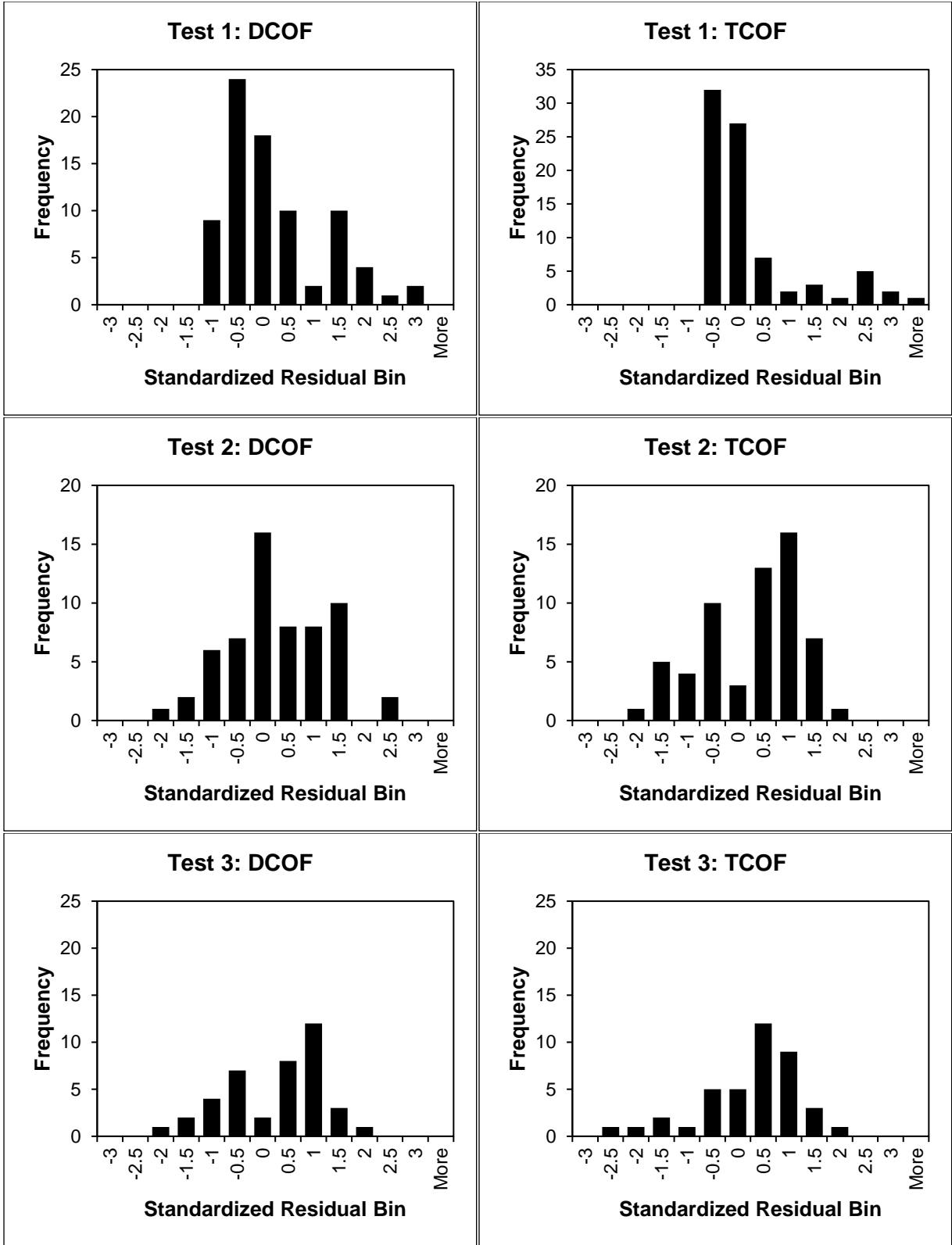


Figure C2: Histograms of friction data for shovelled snow experiments.

Table C1: Winter maintenance activities carried out on pavement cells.

Measurement	Friction	Kurtosis ^{a,b} (-1 to 1)	Skewness ^{a,b} (-1 to 1)	Shapiro Wilk p-value ^{a,b} (p > 0.05)
Test 1	DCOF	0.04	0.93	< 0.01
	TCOF	1.80	2.24	< 0.01
Test 2	DCOF	0.06	-0.18	0.73
	TCOF	-0.59	-0.59	< 0.01
Test 3	DCOF	-0.34	-0.86	0.11
	TCOF	-0.9	0.37	0.02

^a Criteria for passing normality test indicated in parenthesis.

^b Bold values in table indicate that dataset failed normality test.

References

Blanca, M. J., Alarcón, R., Arnau, J., Bono, R., and Bendayan, R. (2017). “Non-normal data: Is ANOVA still a valid option?” *Psicothema*, 29(4), 552–557.

**Appendix D: State-of-the-Art Review Paper on Phosphorus Sorption Amendments in
Bioretention Media**

State-of-the-Art Review of Phosphorus Sorption Amendments in Bioretention Media: A Systematic Literature Review

Jeffrey T. Marvin¹; Elodie Passeport²; and Jennifer Drake³

¹Department of Civil & Mineral Engineering, University of Toronto, 35 St. George St., Toronto ON M5S 1A4, Canada

²Assistant Professor, Department of Civil & Mineral Engineering, Dept. of Chemical Engineering & Applied Chemistry, University of Toronto, 35 St. George St., Toronto ON M5S 1A4, Canada

³Assistant Professor, Department of Civil & Mineral Engineering, Daniels Faculty of Architecture, Landscape & Design, University of Toronto, 35 St. George St., Toronto ON M5S 1A4, Canada

Abstract: The ability of bioretention systems to treat phosphorus heavily depends on the filter media composition. Dissolved phosphorus is primarily removed from influent stormwater runoff through sorption processes, although the organic material contained within bioretention media can also leach phosphorus. Amendments containing sorptive metals such as aluminum, iron, and calcium have been introduced in recent years to increase the phosphorus sorption capacities and rates of bioretention media. This study is a state-of-the-art review that uses a systematic literature review process to identify, integrate, and critically evaluate the findings of all published column, mesocosm, and field studies identified from two database platforms that have provided quantitative analyses of phosphorus sorption amendments for bioretention systems. These amendment materials were grouped into four categories: (1) waste products, (2) natural materials, (3) processed materials, and (4) proprietary products. A total of 51 amendment materials or material combinations were evaluated across 59 studies, of which only four have been evaluated within a field setting (expanded slate, fly ash, Sorbtive MediaTM, and aluminum-based water treatment residuals) and only one (fly ash) has been evaluated within an aged system. The study provides a detailed discussion on the performance, applicability, constructability, and operational challenges of phosphorus sorption amendments used in bioretention systems. Recommendations for amendment selection and installation methods are provided to support both engineering practice and future research on the topic.

1 Introduction

Urban development impacts the hydrology of a watershed by modifying the flow rates, runoff volumes, and water quality of stormwater runoff discharged to the environment (Line and White 2007; Paul and Meyer 2001). Over the past two decades, the driving design objective of stormwater management practices has shifted from preserving pre-development peak runoff flows to also maintaining pre-development runoff volumes and water quality. Bioretention systems, also known as *rain gardens*, are a type of Low Impact Development (LID) stormwater Best Management Practice (BMP) and Green Infrastructure (GI) that treat, infiltrate, and evapotranspire stormwater runoff. A typical bioretention cell is installed within a shallow depression and consists of a plant and mulch layer above a coarse filter media bed and a washed gravel drainage layer (Davis et al. 2009). The drainage layer typically contains an underdrain if the native soil below has low infiltration rates.

While bioretention systems with underdrains are shown by numerous studies to effectively treat pollutants from stormwater runoff (LeFevre et al. 2014 and references therein), the ability of bioretention to treat phosphorus (P) varies (e.g., Bratieres et al. 2008; Hsieh and Davis 2005; Hunt et al. 2006). In urban stormwater runoff, P mostly originates from lawn fertilizers, pet waste, leaf litter, road salts, atmospheric deposition, and soil erosion (USEPA 1999; Waschbusch et al. 1999). Bioretention media with a high phosphorus index (P-index) can also potentially desorb P into the discharged stormwater (Hunt et al. 2006; Jay et al. 2017). Leaching may, however, decrease over time as the media ages (Hatt et al. 2009).

Phosphorus in stormwater runoff is present in two forms, particulate phosphorus (PP) and dissolved phosphorus (DP). In bioretention systems, PP is removed by filtration, whereas DP is removed by plant uptake, microbial uptake, and sorption to the filter media (Lucas and Greenway 2008). These sorption mechanisms include ion exchange, adsorption, and precipitation (Li and Davis 2016). Dissolved phosphorus is further divided into soluble reactive phosphorus (SRP), which is also referred to as *soluble inorganic phosphorus* or *orthophosphates*, and dissolved organic phosphorus (DOP). The concentrations of SRP and DOP in typical stormwater runoff are believed to be nearly equal (Liu and Davis 2014). Soluble reactive phosphorus is typically considered to be the only form of P that is bioavailable for plants and to be the primary contributor to unwanted algae growth downstream of urban developments. However, some forms

of DOP, such as adenosine-5'-monophosphate, guanosine diphosphate, uridine diphosphate, adenosine-5'-triphosphate, deoxyribonucleic acid, ribonucleic acid, and phosphatidylcholine, are potentially also bioavailable for algae (Li and Brett 2013). A diagram depicting the different forms of P and their removal processes in a bioretention system is shown in Figure D1.

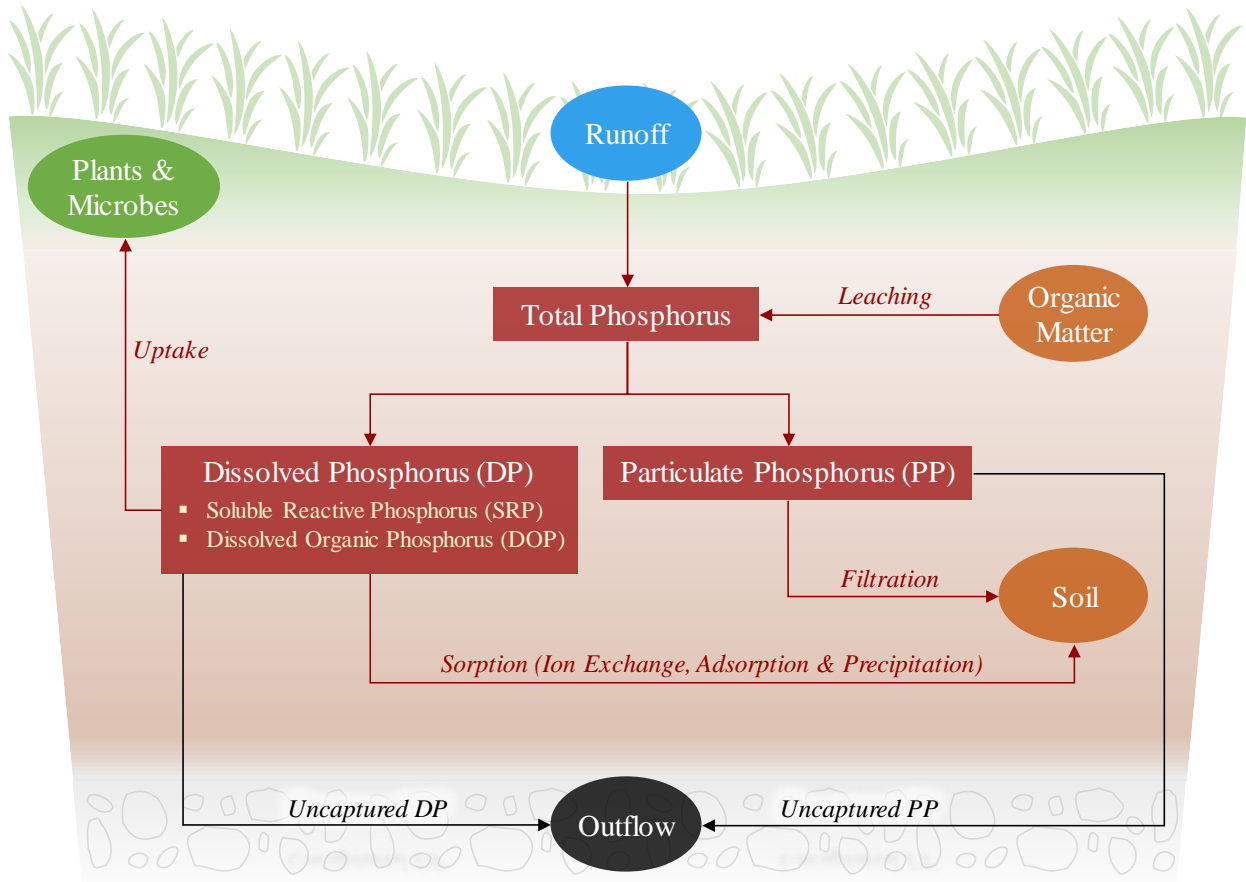


Figure D1: Phosphorus forms and removal processes in a bioretention system.

The dominant SRP removal mechanism in bioretention systems is media sorption (Lucas and Greenway 2011). In alkaline environments, SRP removal mechanisms are primarily through precipitation reactions with calcium (Ca), forming compounds such as dicalcium phosphate dihydrate, octocalcium phosphate, and hydroxyapatite (Stevenson and Cole 1999; Zhang et al. 2008). In neutral to acidic environments, SRP is primarily eliminated through aluminum (Al) and iron (Fe) oxide sorption processes (Stumm and Morgan 1996). During storm events, highly reversible ion-exchange reactions occur rapidly with Al and Fe oxides on particle surfaces, enabling the transfer of SRP from stormwater to soil (Bolan 1991; Hsieh et al. 2007). The slower

and less reversible adsorption reactions then continue to occur during dry periods, diffusing sorbed P into particle interiors and forming monodentate and bidentate complexes (Bolan 1991; Lucas and Greenway 2008). These slower processes also free available adsorptive surfaces for additional sorption during future storm events (O'Neill and Davis 2012b). However, crystallization of hydrous oxide mineral surfaces is also induced by media drying, which converts amorphous Al and Fe to less reactive crystalline forms (O'Neill and Davis 2012a). Other slower, irreversible reactions take place over longer periods of time that strongly bind P to the media (Kendal et al. 2017). While less research is available on DOP sorption in bioretention systems, the sorption mechanisms are believed to be similar (Liu and Davis 2014).

Vegetation in bioretention systems improves P removal and retention due to a combination of plant and microbial biomass uptake (Brown et al. 2016; Glaister et al. 2014; Lucas and Greenway 2008; Lucas and Greenway 2011). While filtration and sorption processes are the primary mechanisms for removing P in bioretention systems, plants require nutrients for growth and therefore uptake P from the media over time (Lucas and Greenway 2008). Plant uptake rates in bioretention systems have been found to be in the range of 0.85 to 2.31 mg of P per g of plant mass (Rycewicz-Borecki et al. 2017), and plant harvesting has been suggested to prevent plant decay from releasing phosphorus back into the system (Davis et al. 2006). Plant uptake rates are further enhanced when mycorrhiza fungi are present, which also provide nutrients to the plants that originate beyond the plant root zone in the soil (Bolan 1991; Stevenson and Cole 1999; Van Tichelin and Colpaert 2000). Poor et al. (2018a) demonstrated this increase in P uptake by mycorrhiza fungi for bioretention systems where mesocosms containing mycorrhizae were found to reduce TP leaching by 13 to 48% and SRP leaching by 14 to 60%. Other fungi including *Stropharia rugoso-annulata* have been shown to reduce SRP leaching in bioretention systems by up to 46% (Taylor et al. 2018). Vegetation also provides oxygen to the media through plant roots, which helps to oxidize Fe(II) in the soil to Fe(III) (Mendelsohn et al. 1995). This increases P sorption in the media, as Fe(III) is insoluble and has a higher P sorption capacity than the soluble Fe(II) form. Finally, vegetation also improves soil structure, providing resilience to cracking and formation of preferential flow paths during dry periods and in the winter when plant roots die (Glaister et al. 2014). These effects on soil porosity could reduce contact time and sorption rates in the media, particularly in cold climates where freeze-thaw cycles create larger and more connected pores (Ding et al. 2019).

Over time, the sorption capacity of the filter media is impacted by the balance of the physical, chemical, and biological processes described above. As the filter media becomes saturated with sorbed P, its ability to remove P from stormwater is reduced. While evaluations of P sorption in aged bioretention cells are limited, field evaluations have shown that P becomes tightly bonded to the media over time and is mostly present near the top of the media layer (Johnson and Hunt 2016; Kandel et al. 2017; Komlos and Traver 2012; Muerdter et al. 2016; Willard et al. 2017). To increase the P sorption capacity of the filter media, various amendments have been introduced to bioretention systems that are typically composed of Al-, Fe-, and Ca-containing compounds. These amendments are also used to increase the sorption of P introduced from both runoff and organic matter leachate throughout the lifespan of the bioretention system. Apart from investigations specific to bioretention cells, many P sorption amendments have been evaluated for various forms of wastewater and stormwater treatment systems, particularly constructed wetland systems. The reader is invited to look at the reviews by Ballantine and Tanner (2010), Cucarella and Renman (2009), Kadlec and Wallace (2008), and Penn et al. (2017) for detailed information on P sorption amendments for these systems. However, an inclusive comparison of P sorption amendments has not yet been performed for bioretention systems, and over half the research to date on the use of P sorption amendments in bioretention media has been published in the past three years. Thus, the first objective of this study is to systematically review and evaluate the performance and applicability of all P sorption amendments that have been proposed in the literature for bioretention media. The second objective is to provide recommendations for amendment selection and installation based on common characteristics while highlighting constructability and operational challenges associated with similar amendment types.

2 Methodology

The literature reviewed for this study was collected by searching selected terms within two electronic database platforms, Engineering Village and Web of Science, and filtering the results based on inclusion and exclusion criteria. These two database platforms were selected because bioretention research in relation to P treatment lies within the fields of engineering and science. The *all fields* search option was selected for Engineering Village and the *topic* search option was selected for Web of Science. Both search options identify terms within the titles, abstracts, controlled key words, and uncontrolled key words.

A final search of the two database platforms was performed on February 4, 2019 using search terms that were intended to first identify all bioretention and sand filter studies from these databases which evaluated P removal in stormwater runoff. Sand filter studies were included in the search because laboratory experiments for bioretention systems often use similar testing methods and media compositions as those for sand filter systems (Adhikari et al. 2016; Erickson et al. 2012). For example, column and mesocosm studies for bioretention media amendments often eliminate the impacts of organic matter leaching by using pure sand for the media composition, or they eliminate the impacts of plant uptake by not including vegetation. Thus, records were identified by searching the database platforms for the terms *phosphorus*, *phosphorous*, or any word ending in *phosphate*. Of these records, only those that included the terms *bioretention*, *biofiltration*, *bioinfiltration*, *biofilter*, or *rain garden* were collected for bioretention studies, and only those that included the terms *stormwater*, *storm water*, *rainwater*, *rain water*, or *drainage* in combination with the word *sand* or *filter* were collected for sand filter studies. This selection of terms allowed for records to be identified that do not exclusively use the terms *bioretention* or *sand filter*. An exclusive list of specific media amendments was not included in the search because the aim of this study was to review all types of media amendments that have been researched. A total of 3,183 records were found using these search criteria, which was reduced to 2,013 after duplicates were removed.

The records were then screened in two phases using inclusion and exclusion criteria based on the titles and abstracts alone. A summary of this procedure is depicted in the flow diagram in Figure D2. The initial screening was performed to eliminate the large amount of undesired articles within other fields of research such as wastewater treatment, drinking water treatment, and soil nutrient loss. Included records for the initial screening were quantitative or review studies on reducing P in stormwater runoff using either bioretention or sand filter systems. Excluded records were (1) records that were not provided as full-text in English, (2) abstracts of presentations that had no full-text manuscript, (3) patents, (4) records that were not peer-reviewed, and (5) records that were unavailable from the University of Toronto library network. A total of 278 records remained following this inclusion and exclusion procedure. A second screening was then performed to exclude (1) studies that did not include media amendments, (2) studies that did not include appropriate media amendments for P sorption such as carbon-based materials intended for nitrogen removal, (3) studies that were field assessments of stormwater

sand filters, and (4) conference proceedings that had been superseded by journal articles or more recent conference proceedings with updated results. Only laboratory studies on stormwater sand filters were included because this review was limited to bioretention applications, whereas other field applications of stormwater sand filters include retention ponds and constructed wetlands. A total of 97 records remained following the secondary screening of the titles and abstracts.

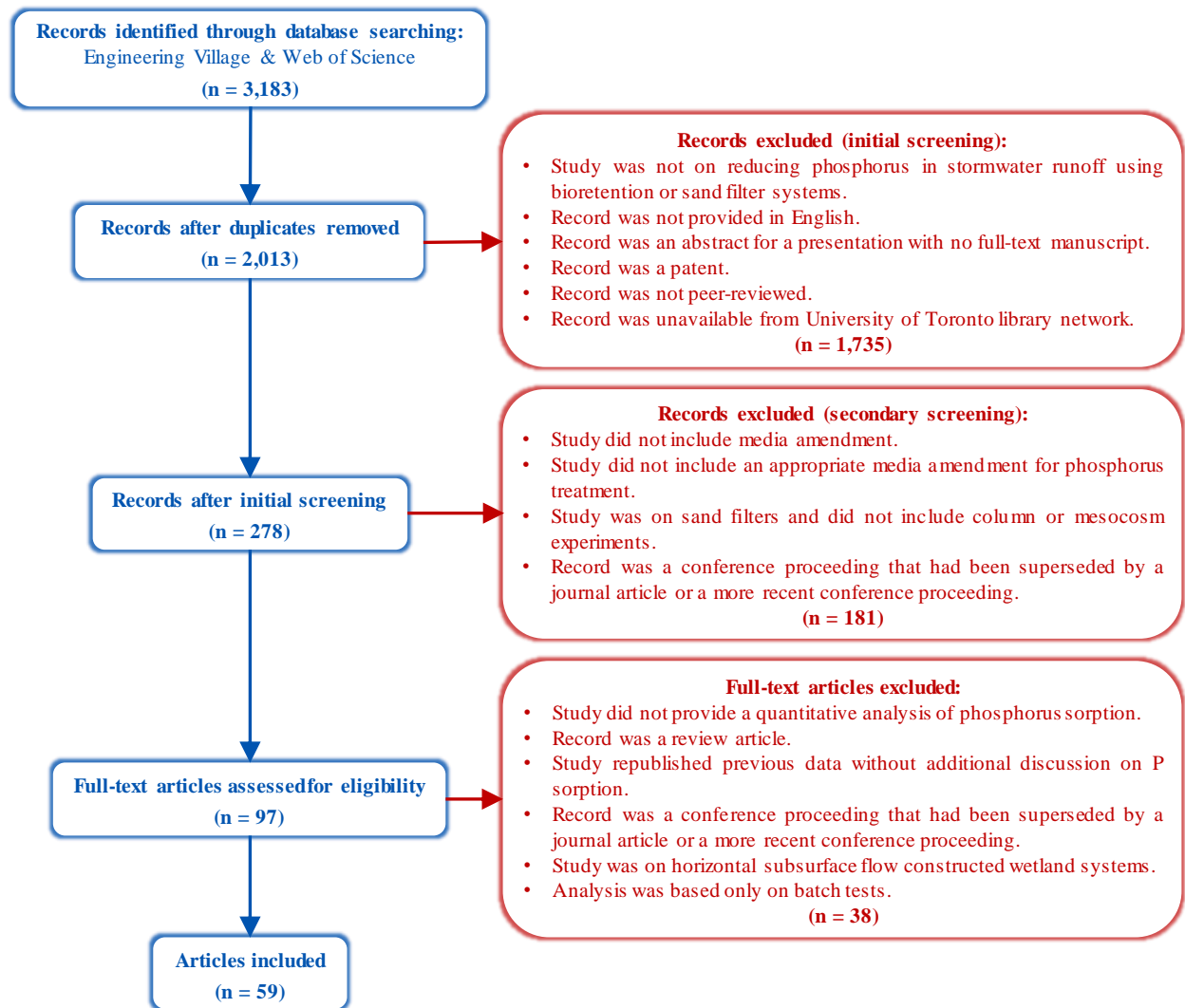


Figure D2: Flow diagram for systematic literature review process.

Full-text sifting of the remaining 97 records was then carried out to exclude (1) studies that did not provide a quantitative analysis of P sorption, (2) review articles, (3) studies that republished previous data without additional discussion on P sorption, (4) records that were conference proceedings superseded by journal articles or more recent conference proceedings, (5) studies that were on horizontal subsurface flow constructed wetland systems, and (6) studies that

analysed P sorption based only on batch test results. Batch tests are experiments where the amendment is well-mixed with a solution for a specified duration, whereas column (indoor) and mesocosm (outdoor) tests are controlled flow-through experiments where a solution is either pumped or percolated through the amendment. Batch tests typically consist of (1) equilibrium tests, which measure P sorption after mixing and shaking the amendment with a P solution for a specified period of time, (2) kinetic tests, which measure the rate of P sorption over a period of time, and (3) desorption tests, which measure the amount of P that desorbs from the amendment when mixed with water following a sorption test. Adsorption isotherm models such as the Langmuir model can then be used to estimate the maximum adsorption capacity of the amendment based on the equilibrium test results. Adsorption capacities of many P sorption materials have already been comparatively evaluated under batch test conditions; see for example the reviews by Cucarella and Renman (2009) and Kadlec and Wallace (2008). While batch tests provide information about the sorption rate and capacity of the amendment material, they do not simulate the flow-through conditions present in bioretention systems, can overestimate sorption capacity, and are often followed up by column, mesocosm, or field tests (Chang et al. 2018; Erickson et al. 2007; Liu and Davis 2012a; Sellner et al. 2019; Stoner et al. 2012; Yan et al. 2017; Zhang et al. 2018; Zhang et al. 2008). Batch tests are also typically carried out on the amendment material alone, whereas column and mesocosm tests are often carried out on amended media. For these reasons, this study was limited to reviewing only column, mesocosm, and field studies. Following full-text sifting, a total of 59 records remained and were selected for review. Of these records, 53 were peer-reviewed journal articles and six were peer-reviewed conference proceedings.

3 Results and Discussion

3.1 Amendment Materials

A list of all amendment materials evaluated by the reviewed articles using column, mesocosm, and field experiments is provided in Table D1 along with the associated references listed chronologically. The dominant metals found within each amendment material that are responsible for the sorption processes are also noted within the table. Only amendments that were intended to enhance P sorption through their metal composition were included, whereas other amendments used within the studies for other purposes, such as carbon sources for

enhancing denitrification, were not included. As shown in Table D1, a total of 51 amendment materials or material combinations were evaluated across the 59 studies. These amendment materials can be grouped into the following four categories: (1) waste products, (2) natural materials, (3) processed materials, and (4) proprietary products.

Waste products are materials leftover from industrial activities such as coal combustion, material processing, mining, and water treatment. They are typically evaluated for their use as media amendments due to their low costs, high availability, and reuse applications (Adhikari et al. 2016; Palmer et al. 2013; Poor et al. 2018; Sellner et al. 2019; Wendling et al. 2013; Zhang et al. 2008). However, waste products can lack consistency due to the high variability of their source materials and components (Guo et al. 2015; O'Neill and Davis 2012a; Poor et al. 2018; McTaggart et al. 2015; Stoner et al. 2012). Waste products evaluated by the reviewed articles include water treatment residuals (WTR), coal combustion waste products (bottom ash, coal ash, fly ash), metallurgical processing waste products (blast furnace slag, red mud, steel chips, steel slag), acid mine drainage residuals, iron coated sand, and recycled concrete aggregate. Water treatment residuals can be further categorized into aluminium-based (Al-WTR), iron-based (Fe-WTR), and calcium-based (Ca-WTR) varieties depending on the type of products used within the water treatment processes. The most commonly studied amendment material for bioretention systems is Al-WTR. Some studies have attempted to further enhance the use of Al-WTR by mixing it with additional materials such as alum (Yan et al. 2017; Yan et al. 2018), partially hydrolyzed aluminum (Yan et al. 2018), and Krasnozem soil (Lucas and Greenway 2011; Greenway 2016).

Natural materials include rocks, minerals, and local soils that have not undergone further processing, and they also include shell remains from marine species such as cockles. While natural materials are sometimes evaluated for their use as media amendments due to their local availabilities (Glaister et al. 2014; Lucas and Greenway 2011), this regional availability may also limit widespread implementation of some materials. Moreover, consistency can vary due to differences in regional geology or species. Natural materials evaluated by the reviewed articles include cockle shells, seashells, shell sand, biotite, glauconite, limestone, medical stone, olivine, zeolite, iron-rich sand, Krasnozem soil, and Skye sand.

Table D1: List of amendment materials evaluated in reviewed studies

Category	Sub-Category	Amendment Abbreviation	Amendment Name	Dominant Metal(s)	Reference
Waste Products	Water Treatment Residuals	Al-WTR	Aluminum-Based Water Treatment Residuals	Al	(Lucas and Greenway 2011; O'Neill and Davis 2012a; O'Neill and Davis 2012b; Stoner et al. 2012; Palmer et al. 2013; Randall and Bradford 2013; Liu et al. 2014; Liu and Davis 2014; Duranceau and Biscardi 2015; Guo et al. 2015; Lee et al. 2015; McTaggart et al. 2015; Adhikari et al. 2016; Greenway 2016; Soleimanifar et al. 2016; Yan et al. 2017; Li et al. 2018a; Poor et al. 2018b; Yan et al. 2018; Zhang et al. 2018)
		Ca-WTR	Calcium-Based Water Treatment Residuals	Ca	(Wendling et al. 2013; Adhikari et al. 2016)
		Fe-WTR	Iron-Based Water Treatment Residuals	Fe	(Brown et al. 2016; Jay et al. 2017)
		Fe-Ca-WTR	Iron- and Calcium-Based Water Treatment Residuals	Fe & Ca	(Wendling et al. 2013)
Coal Combustion Waste Products		BA	Bottom Ash	Al	(Kim et al. 2018)
		CA	Coal Ash	Al, Fe & Ca	(Wang et al. 2018)
		FA	Fly Ash	Ca	(Zhang et al. 2008; Brown et al. 2009; Wendling et al. 2013; Li et al. 2016a; Li et al. 2016b; Houle et al. 2017; Kandel et al. 2017; Li et al. 2018a; Li et al. 2018b; Zhang et al. 2018)
Metallurgical Waste Products		BFS	Blast Furnace Slag	Ca	(Li et al. 2016a; Li et al. 2016b; Sanford and Larson 2016; Li et al. 2018b;
		RM	Red Mud	Al	(Lucas and Greenway 2011; Greenway 2016)
		SC	Steel Chips	Fe	(Sellner et al. 2019)
		SS	Steel Slag	Fe & Ca	(Klimeski et al. 2014; Sellner et al. 2019)
Other		AMDR	Acid Mine Drainage Residual	Fe	(Klimeski et al. 2014)
		ICS	Iron Coated Sand	Fe	(Vandermoere et al. 2018)
		RCA	Recycled Concrete Aggregate	Ca	(Guo et al. 2015)

Table D1 (continued).

Natural Materials	Animal Shells	CS	Cockle Shell	Ca	(Goh et al. 2015; Goh et al. 2017)
		S-Sh	Seashells	Ca	(Canga et al. 2016)
		Sh-S	Shell Sand	Ca	(Wium-Andersen et al. 2012)
	Rocks & Minerals	B	Biotite	Al, Fe & Ca	(Klimeski et al. 2014)
		L	Limestone	Ca	(Chang et al. 2011; Wium-Andersen et al. 2012; Canga et al. 2016)
		MS	Medical Stone	Al	(Li et al. 2018a; Zhang et al. 2018)
		O	Olivine	Fe	(Wium-Andersen et al. 2012)
		Z	Zeolite	Al	(Wium-Andersen et al. 2012; Li et al. 2018a)
	Local Soils	IRS	Iron-Rich Soil	Fe	(Zhou et al. 2016)
		KS	Krasnozern Soil	Al & Fe	(Lucas and Greenway 2011; Greenway 2016)
Sk-S		Skye Sand	Al & Fe	(Glaister et al. 2014)	
Processed Materials	Expanded Soils	CDE	Calcined Diatomaceous Earth	Al & Fe	(Canga et al. 2016)
		EC	Expanded Clay	(not specified)	(Canga et al. 2016)
		E-Sh	Expanded Shale	Al & Fe	(Zhang et al. 2008)
	Aluminum Products	E-Sl	Expanded Slate	Al & Fe	(Passeport et al. 2009)
		AOCM	Aluminum Oxide Coated Media	Al	(Ma and Sansalone 2007)
	Iron Products	Fe-F	Iron Filings	Fe	(Erickson et al. 2012; Allred and Racharaks 2014; Weiss et al. 2016; Chang et al. 2018)
		Fe(III)-OH	Iron(III) Hydroxide	Fe	(Canga et al. 2016; Allred et al. 2017)
		IMB	Iron Modified Biochar	Fe	(Liu et al. 2015)
		Fe-O	Iron Oxide	Fe	(Lyngsie et al. 2014)
		Fe-O/OH	Iron Oxide/Hydroxide	Fe	(Allred and Racharaks 2014)
PICP		Porous Iron Composite Powder	Fe	(Allred and Racharaks 2014)	
SW-G		Steel Wool (granular)	Fe	(Erickson et al. 2007; Kratky et al. 2018)	
SW-F		Steel Wool (fabric)	Fe	(Erickson et al. 2007)	
SMIP	Sulfur-Modified Iron Powder	Fe	(Allred and Racharaks 2014)		

Table D1 (continued).

Proprietary Products	Expanded Soils	B&G	Bold & Gold™ (Expanded Clay)	Al & Fe	(Hood et al. 2013)
		FL-P	Filtralite-P™ (Expanded Clay)	Al, Fe & Ca	(Klimeski et al. 2014; Lyngsie et al. 2014; Canga et al. 2016)
	Other	F-P	Filtra P™ (Lime + Iron-Rich Gypsum)	Fe & Ca	(Klimeski et al. 2014)
		P	Phoslock™ (Lanthanum Bentonite Clay)	La	(Randall and Bradford 2013)
		S	Sachtofer™ (Iron(III) Sulfate + Lime)	Fe & Ca	(Klimeski et al. 2014)
SM	Sorbtive Media™ (Aluminum & Iron Oxides)	Al & Fe	(Randall and Bradford 2013; Duranceau and Biscardi 2015; Cording et al. 2018; Shrestha et al. 2018; Ding et al. 2019)		
Material Combinations	Al-WTR Variations	Al-WTR + A + L	Al-WTR + Alum + Limestone	Al & Ca	(Yan et al. 2017; Yan et al. 2018)
		Al-WTR + KS	Al-WTR + Krasnozem Soil	Al & Fe	(Lucas and Greenway 2011; Greenway 2016)
		Al-WTR + PHA + L	Al-WTR + Partially Hydrolyzed Al + Limestone	Al & Ca	(Yan et al. 2018)
	Other	A + L	Alum + Limestone	Al & Ca	(Yan et al. 2017)
		EC + C + L	Expanded Clay + Cement Sand + Limestone	Al, Fe & Ca	(Jones et al. 2015)
ICS + G	Iron Coated Sand + Glauconite	Al + Fe	(Vandermoere et al. 2018)		

Processed materials are rocks, minerals, and local soils that have been modified to create chemical compounds or commercial products. Unlike several of the waste and natural products, processed products are more consistent in their material compositions and can often be easily purchased from a manufacturer. Processed materials evaluated by the reviewed articles include expanded soils (calcined diatomaceous earth, expanded clay, expanded shale, expanded slate), Al products (aluminum oxide coated media), Fe products (iron filings, iron(III) hydroxide, iron modified biochar, iron oxide, iron oxide/hydroxide, porous iron composite powder, granular steel wool, steel wool fabric, sulfur-modified iron powder), and cement sand.

Proprietary products, in the context of this review, are media or media amendments specifically designed to remove P from water. Similar to processed materials, proprietary products are consistent in their material compositions and easy to purchase. Proprietary products evaluated by the reviewed articles include Bold & Gold™, Filtralite-P™, Filtra P™, Phoslock™, Sachtofer™, and Sorbtive Media™. Phoslock™ is a unique material within the evaluated amendments because its dominant metal used for sorption is lanthanum (La), whereas all other amendments are composed of Al, Fe, or Ca.

3.2 Test Methods for Laboratory Evaluations

Of the 59 records identified for this review, 39 were column studies, 13 were mesocosm studies, and 7 were field studies. Two of the field studies evaluated the same bioretention installation (Cording et al. 2018; Shrestha et al. 2018), thus leading to only six unique field installations that were identified by this review. Amendments evaluated by the field studies included expanded slate (Passeport et al. 2009), fly ash (Brown et al. 2009; Kendel et al. 2017), Sorbtive Media™ (Cording et al. 2018; Shrestha et al. 2018), and Al-WTR (Houle et al. 2017; Liu and Davis 2014). Thus, the performance of all other amendments has only been evaluated under controlled laboratory conditions, which do not account for the impacts of external factors including natural stormwater loadings and the spatial heterogeneity of full-scale bioretention systems (Johnson and Hunt 2016). Test methods used for laboratory evaluations also vary between studies, as some studies aim to simulate conditions that are more representative of actual bioretention systems, whereas other studies simplify the experiments to reduce the number of variables affecting the P balance in the system. Key factors that differ between laboratory studies include the type and concentration of P used in the influent, the method used to pass influent through the system, the

presence of vegetation, the media composition, the establishment period, and the degree of P sorption exhaustion achieved during the experiment. A summary of the test methods used to evaluate the amendment materials for the 52 laboratory studies is provided in Table D2.

While bioretention systems evaluated in field studies receive natural stormwater runoff, artificial stormwater loadings are needed for column and mesocosm studies. Due to the variability of P in stormwater runoff, most (81%) of the laboratory studies synthesized stormwater influent by mixing phosphates with deionized water, drinking water, collected runoff, or treated effluent from wastewater treatment plants to achieve desired or representative P concentrations. Some of these studies also used a range of concentrations to represent the natural variability in stormwater (Chang et al. 2018; Erickson et al. 2007; Erickson et al. 2012; Jones et al. 2015; Li et al. 2016a; Li et al. 2018a; Li et al. 2016b; Li et al. 2018b; Liu et al. 2014; Lyngsie et al. 2014; O'Neill and Davis 2012b; Stoner et al. 2012; Wium-Andersen et al. 2012). While most of the studies that synthesized the stormwater influent used P concentrations less than 5 mg/L, some studies used very high concentrations (between 5 and 80 mg/L) to accelerate sorption capacity exhaustion or evaluate sorption performance under higher loadings (Adhikari et al. 2016; Allred et al. 2017; Allred and Racharaks 2014; Ding et al. 2019; Klimeski et al. 2014, Sellner et al. 2019; Stoner et al. 2012; Wium-Andersen et al. 2012). As shown in Table D2, no standard P concentrations were used between the various studies that used synthetic stormwater. Furthermore, the common practice of synthesizing stormwater runoff using SRP solutions indicates that PP and other types of DP were generally not considered in laboratory experiments. In particular, DOP was included in the synthetic stormwater for only three of the laboratory studies (Lucas and Greenway 2011; Yan et al. 2018; Yan et al. 2017). More research is therefore needed on the performance of bioretention amendments with respect to DOP, as most studies have only analysed SRP, and both forms of DP can have variants that are bioavailable (Li and Brett 2013).

Table D2: Characteristics of test methods for laboratory studies.

Reference	Type of Test	Influent Type	TP Influent Concentration (mg/L)	Gravity Fed Influent?	Intermittent Flow?	Vegetated Surface?	Bioretention Media?	Establishment Period?	Sorption Capacity Exhausted?
(Adhikari et al. 2016)	Column	Synthetic (SRP)	80						✓
(Allred et al. 2017)	Column	Agricultural Runoff + SRP	1, 10						
(Allred and Racharaks 2014)	Column	Agricultural Runoff + SRP	1, 10						
(Brown et al. 2016)	Column	Synthetic (SRP)	1	✓	✓	✓	✓	✓	
(Canga et al. 2016)	Column	Synthetic (SRP)	0.3						
(Chang et al. 2011)	Column	Runoff + SRP	(not specified)						
(Chang et al. 2018)	Column	Synthetic (SRP)	(0.3, 0.5, 0.7)						
(Ding et al. 2019)	Column	Synthetic (SRP)	8.33 + 0.93	✓	✓		✓	✓	
(Duranceau and Biscardi 2015)	Column	Surface Water	0.05 to 0.11						
(Erickson et al. 2007)	Column	Synthetic (SRP)	0.1 to 0.8	✓	✓				
(Erickson et al. 2012)	Column	Synthetic (SRP)	0.233 to 0.531	✓	✓				
(Glaister et al. 2014)	Column	Synthetic (SRP + Sediment)	0.35	✓	✓	✓	✓	✓	
(Goh et al. 2015)	Column	Runoff	5.25	✓			✓		
(Goh et al. 2017)	Mesocosm	Runoff	5.67	✓		✓	✓	✓	
(Greenway 2016)	Mesocosm	Tertiary Effluent	3.63, 4.80	✓	✓	✓	✓		
(Guo et al. 2015)	Column	Runoff, Runoff + SRP	0.22, 1.8	✓	✓		✓		
(Hood et al. 2013)	Mesocosm	Runoff + SRP	0.25	✓	✓	✓		✓	
(Jay et al. 2017)	Column	Synthetic (SRP), Runoff	1.71, 0.08	✓	✓		✓		
(Jones et al. 2015)	Column	Synthetic (SRP), Runoff + SRP	0.5, 1						✓
(Kim et al. 2018)	Column	Runoff	0.3 to 1						
(Klimeski et al. 2014)	Column	Synthetic (SRP)	50	✓					✓
(Kratky et al. 2018)	Column	Synthetic (SRP + Sediment)	2	✓	✓	✓	✓		
(Lee et al. 2015)	Column	Secondary Effluent	1.52		✓		✓		
(Li et al. 2016a)	Mesocosm	Synthetic (SRP)	0.5, 1.5, 2.5	✓	✓		✓		
(Li et al. 2018a)	Mesocosm	Synthetic (SRP)	1, 1.5, 2.5	✓	✓	✓	✓	✓	

(Li et al. 2016b)	Mesocosm	Synthetic (SRP)	0.5, 1.5, 2.5	✓	✓	✓	✓		
-------------------	----------	-----------------	---------------	---	---	---	---	--	--

Table D2 (continued).

(Li et al. 2018b)	Mesocosm	Synthetic (SRP)	1, 2.5	✓	✓	✓	✓		✓
(Liu et al. 2014)	Mesocosm	Synthetic (SRP)	0.1 to 1	✓	✓	✓	✓	✓	
(Liu et al. 2015)	Column	Agricultural Runoff	1.86 to 2.47	✓	✓				
(Lucas and Greenway 2011)	Mesocosm	Synthetic (SRP + DOP)	0.37 to 0.49	✓	✓	✓	✓	✓	
(Lyngsie et al. 2014)	Column	Synthetic (SRP)	0.05 to 1						✓
(Ma and Sansalone 2007)	Column	Synthetic (SRP)	0.5						✓
(McTaggart et al. 2015)	Column	Synthetic (SRP + Sediment)	0.27 to 0.37						
(O'Neill and Davis 2012a)	Column	Synthetic (SRP)	0.12		✓		✓		✓
(O'Neill and Davis 2012b)	Column	Synthetic (SRP)	0.0685 to 0.437	✓	✓	✓	✓		
(Palmer et al. 2013)	Mesocosm	Runoff + SRP	0.397 to 0.485	✓	✓	✓	✓	✓	
(Poor et al. 2018b)	Mesocosm	Runoff	0.04 to 0.5	✓	✓	✓	✓	✓	
(Randall and Bradford 2013)	Mesocosm	Synthetic (SRP)	0.568	✓	✓	✓	✓	✓	
(Sanford and Larson 2016)	Column	Synthetic (SRP)	2		✓				
(Sellner et al. 2019)	Column	Synthetic (SRP), Agricultural Runoff + SRP, Runoff + SRP, Tertiary Effluent + SRP	1, 10, 50						✓
(Soleimanifar et al. 2016)	Column	Synthetic (SRP)	2.3	✓					
(Stoner et al. 2012)	Column	Synthetic (SRP)	0.5, 1, 5, 10, 15						✓
(Vandermoere et al. 2018)	Column	Synthetic (SRP)	0.5	✓					
(Wang et al. 2018)	Column	Synthetic (SRP)	3	✓	✓		✓		
(Weiss et al. 2016)	Mesocosm	Drinking Water	0.54	✓	✓	✓	✓		
(Wendling et al. 2013)	Column	Surface Water	0.69						✓
(Wium-Andersen et al. 2012)	Column	Synthetic (SRP)	0.09 to 9.7						
(Yan et al. 2017)	Column	Synthetic (SRP + DOP)	0.2				✓		✓
(Yan et al. 2018)	Column	Synthetic (SRP + DOP)	0.1						✓
(Zhang et al. 2018)	Column	Synthetic (SRP)	1				✓		✓
(Zhang et al. 2008)	Column	Synthetic (SRP)	1						✓
(Zhou et al. 2016)	Column	Synthetic (SRP)	0.8	✓	✓			✓	
Total number of laboratory studies meeting criteria (out of 52)				29	27	16	25	12	14

In lieu of synthesizing stormwater influent, six of the laboratory studies directly used unaltered urban stormwater runoff as influent in the experiments (Goh et al. 2015; Goh et al. 2017; Guo et al. 2015; Jay et al. 2017; Kim et al. 2018; Poor et al. 2018b). The concentrations of TP in the collected runoff ranged from 0.04 mg/L to 5.67 mg/L within these studies, whereas TP concentrations in bioretention influent are typically in the range of 0.07 mg/L to 0.26 mg/L (Clary et al. 2017). Thus, while the use of actual stormwater better represents field conditions, the collected stormwater can introduce additional variability in controlled laboratory experiments, and P concentrations in collected stormwater may not be representative of typical concentrations. Other direct sources for stormwater influent in the laboratory studies included agricultural runoff, surface water, drinking water, and treated effluent from wastewater treatment plants. The use of drinking water in the study by Weiss et al. (2016) was because the local water supply was treated with phosphates to inhibit corrosion and leaching of lead, which resulted in an SRP concentration in the drinking water of 0.50 mg/L. Similarly, drinking water containing 0.91 mg/L SRP was used in the study by Ding et al. (2019) to create a 5 cm layer of artificial snow on top of the column that was tested under freeze-thaw cycles in addition to the regular influent dosing.

Dosing methods for stormwater influent varied between the laboratory studies. Influent was gravity fed through the media for 56% of the laboratory studies and pumped through the media, typically using an upward flow configuration, for the remaining studies. While pumping influent through the column or mesocosm allows for better control over flow rates and contact time with the media, gravity feeding the influent better simulates field conditions and actual contact times by allowing for stormwater to percolate through the system based on the media's hydraulic conductivity. To simulate the natural wetting and drying periods that occur in the field, 52% of the laboratory studies used intermittent flow dosing. This cycling better represents P removal processes, as it allows for the slower irreversible adsorption processes to occur during dry periods, freeing up available adsorptive surfaces for subsequent tests (Lucas and Greenway 2011). These freed-up surfaces are then quickly filled when influent is re-introduced to the media (O'Neill and Davis 2012b). For Fe-based media amendments, dry periods promote rust formation, which creates new sorption sites (Erickson et al. 2012; Sellner et al. 2019; Weiss et al. 2016). Dry periods can, however, also convert amorphous Al and Fe oxides to less-reactive crystalline forms, reducing the number of available sorption sites (O'Neill and Davis 2012a).

Experiment durations varied greatly between the laboratory studies, ranging from single events to several years of data collection. Cumulative P loadings were therefore inconsistent, resulting in decreased sorption performance for experiments where amended media became partially or fully exhausted. As shown in Table D2, 27% of the studies loaded the columns or mesocosms until sorption capacity was exhausted. This practice was typically carried out to measure the sorption capacity of amended media under flow-through conditions, providing a more realistic capacity measurement compared to the equilibrium conditions of batch tests (Lyngsie et al. 2014). As a result, such laboratory experiments typically accelerate media exhaustion by introducing high P concentrations in the influent or continuously pumping influent through the media, which cannot be achieved in the field.

Column and mesocosm studies typically test new systems where the media and vegetation have not yet been established at the beginning of the experiments. This can result in P leaching from the media throughout the test period or during the initial phases of the experiment (Brown et al. 2016; Hood et al. 2013; Jay et al. 2017; Lucas and Greenway 2011; Zhang et al. 2018). As shown in Table D2, only 23% of the laboratory studies provided establishment periods prior to carrying out the experiments to allow for vegetation growth, microbial development, media settling, and initial leaching of mobile P from organic material in the media. These establishment periods typically consisted of irrigating the columns or mesocosms for a duration of four weeks or greater. In addition to or in lieu of irrigation, three of the studies dosed the experiments with the same stormwater influent used in the subsequent testing period (Glaister et al. 2014; Lucas and Greenway 2011; Palmer et al. 2013).

As shown in Table D2, only 31% of the evaluated laboratory studies included a living vegetation layer in their experiments. While this percentage is partially attributed to the inclusion of sand filter studies in this review, it still indicates that only 16 laboratory studies have evaluated the combined impacts of vegetation and media amendments on P removal in bioretention systems. However, plant and microbial uptake have been shown to increase the amount of P removed in both amended and non-amended bioretention media (Brown et al. 2016; Glaister et al. 2014; Lucas and Greenway 2008; Lucas and Greenway 2011). The overall performance of the system therefore depends on the presence and type of vegetation. Bioretention vegetation also requires a proper growing medium, and while none of the evaluated studies identified toxicity concerns for

the plants, the impact of the amendment materials on the survivability of bioretention plants cannot be evaluated for studies that do not include vegetation.

The composition of the filter media also varied between the laboratory studies, creating additional variation in the performance of the amended media. For example, leaching was observed in the study by Jay et al. (2017) where organic material was intentionally mixed at unconventionally high ratios (17.5% and 35% by volume) to evaluate the impacts of Fe-WTR on P leaching. The type of organic material mixed into the bioretention media also impacts P sorption performance, as the use of hardwood bark mulch in lieu of compost products can increase moisture retention in the media during dry periods, preventing crystallization and adsorption capacity loss (O'Neill and Davis 2012a). As shown in Table D2, 48% of the laboratory studies used a typical bioretention mixture that included both soils and organic materials, whereas the remaining studies (including all sand filter studies) omitted organic materials or performed experiments on the amendment material only. Experiments that omit organic materials or that use media containing impractically high ratios of the amendment materials may therefore overestimate the performance of the amendment compared to using a media that is intended to support vegetation growth. In addition to the filter media composition, only 32% of the laboratory studies that used a bioretention mixture also reported using an organic-based or unspecified mulch layer on top (Ding et al. 2019; Kratky et al. 2018; Li et al. 2016a; Li et al. 2018a; Li et al. 2018b; Li et al. 2016b; Randall and Bradford 2013; Weiss et al. 2016). While an organic-based mulch layer is commonly used in bioretention systems to help with plant survival, pre-treatment, and erosion protection, the organic material contained within the mulch can potentially leach DP into the system (Hsieh and Davis 2005).

Finally, nine of the laboratory studies included experiments where an amended layer was placed above or below the media layer (Chang et al. 2018; Kim et al. 2018; Kratky et al. 2018; Li et al. 2016a; Li et al. 2016b; Poor et al. 2018b; Randall and Bradford 2014; Weiss et al. 2016; Wendling et al. 2013). Having the amended layer above the media layer concentrates P treatment near the top, which is where most of the P is treated in unamended bioretention systems (Johnson and Hunt 2016; Komlos and Traver 2012; Muerdter et al. 2016; Willard et al. 2017).

Alternatively, having the amended layer below the media layer allows for any potential leaching from the organic matter content to occur prior to sorption processes with the amendment material. For one study, the amended layer was placed between an organic matter layer and a

sand layer (Poor et al. 2018b), maximizing both potential benefits while maintaining the components of the bioretention media. These alternative amendment configurations therefore impact the treatment processes in the system compared to amending the entire media.

3.3 Phosphorus Removal

Most published studies report *removal efficiencies* or *removal rates* calculated as a relative percent decrease in either concentration or mass of P between the inlet and outlet of a bioretention system. Here, for clarity, these quantities are reported using the terms *percent concentration reductions* or *percent mass reductions*. The TP and SRP percent concentration and mass reductions reported by the reviewed articles for each amendment are summarized in Figure D3(i), D3(ii) D3(iii) and D3(iv). Results for the individual experiments are provided in Table D3, which also includes reported effluent concentrations. Overall, highly variable results were observed between the different amendments and between experiments on the same amendments, with both percent concentration and mass reductions of P ranging from negative (leaching) to 100% (complete removal). While only zero and positive percent reductions were reported in Figure D3(i), D3(ii), D3(iii), and D3(iv), leaching was observed in some of the experiments for calcined diatomaceous earth, expanded slate, fly ash, iron filings, Kraznozern soil, steel wool, Al-WTR, Fe-WTR, and zeolite (Canga et al. 2016; Chang et al. 2018; Erickson et al. 2007; Jay et al. 2017; Lucas and Greenway 2011; O'Neill and Davis 2012a; Palmer et al. 2013; Passeport et al. 2009; Poor et al. 2018b; Wium-Andersen et al. 2012; Zhang et al. 2018). The variability in the results was partially attributed to the differences in reporting methods, as some studies reported all measured values, others provided average values for each of the tested stormwater events, and others provided average or median values for the entire experiment. Variability was also attributed to the differences in the test methods used for the laboratory experiments, as previously described.

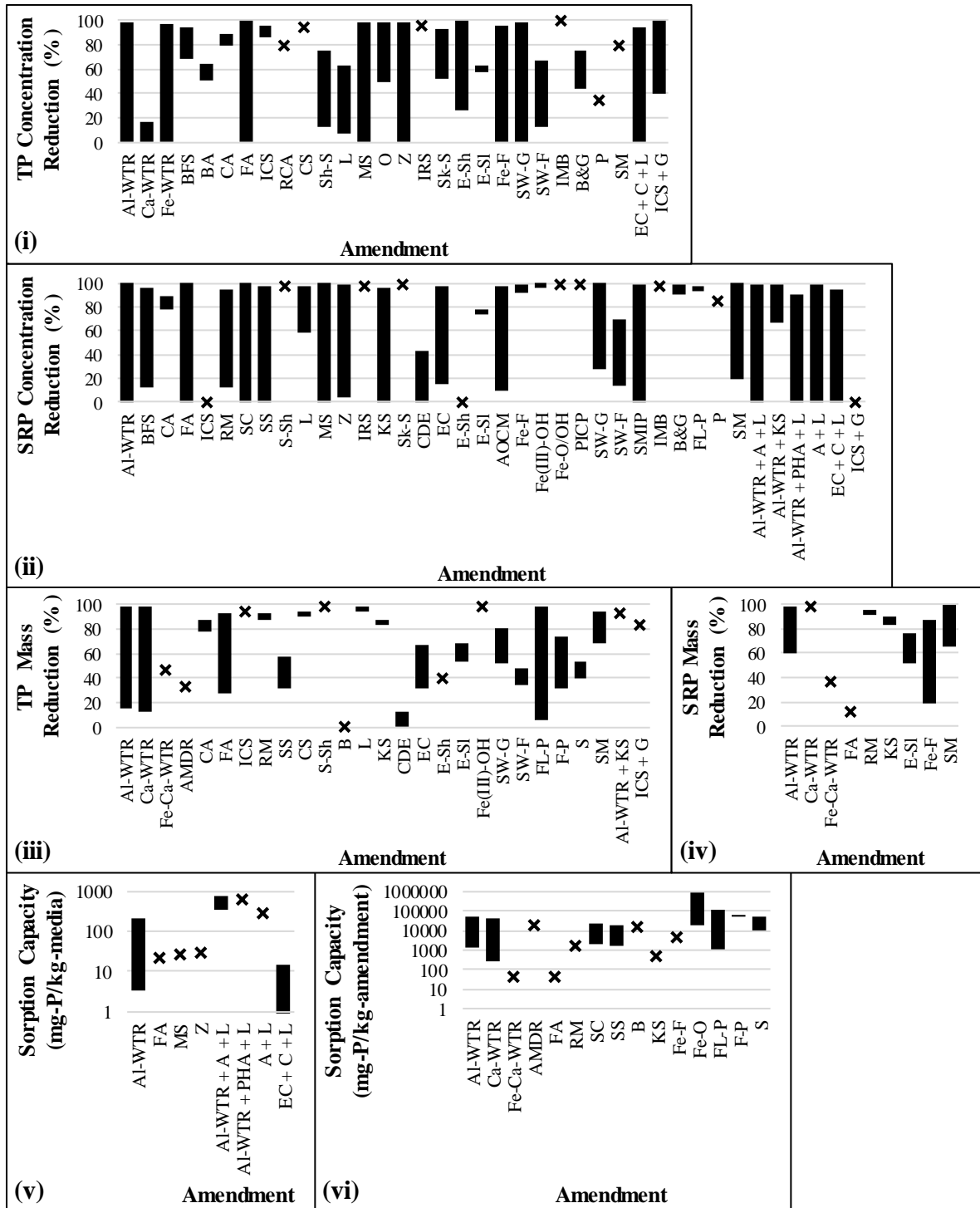


Figure D3: Percent concentration reductions for (i) TP and (ii) SRP; percent mass reductions for (iii) TP and (iv) SRP; and P sorption capacities reported as mg of P per (v) kg of media and (vi) kg of amendment. Bars represent the full range of reported values and points represent singular reported values if there is no range. Only percent reductions equal to or greater than zero were included in D3(i), D3(ii), D3(iii), and D3(iv).

Table D3: Summary of phosphorus removal results reported in reviewed studies.

Amendment Material(s)	Reference	Fraction of Amendment in Media ^{a,b}	Percent Mass Reduction ^c		Percent Concentration Reduction ^{c,d}		Effluent Concentration ^{c,d}	
			TP (%)	SRP (%)	TP (%)	SRP (%)	TP (µg/L)	SRP (µg/L)
Acid Mine Drainage Residual	(Klimeski et al. 2014)	100%	33	-	-	-	-	-
Alum + Limestone	(Yan et al. 2017)	30% (M)	-	-	-	0 to 99	-	< 10 to 200
Aluminum & Iron Oxides (Sorbitive Media TM)	(Randall and Bradford 2013)	100% (LB)	-	-	79	90	113	55
	(Duranceau and Biscardi 2015)	10% (V)	-	-	-	20 to 100	-	10 to 80
	(Cording et al. 2018)	100% (LB)	68 to 71	65 to 94	-	-	17 to 151	2 to 32
	(Ding et al. 2018)	3.7% (V)	-	98 to 100	-	-	-	< 90
	(Shrestha et al. 2018)	100% (LB)	86 to 94	94	-	-	1.4	1.3
Aluminum Oxide Coated Media	(Ma and Sansalone 2007)	100%	-	-	-	9 to 97	-	-
Biotite	(Klimeski et al. 2014)	100%	1	-	-	-	-	-
Blast Furnace Slag	(Li et al. 2016a)	50% (V)	-	-	81 to 94	89 to 96	-	-
	(Li et al. 2016a)	100%	-	-	91 to 95	94 to 96	-	-
	(Li et al. 2016b)	50% (V)	-	-	71 to 79	-	-	-
	(Li et al. 2016b)	100%	-	-	68 to 79	-	-	-
	(Sanford and Larson 2016)	100%	-	-	-	12 to 62	-	-
	(Sanford and Larson 2016)	(NS)	-	-	-	12 to 48	-	-
	(Li et al. 2018b)	100%	-	-	-	63 to 94	-	60 to 780
	(Li et al. 2018b)	50% (V)	-	-	-	40 to 88	-	120 to 720
Bottom Ash	(Kim et al. 2018)	100% (LB)	-	-	52 to 64	-	-	-
	(Kim et al. 2018)	100% (LA)	-	-	51 to 65	-	-	-
Calcined Diatomaceous Earth	(Canga et al. 2016)	100%	-83 to 13	-	-	-1,420 to 43	-	171 to 725
Coal Ash	(Wang et al. 2018)	50%	80 to 88	-	79 to 89	78 to 89	-	330 to 650
	(Wang et al. 2018)	33%	78 to 88	-	82 to 89	81 to 88	-	350 to 560
Cockle Shell	(Goh et al. 2015)	10% (V)	-	-	94 to 96	-	230 to 320	-
	(Goh et al. 2017)	10% (V)	90 to 95	-	-	-	450	-
Expanded Clay	(Canga et al. 2016)	100%	31 to 67	-	-	15 to > 97	-	< 10 to 254

Table D3 (continued).

Expanded Clay (Bold & Gold™)	(Hood et al. 2013)	75% (V)	-	-	44 to 76	90 to 99	-	-
Expanded Clay (Filtralite-P™)	(Klimeski et al. 2014)	100%	6 to 8	-	-	-	-	-
	(Lyngsie et al. 2014)	(NS)	-	-	-	-	-	-
	(Canga et al. 2016)	100%	95 to 99	-	-	93 to > 97	-	< 10 to 22
Expanded Clay + Cement Sand + Limestone	(Jones et al. 2015)	80% (V)	-	-	0 to 95	0 to 95	50 to 1,000	50 to 1,000
Expanded Shale	(Zhang et al. 2008)	100%	40	-	26 to 100	-	-	-
Expanded Slate	(Passeport et al. 2009)	80%	53 to 68	52 to 77	58 to 63	74 to 78	51 to 58	13 to 15
Fly Ash	(Zhang et al. 2008)	2.5% (M)	66	-	24 to 100	-	0 to 760	-
	(Zhang et al. 2008)	5% (M)	85	-	72 to 100	-	0 to 280	-
	(Brown et al. 2009)	5% (M)	-	-	-	-	-	50 to 70
	(Waldrop et al. 2009)	50% (V)	-	-	-	57 to 98	-	10 to 90
	(Wendling et al. 2013)	50% (M) (LB)	27	12	-	-	-	-
	(Li et al. 2016a)	50% (V)	-	-	98 to 100	95 to 99	-	-
	(Li et al. 2016b)	20% (V)	-	-	81 to 87	-	-	-
	(Houle et al. 2017)	10% (V)	-	-	32	-	-	-
	(Kandel et al. 2017)	5% (M)	76 to 93	-	64 to 75	-	30 to 80	-
	(Li et al. 2018a)	10% (M)	-	-	86 to 99	91 to 100	-	-
	(Li et al. 2018b)	50% (V)	-	-	-	63 to 97	-	30 to 500
(Zhang et al. 2018)	10% (M)	-	-	-62 to 55	-23 to 77	430 to 1,550	220 to 1,180	
Iron Coated Sand	(Vandermoere et al. 2018)	100%	94	-	86 to 96	-	20 to 70	-
Iron Coated Sand + Glauconite	(Vandermoere et al. 2018)	100%	84	-	40 to 100	-	0 to 300	-

Table D3 (continued).

Iron Filings	(Erickson et al. 2012)	0.3 (M)	-	18	-	-	-	271
	(Erickson et al. 2012)	2% (M)	-	79	-	-	-	66
	(Erickson et al. 2012)	5% (M)	-	88	-	-	-	36
	(Allred and Racharaks 2014)	100%	-	-	-	94 to > 99	-	< 9 to 63
	(Weiss et al. 2016)	5% (M) (LB)	-	-	75 to 93	92 to 98	-	-
	(Chang et al. 2018)	3.8% (V)	-	-	47 to 83	-	100 to 180	-
	(Chang et al. 2018)	3.8% (V) (LA)	-	-	-167 to 64	-	240 to 1300	-
	(Chang et al. 2018)	5% (V)	-	-	-695 to 96	-	28 to 2400	-
Iron(III) Hydroxide	(Canga et al. 2016)	100%	98 to 100	-	-	> 97	-	< 10
	(Allred et al. 2017)	100%	-	-	-	96 to 100	-	4 to 40
Iron Modified Biochar	(Liu et al. 2015)	5% (M)	-	-	99 to 100	97 to 98	10 to 20	10 to 20
Iron Oxide	(Lyngsie et al. 2014)	(NS)	-	-	-	-	-	-
Iron Oxide/Hydroxide	(Allred and Racharaks 2014)	100%	-	-	-	> 99	-	< 9
Iron-Rich Gypsum + Lime (Filtru P™)	(Klimeski et al. 2014)	100%	32 to 74	-	-	-	-	-
Iron-Rich Soil	(Zhou et al. 2016)	15% (M)	-	-	95 to 97	96 to 98	-	-
Iron(III) Sulfate + Lime (Sachtofer™)	(Klimeski et al. 2014)	100%	40 to 54	-	-	-	-	-
Krasnozem Soil	(Lucas and Greenway 2011)	14% (M)	-	-	-	-100 to 96	-	12 to 1000
	(Lucas and Greenway 2011)	30% (M)	-	-	-	0 to 92	-	44 to 340
	(Greenway 2016)	14% (M)	87	90	-	-	-	-
	(Greenway 2016)	30% (M)	83 to 86	83 to 89	-	-	-	-
Lanthanum Bentonite Clay (Phoslock™)	(Randall and Bradford 2013)	14% (M)	-	-	34	85	365	77
Limestone	(Chang et al. 2011)	10% (M)	-	-	-	59 to 67	-	-
	(Wium-Andersen et al. 2012)	100%	-	-	7 to 63	-	-	-
	(Canga et al. 2016)	100%	95 to 99	-	-	87 to > 97	-	< 10 to 38
Medical Stone	(Li et al. 2018a)	10% (M)	-	-	92 to 99	92 to 100	-	-
	(Li et al. 2018a)	2.5% (M)	-	-	93 to 99	92 to 99	-	-
	(Zhang et al. 2018)	10% (M)	-	-	-35 to 83	-2 to 93	170 to 1,300	70 to 980
Olivine	(Wium-Andersen et al. 2012)	100%	-	-	49 to 98	-	-	-

Table D3 (continued).

Porous Iron Composite Powder	(Allred and Racharaks 2014)	100%	-	-	-	> 99	-	< 9
Red Mud	(Lucas and Greenway 2011)	5% (M)	-	-	-	12 to 95	-	16 to 330
	(Lucas and Greenway 2011)	9% (M)	-	-	-	44 to 91	-	28 to 290
	(Greenway 2016)	5% (M)	88	92	-	-	-	-
	(Greenway 2016)	9% (M)	93	96	-	-	-	-
Recycled Concrete Aggregate	(Guo et al. 2015)	10% (M)	-	-	80	-	-	-
Seashells	(Canga et al. 2016)	100%	99	-	-	> 97	-	< 10
Shell Sand	(Wium-Andersen et al. 2012)	100%	-	-	12 to 75	-	-	-
Skye Sand	(Glaister et al. 2014)	95% (V)	-	-	52 to 93	98 to 99	25 to 190	1 to 4
Steel Chips	(Sellner et al. 2019)	100%	-	-	-	0 to 100	-	0 to 50,000
Steel Slag	(Klimeski et al. 2014)	100%	32 to 58	-	-	-	-	-
	(Sellner et al. 2019)	100%	-	-	-	0 to 98	-	200 to 10,000
Steel Wool (granular)	(Erickson et al. 2007)	2% (M)	52 to 81	-	-3 to 98	28 to 100	-	-
	(Kratky et al. 2018)	0.5% (M) (LB)	-	-	-	88 to 100	-	-
Steel Wool (fabric)	(Erickson et al. 2007)	100% (LB)	34 to 48	-	-13 to 67	14 to 70	-	-
Sulfur-Modified Iron Powder	(Allred and Racharaks 2014)	100%	-	-	-	> 99	-	< 9

Table D3 (continued).

Al-WTR	(Lucas and Greenway 2011)	20% (M)	-	-	-	82 to 99	-	2 to 90
	(O'Neill and Davis 2012a)	4% (M)	-	-	-37 to 79	15 to 80	-	-
	(O'Neill and Davis 2012b)	5% (M)	89	-	42 to > 92	> 85 to > 98	<10 to 70	<10 to 20
	(Stoner et al. 2012)	(NS)	-	-	11 to 55	-	-	-
	(Palmer et al. 2013)	10% (V)	-	-	-67 to 27	58 to 81	330 to 680	73 to 160
	(Randall and Bradford 2013)	20% (M)	-	-	78	85	120	76
	(Liu et al. 2014)	3% (V)	-	-	81 to 95	-	-	-
	(Liu et al. 2014)	12% (V)	-	-	85 to 97	-	-	-
	(Liu and Davis 2014)	5% (M)	84	60	-	-	50 to 117	10 to 280
	(Duranceau and Biscardi 2015)	10% (V)	-	-	-	12 to 100	-	3 to 74
	(Guo et al. 2015)	10% (M)	-	-	87 to 93	-	-	-
	(Lee et al. 2015)	10% (M)	-	-	87 to 98	94 to 100	30 to 200	0 to 94
	(McTaggart et al. 2015)	100%	-	-	7 to 77	-	-	-
	(Adhikari et al. 2016)	100%	16	-	0 to 23	-	61,500 to 80,000	-
	(Greenway 2016)	20% (M)	98	97 to 99	-	-	-	-
	(Soleimanifar et al. 2016)	33% (M)	-	-	48 to 94	-	-	-
	(Yan et al. 2017)	10% (M)	-	-	-	0 to 99	-	< 10 to 200
	(Li et al. 2018a)	10% (M)	-	-	91 to 99	91 to 100	-	-
	(Poor, Conkle et al. 2018)	10%	-	-	-3,200 to -150	-14,000 to -500	600 to 2,800	400 to 2,300
	(Poor, Conkle et al. 2018)	10% (LB)	-	-	-880 to 26	-560 to -16	200 to 400	50 to 200
(Yan et al. 2018)	10% (M)	-	-	-	0 to > 90	-	< 10 to 100	
(Zhang et al. 2018)	10% (M)	-	-	16 to 92	17 to 93	70 to 810	70 to 800	
Al-WTR + Alum + Limestone	(Yan et al. 2017)	40% (M)	-	-	-	5 to 99	-	< 10 to 200
	(Yan et al. 2018)	(NS)	-	-	-	0 to > 90	-	< 10 to 100
Al-WTR + Krasnozem Soil	(Lucas and Greenway 2011)	29% (M)	-	-	-	67 to 99	-	3 to 200
	(Greenway 2016)	29% (M)	93	94	-	-	-	-

Table D3 (continued).

Al-WTR + Partially Hydrolyzed Al + Limestone	(Yan et al. 2018)	(NS)	-	-	-	0 to > 90	-	< 10 to 100
Ca-WTR	(Adhikari et al. 2016)	100%	13	-	<i>0 to 16</i>	-	67,000 to 80,000	-
	(Wendling et al. 2013)	50% (M) (LB)	98	98	-	-	-	-
Fe-WTR	(Brown et al. 2016)	2% (M)	-	-	<i>91 to 97</i>	-	30 to 90	-
	(Brown et al. 2016)	4% (M)	-	-	<i>77 to 90</i>	-	100 to 230	-
	(Jay et al. 2017)	1% (M)	-	-	<i>-6,200 to -3,700</i>	-	3,000 to 5,000	-
	(Jay et al. 2017)	2% (M)	-	-	<i>-6,200 to -4,900</i>	-	4,000 to 5,000	-
Fe-Ca-WTR	(Wendling et al. 2013)	50% (M) (LB)	46	37	-	-	-	-
Zeolite	(Wium-Andersen et al. 2012)	100%	-	-	<i>-2 to 31</i>	-	-	-
	(Li et al. 2018a)	10% (M)	-	-	<i>89 to 99</i>	86 to 99	-	-
	(Li et al. 2018a)	2.5% (M)	-	-	<i>94 to 99</i>	90 to 98	-	-
	(Zhang et al. 2018)	10% (M)	-	-	<i>-40 to 78</i>	4 to 90	220 to 1,350	90 to 920

^aNS = value not specified in record.

^bM = fraction of amendment material in media is measured on a mass basis; V = fraction of amendment material in media is measured on a volume basis; LA = amendment layer was placed above the media layer; LB = amendment layer was placed below the media layer, between two media layers, or between a media layer and an organic matter layer

^cThe full range of values provided by each study is reported. If a study presented data graphically, the range was read visually from the graph (when legible). Results for vegetated systems are reported if a study includes both vegetated and non-vegetated experiments. Results for intermittent flow conditions are reported if the study includes both intermittent and continuous flow experiments.

^d*Italicized numbers indicate percent concentration reductions calculated from influent and effluent concentrations, or effluent concentration was calculated from percent concentration reduction and influent concentration.*

The impacts of accelerated loading on P sorption capacity during column and mesocosm experiments also contributed to several of the large ranges and low values of P percent concentration and mass reductions reported in Figure D3(i), D3b(ii) D3(iii), and D3(iv). Column and mesocosm experiments are sometimes used to evaluate the sorption capacity of the amended media by loading the experimental system until the sorption capacity of the media is exhausted, as these types of laboratory experiments can allow for the media to be subject to high stormwater loads in shorter periods of time than what would occur in a natural outdoor environment. A summary of the sorption capacity results from these studies expressed as mass of P removed per mass of media or per mass of amendment is provided in Figure D3(v) and D3(vi), respectively. Results for the individual experiments are provided in Table D4. As shown in Figure D3(v) and D3(vi), the media P sorption capacities also vary between amendments and between experiments on the same amendments, which is partially attributed to the previously discussed differences in evaluation methods and media compositions. Furthermore, sorption capacities were likely underestimated in four of the studies for some of the experiments where the media was not fully exhausted at the end of the experiments (Erickson et al. 2012; Lucas and Greenway 2011; O'Neill and Davis 2012; Sellner et al. 2019).

Table D4: Sorption capacities estimated from column and mesocosm exhaustion tests.

Amendment Material	Reference	P Sorption Capacity (mg-P / kg-media)^b	P Sorption Capacity (mg-P / kg-amendment)^b
Acid Mine Drainage Residual	Klimeski et al. (2014)	-	18,600
Alum + Limestone	Yan et al. (2017)	293	-
Biotite	Klimeski et al. (2014)	-	16,000
Expanded Clay (Filtralite-P TM)	Klimeski et al. (2014)	-	1,100 to 1,600
	Lyngsie et al. (2014)	-	3,200 to 116,000
Expanded Clay + Cement Sand + Limestone	Jones et al. (2015)	0.143 to 15.1	-
Fly Ash	Wendling et al. (2013)	-	42
	Zhang et al. (2018)	22.09	-
Iron Filings	Erickson et al. (2012) ^a	-	4,800
Iron Sulfate & Lime (Sachtofer TM)	Klimeski et al. (2014)	-	9,900 to 55,200
Iron Oxide	Lyngsie et al. (2014)	-	17,000 to 889,000
Iron-Rich Gypsum + Lime (Filtra P TM)	Klimeski et al. (2014)	-	53,200 to 69,000
Krasnozern Soil	Lucas and Greenway (2011) ^a	-	500
Medical Stone	Zhang et al. (2018)	25.95	-
Red Mud	Lucas and Greenway (2011) ^a	-	1,700
Steel Chips	Sellner et al. (2019) ^a	-	2,180 to 22,700
Steel Slag	Klimeski et al. (2014)	-	6,100 to 19,800
	Sellner et al. (2019)	-	1,500
Al-WTR	Lucas and Greenway (2011) ^a	-	1,400
	O'Neill and Davis (2012a)	8.1 to 52.2	-
	O'Neill and Davis (2012b) ^a	3.18	-
	Adhikari et al. (2016)	-	55,300
	Yan et al. (2017)	156	-
	Yan et al. (2018)	214	-
	Zhang et al. (2018)	94.29	-
Al-WTR + Alum + Limestone	Yan et al. (2017)	750	-
	Yan et al. (2018)	337	-
Al-WTR + Partially Hydrolyzed Al + Limestone	Yan et al. (2018)	660	-
Ca-WTR	Adhikari et al. (2016)	-	44,500
	Wendling et al. (2013)	-	254
Fe-Ca-WTR	Wendling et al. (2013)	-	40
Zeolite	Zhang et al. (2018)	29.38	-

^aSorption capacity of media was not fully exhausted.

^bThe full range of values provided by each study is reported. Results for vegetated systems are reported if a study includes both vegetated and non-vegetated experiments. Results for intermittent flow conditions are reported if the study includes both intermittent and continuous flow experiments.

For the seven field studies, the percent concentration reductions ranged from 32 to 75% for TP and from 74 to 78% for SRP, and the percent mass reductions ranged from 53 to 94% for TP and from 52 to 94% for SRP. Four of the studies also compared the monitoring results with those from similar unamended bioretention cells and found that the use of amendments significantly improved P removal (Brown et al. 2009; Cording et al. 2018; Liu and Davis 2014; Shrestha et al. 2018). For example, Brown et al. (2009) evaluated a bioretention cell that was hydraulically

divided into a fly ash amended region and an unamended region, and the study found that the use of fly ash reduced effluent SRP concentrations by approximately half. Liu and Davis (2014) rototilled Al-WTR into the top 400 mm of a bioretention cell, which increased the TP percent mass reduction from 55 to 84%. Shrestha et al. (2018) demonstrated that a Sorptive Media layer decreased both TP and SRP masses in a bioretention cell by up to 94%, whereas a similar bioretention cell without the amendment leached P. These results confirmed those from a previous monitoring period of the same bioretention installation where TP and SRP percent mass reductions were observed to be up to 71% and 94%, respectively (Cording et al. 2018). Whereas six of the studies evaluated relatively new bioretention systems that were less than five years in age, one study evaluated a seven-year old system and found that the amendment material (fly ash) was not yet exhausted and that the sorbed P was tightly bond to the media (Kandal et al. 2017). While the results from these seven studies indicate that amended bioretention cells generally performed well at retaining P, they only provided singular examples for the individual amendments, highlighting the current lack of field studies on amended bioretention systems.

The remaining 52 column and mesocosm studies generally also reported high percent concentration reductions, percent mass reductions, and sorption capacities for most of the amendments, or they demonstrated that the amendments improved P removal compared to unamended conditions. For example, a 75% concentration or mass reduction was achieved during the column and mesocosm experiments for 71% of the amendments with respect to TP and 85% of the amendments with respect to SRP. However, evaluation methodologies and media composition differed greatly between studies. The relative performance between different amendments can therefore only be compared within individual studies where the test methods were similar for the different amendments. Furthermore, aside from the sorption capacity estimations provided by some of the column and mesocosm studies, current research does not provide evidence supporting sorption lifespans of amendments in a bioretention media setting.

3.4 Constructability and Operational Challenges

While the bioretention media amendments presented in Table D1 generally improved P sorption, various constructability and operational challenges have been identified for several of the amendments. For example, some amendments require initial processing prior to or while being

incorporated into the bioretention media. Waste materials such as steel chips and steel slag may need to be washed to remove fine particles and oil then dried and sieved to obtain desired particle sizes (Sellner et al. 2019), and materials such as iron filings may need to be ground to achieve specific particle sizes (Chang et al. 2018). Similarly, while raw Al-WTR obtained from treatment plants are sometimes available as a fine powder that can be easily mixed into bioretention media (Poor et al. 2018b), more often they are heterogeneous, clumpy, moist, and consist of variable particle sizes that first need to be mixed, dried, broken up and sieved (Adhikari et al. 2016; Duranceau and Biscardi 2015; McTaggart et al. 2015; O'Neill and Davis 2012a; Palmer et al. 2013; Randall and Bradford 2013; Soleimanifar et al. 2016; Yan et al. 2018; Yan et al. 2017; Zhang et al. 2018). The resultant particle size distribution after sieving also impacts the performance of Al-WTR, as smaller particles have higher specific surface areas and increased sorption potential than coarser particles (Lucas and Greenway 2011; Randall and Bradford 2013). The initial preparation performed for Al-WTR in several of the studies highlights the need to develop best practices for incorporating Al-WTR into bioretention cells. While the above preparation methods are relatively simple processes, some amendment materials such as alum require more complex mixing processes and alkaline consumption that may not be practical for field-scale implementation (Yan et al. 2017; Yan et al. 2018).

It has been suggested that some Fe-based amendments may present operational issues if the bioretention media is exposed to prolonged saturated conditions (Ding et al. 2019; O'Neill and Davis 2012a; Shrestha et al. 2018), as this may produce anaerobic conditions that reduce and solubilize Fe(III) to Fe(II), thus releasing Fe(III)-adsorbed P (Mitsch and Gosselink 2015). These conditions are more likely to occur if the bioretention system contains an internal saturated zone intended to promote denitrification (Palmer et al. 2013). The P released during this process may, however, be redistributed within the media, including sorption to newly formed solid-phase Fe(II) compounds (Shober and Sims 2009). Nevertheless, the impacts of saturated conditions on the solubility of Fe-based amendments and associated release of Fe(III)-adsorbed P have not yet been researched for bioretention media, as all experiments performed on Fe-based amendments installed within internal saturated zones used materials that contain high amounts of both Fe and Al (Ding et al. 2019; Passeport et al. 2009). Reducing conditions can also be avoided by installing the Fe-based amendment within a layer that is above the internal saturated zone (Glaister et al. 2014; Kratky et al. 2018). Still, saturated conditions remain a concern for Fe-

based amendments due to the possibility of Fe particles clumping and forming conglomerates with the filter material (Erickson et al. 2017; Erickson et al. 2018). This would not only reduce the contact time and area with the amendment material, but would also create maintenance requirements to break up the clumped particles.

Amendments that are Ca-based present constructability and operational challenges due to the presence of Ca oxides or Ca carbonates in the materials that can dissolve when exposed the neutral to acidic pH conditions that are typical in stormwater runoff (Stevenson and Cole 1999; Stumm and Morgan 1996). This can cause clumping of the materials and clogging of the filter media, reduced P sorption, and leaching of Ca and P into the discharge (Adhikari et al. 2016; Brown et al. 2009; Chavez et al. 2015; Duranceau and Biscardi 2015; Elliott et al. 2002; Li et al. 2018a, Lyngsie et al. 2015; Zhang et al. 2018). Fly ash, which is the most commonly used Ca-based amendment, presents multiple constructability challenges due to its small particle size and because it clots when exposed to small levels of moisture (Brown et al. 2009; Chavez et al. 2015). While clotting can potentially reduce sorption capabilities, it also creates material storage challenges and difficulties in achieving homogeneous mixtures within bioretention media (Chavez et al. 2015; Duranceau and Biscardi 2015; Kandel et al. 2017). Previous efforts made in the field to incorporate fly ash into bioretention media by mixing it with a loader bucket and rototilling have resulted in considerable heterogeneity in fly ash distribution in the media (Chavez et al. 2015). However, heterogeneity may not greatly reduce performance, as poorly mixed fly ash in bioretention media does not result in significant preferential flow (Chavez et al. 2013).

Another concern with fly ash and other Ca-based amendments is that they increase the pH of stormwater runoff from near neutral to alkaline levels. For example, the pH of the effluent in fly ash amended systems was found to be in the range of 7.7 to 10.3 from column studies (Wendling et al. 2013; Zhang et al. 2008) and in the range of 7.5 to 10.4 from field studies (Brown et al. 2009; Kandel et al. 2017). Other amendments including blast furnace slag, steel slag, recycled concrete aggregate, cockle shells, limestone, olivine, shell sand, Filtralite-PTM, Filtra PTM, SachtoferTM, and Ca-WTR were found to increase the pH of the stormwater runoff influent to between 7.6 and 13.0 (Goh et al. 2015; Goh et al. 2017; Guo et al. 2015; Klimeski et al. 2014; Sanford and Larson 2016; Wendling et al. 2013; Wium-Andersen et al. 2012). In the USA, stormwater runoff discharged from an industrial site must have a pH in the range of 6.0 to 9.0,

although these values may be superseded by local guidelines (USEPA 2015). This increase in pH should therefore be considered if Ca-based amendments are selected, as alkaline discharge may not be desired or may exceed regulated limits. Furthermore, stormwater runoff having a neutral to acidic pH level does not present ideal conditions for Ca-based amendments, as P sorption through precipitates are favoured at higher pH levels (Adhikari et al. 2016; Sanford and Larson 2016; Stevenson and Cole 1999; Zhang et al. 2008).

Some amendments may also present clogging concerns by reducing the hydraulic conductivity of the bioretention media if the particle sizes of the amendments are smaller than those of the media. In particular, clogging and hydraulic conductivity concerns were highlighted in reviewed studies for alum, fly ash, and Phoslock™ (Duranceau and Biscardi 2015; Randall and Bradford 2013; Yan et al. 2018; Zhang et al. 2008). Alum was found to reduce the hydraulic conductivity of bioretention media from 90 mm/h to below 10 mm/h when mixed at 10% by mass (Yan et al. 2018), fly ash was found to reduce the hydraulic conductivity of the media from 340 mm/h to 9.1 mm/h when mixed at 5% by mass (Zhang et al. 2008), and Phoslock™ was found to clog the media and provide inadequate phosphorus treatment due to runoff bypassing the system (Randall and Bradford 2013). While reducing the percent composition of these amendments within the media would mitigate their impacts on hydraulic conductivities, adequate quantities of the amendments are still needed to provide P sorption benefits. For example, the 5% by mass mixture of fly ash is the amount recommended by Zhang et al. (2008) to provide adequate P sorption, and it is also the typical amount used in field installations (Brown et al. 2009; Chavez et al. 2015; Kandel et al. 2017). Another way to prevent inadequate hydraulic conductivities for amended media is to use a coarser soil mixture (Yan et al. 2018), although fine amendment material particles in coarser mixtures may move downward towards the bottom of the system (Duranceau and Biscardi 2015).

4 Conclusions and Recommendations

This review provides a systematic evaluation of research to date on P sorption amendments applied to bioretention systems. While the focus of this study is on bioretention systems containing components such as vegetation and organic matter, many of the findings discussed in this review may also be applied to other media-based stormwater control measures such as permeable pavement systems, infiltration galleries, and green roofs. This review identified 51

amendments that have been investigated by researchers in laboratory settings, of which only four have been evaluated in the field (Brown et al. 2009; Cording et al. 2018; Houle et al. 2017; Kandel et al. 2017; Liu and Davis 2014; Passeport et al. 2009; Shrestha et al. 2018) and only one has been evaluated in an aged system (Kandel et al. 2017). The application of these materials to a field setting and their corresponding long-term P removal performance therefore needs further investigation. For many of the amendments studied, additional research still needs to be conducted to determine their proportion in the bioretention media that would simultaneously enhance P sorption without reducing infiltration. Moreover, the integration of amendments within internal storage layers and mixtures containing carbon-based amendments intended for nitrogen removal requires additional research (Chang et al. 2011; Chang et al. 2018; Ding et al. 2019; Guo et al. 2015; Hood et al. 2015; Kim et al. 2018; Kratky et al. 2018; Li et al. 2018a; Liu et al. 2014; Palmer et al. 2013; Passeport et al. 2009; Zhang et al. 2018; Zhou et al. 2016). The ability of P sorption amendments in bioretention media to sorb DOP in addition to SRP is also scarcely evaluated in the literature (Liu and Davis 2014; Lucas and Greenway 2011; Yan et al. 2017; Yan et al. 2018). Overall, the applicability of P sorption amendments for bioretention media can be evaluated by categorizing the amendment materials based on the dominant metal(s) they contain that drive the P sorption. Recommendations for amendment selection based on their dominant metal(s) are summarized in Table D5 and are provided as follows:

- Ca-rich amendments such as Ca-WTR, fly ash, blast furnace slag, steel slag, recycled concrete aggregate, marine animal shells, limestone, Filtralite-P™, Filtra P™, and Sachtofer™ require alkaline conditions for precipitation reactions, can increase the pH of runoff to alkaline levels, can dissolve and leach Ca and P, and can create clumping and clogging at neutral to acidic pH levels (Adhikari et al. 2016; Brown et al. 2009; Chavez et al. 2015; Duranceau and Biscardi 2015; Elliott et al. 2002; Erickson et al. 2007; Goh et al. 2015; Goh et al. 2017; Kandel et al. 2017; Li et al. 2018a; Klimeski et al. 2014; Lyngsie et al. 2015; Wendling et al. 2013; Wium-Andersen et al. 2012; Zhang et al. 2008). These materials should therefore be limited to applications where alkaline conditions are naturally present and are not damaging to the downstream watershed.
- Fe-rich amendments such as Fe-WTR, steel chips, steel slag, acid mine drainage residuals, iron coated sand, olivine, natural and expanded soils, Fe products, and Sorbtive Media™ may present performance concerns if the bioretention media is intended to be saturated for

extended periods of time, as a shift from oxidized conditions to reducing conditions can result in the dissolution of P-containing Fe(III) minerals, thus releasing P to the environment and potentially clogging the soil (Erickson et al. 2017; Erickson et al. 2018; Palmer et al. 2013). However, to date, such negative impacts on the potential release of adsorbed P on Fe(III) has not been demonstrated in a bioretention setting. Indeed, the P cycle is complex and not entirely dependent on Fe minerals. Other components of the bioretention system, e.g., the non redox-sensitive Al oxides that can adsorb released P and precipitates that are stable under reducing conditions, can maintain a high P adsorption capacity of the bioretention media. Consequently, more research is needed on the use of Fe-based amendments during intermittent flow and within internal saturated zones to quantify potential issues on drainage and water quality associated with the temporary presence of anaerobic conditions.

- Al-rich amendments such as Al-WTR, bottom ash, red mud, aluminum oxide coated media, medical stone, zeolite, natural and expanded soils, Sorbtive MediaTM, alum, and partially hydrolyzed aluminum seem to present the lowest performance limitations and are therefore the most promising materials for P sorption amendments in bioretention media. They perform well under a range of neutral to acidic pH levels, can act as a pH buffer, are not known to leach metals, and can potentially be integrated within internal saturated zones (Adhikari et al. 2016; Ding et al. 2019; Lucas and Greenway 2011; O'Neill and Davis 2012a; Poor et al. 2018; Randall and Bradford 2013). However, the selected amendment should not have an alkaline pH that would reduce the sorption capabilities of Al-based amendments (Zhang et al. 2008). Furthermore, alum and partially hydrolyzed aluminum may not be practical due to their processing requirements and negative impacts on infiltration rates.
- Materials composed of other sorptive metals can potentially be used for media amendments. While the study by Randall and Bradford (2011) found that the La-based PhoslockTM product can create clogging concerns, the use of La or other sorptive metals should be further explored.

Table D5: Summary of recommendations for amendment selection and installation methods.

Activity	Item	Applicability	Issues and Concerns
Amendment Selection	Al-based amendments	- Runoff has neutral to acidic pH.	- Weaker sorption reactions if runoff has alkaline pH.
	Fe-based amendments	- Runoff has neutral to acidic pH. - Well-draining bioretention systems. - Amendment installed above internal saturated zones.	- Weaker sorption reactions if runoff has alkaline pH. - Dissolution of Fe(III) under saturated conditions can release previously adsorbed P and/or cause clumping and clogging.
	Ca-based amendments	- Runoff has alkaline pH. - Alkaline runoff does not harm downstream watershed. - Amendment installed above internal saturated zones.	- Weaker precipitation reactions if runoff has neutral to acidic pH. - Can increase pH of runoff. - Can dissolve and leach Ca and P. - Can create clumping and clogging if runoff has neutral to acidic pH.
Installation Method	Mix amendment into media prior to installation	- Conventional installation.	- Challenges in achieving a homogeneous mixture and preventing segregation. - Amendment can potentially reduce the hydraulic conductivity of the media.
	Install amendment as a layer below the media or organic layer	- Amendment layer does not limit the hydraulic conductivity of the system. - Media layer has high organic content or P leaching. - Bioretention system is designed with removable filters.	- Amendment layer can potentially limit drainage or cause clogging. - Amendment layer depth should be limited to above internal saturated zone for some Fe- and Ca-based amendment materials prone to dissolution.
	Rototill amendment into top of media	- Retrofitting an existing bioretention system.	- Only amends the top of the bioretention media. - Additional challenges in achieving a homogeneous mixture.
	Use amendment as bedding layer for underdrain	- Bioretention system includes an underdrain. - Coarse amendment materials.	- Amendment may have low contact time with runoff.

Methods and configurations for installing amendments within bioretention systems also need to be further researched. A summary of recommendations for installation methods and amendment configurations is also provided in Table D5. While many of the reviewed studies reported on amendments that were uniformly mixed within the entire depth of the media, other studies invoked the placement of amendment materials, amended sand, or amended media as layers above or below the media (Cording et al. 2018; Chang et al. 2018; Erickson et al. 2007; Kim et

al. 2018; Kratky et al. 2018; Li et al. 2016a; Li et al. 2016b; Poor et al. 2018b; Randall and Bradford 2013; Shrestha et al. 2018; Weiss et al. 2016; Wendling et al. 2013). Layering has been shown to increase P sorption when using Al-WTR (Poor et al. 2018b), and placing the layer towards the top of the system may further improve performance, provided that the amendment layer is placed below any layer containing organic matter (Chang et al. 2018; Kim et al. 2018; Poor et al. 2018b). The use of an amendment layer may also be beneficial when using Fe- and Ca-based amendments in bioretention systems containing internal saturated zones, as the amendment layer depth can be limited such that it remains above the internal saturated zone, avoiding potential issues associated with Fe- and Ca-based amendments being exposed to prolonged saturated conditions (Brown et al. 2009; Chavez et al. 2015; Glaister et al. 2014; Kratky et al. 2018). Some Fe- and Ca-based amendments that are known to cause clumping and amendments with small particle sizes may need to be mixed with a sufficient proportion of sand or bioretention media prior to installing them as a layer, as this reduces the risk of clogging (Brown et al. 2009; Chavez et al. 2015; Duranceau and Biscardi 2015; Erickson et al. 2017; Erickson et al. 2018). In addition to impacting P sorption performance, layering may also allow for the use of removable filters that could be replaced once the adsorption capacity is exhausted, although no research on the topic was identified by this review and such a configuration would require further engineering design.

Alternatively, bioretention systems can be retrofitted with amendments by rototilling the materials near the top of the media, as demonstrated by Liu and Davis (2014) with Al-WTR. This retrofit method would concentrate the added P removal capacity in the top of the bioretention media, which is where most of the P removal takes place in unamended bioretention systems (Johnson and Hunt 2016; Komlos and Traver 2012; Muerdter et al. 2016; Willard et al. 2017). However, mixing issues have been identified when attempting to rototill other amendments such as iron filings (Erickson et al. 2017) and fly ash (Chavez et al. 2015) into sand, so practical considerations are needed based on the selected amendment. In addition to amending the media layer, coarser amendment materials such as expanded shales can be used to replace the washed gravels within the drainage layers of bioretention systems (Zhang et al. 2008), although no research has been carried out on this type of configuration. Nevertheless, if the coarser material is not likely to solubilize under prolonged saturated conditions, the amended drainage layer could potentially also be used as an internal saturated zone to promote denitrification.

In summary, the following areas were identified from this review as in need of future research:

- Field investigations of the performance of amendments for P sorption.
- Evaluation of the long-term performance of P amendments and estimations of amendment life-spans.
- Determining the appropriate range of proportions of the amendments in the bioretention media that would simultaneously enhance P sorption without reducing infiltration rates.
- Quantifying the performance of P amendments for DOP.
- Providing direct evidence for the potential of Fe-based amendments to release P under realistic durations of saturation conditions and intermittent flow, and for bioretention cells incorporating an internal water storage zone.
- Quantifying the P sorption potential of amendments that were originally not intended for P removal, e.g., carbon-based amendments intended for nitrogen removal.
- Evaluating the performance and clogging potential of La-based amendments.
- Investigating the P sorption potential of amendments incorporating metals other than Al, Fe, Ca, and La.
- Investigating methods and configurations for the proper incorporation of amendments within bioretention systems.
- Evaluating the potential to use removable filters in layered configurations that could be replaced once the P adsorption capacity of the amendments is exhausted.
- Investigating the P sorption potential of coarser amendment materials such as expanded shales to replace the washed gravels within the drainage layers of bioretention systems.

References

- Adhikari, R. A., Bal Krishna, K. C., and Sarukkalige, R. (2016). "Evaluation of phosphorus adsorption capacity of various filter materials from aqueous solution." *Adsorpt. Sci. and Technol.* 34(4–5), 320–330.
- Allred, B. J., Martinez, L. R., and Gamble, D. L. (2017). "Phosphate removal from agricultural drainage water using an iron oxyhydroxide filter material." *Water Air Soil Pollut.* 228(7), 220.
- Allred, B. J., and Racharaks, R. (2014). "Laboratory comparison of four iron-based filter materials for drainage water phosphate treatment." *Water Environ. Res.* 86(9), 852–862.
- Ballantine, D. J., and Tanner, C. C. (2010). "Substrate and filter materials to enhance phosphorus removal in constructed wetlands treating diffuse farm runoff: A review." *N. Z. J. Agric. Res.* 53(1), 71–95.
- Bolan, N. S. (1991). "A critical review on the role of mycorrhizal fungi in the uptake of phosphorus by plants." *Plant Soil*, 134(2), 189–207.
- Bratieres, K., Fletcher, T. D., Deletic, A., and Zinger, Y. (2008). "Nutrient and sediment removal by stormwater biofilters: A large-scale design optimisation study." *Water Res.* 42(14), 3930–3940.
- Brown, G. O., Chavez, R. A., Storm, D. E., and Smolen, M. D. (2009). "Construction and performance of bioretention cells." *Proc., World Environmental and Water Resources Congress 2009: Great Rivers*, ASCE, Kansas City, MO, 981–990.
- Brown, S., Corfman, A., Mendrey, K., Kurtz, K., and Grothkopp, F. (2016). "Stormwater bioretention systems: Testing the phosphorus saturation index and compost feedstocks as predictive tools for system performance." *J. Environ. Qual.* 45(1), 98–106.
- Canga, E., Heckrath, G. J., and Kjaergaard, C. (2016). "Agricultural Drainage Filters. II. Phosphorus Retention and Release at Different Flow Rates." *Water Air Soil Pollut.* 227(8), 276.
- Chang, N.-B., Wanielista, M. P., and Henderson, D. (2011). "Temperature effects on functionalized filter media for nutrient removal in stormwater treatment." *Environ. Prog. Sustainable Energy*, 30(3), 309–317.
- Chang, N.-B., Wen, D., and Wanielista, M. P. (2018). "Impact of changing environmental factors and species competition on iron filings-based green environmental media for nutrient removal in stormwater treatment." *Environ. Prog. Sustainable Energy*.
- Chavez, R. A., Brown, G. O., Coffman, R. R., and Storm, D. E. (2015). "Design, construction and lessons learned from Oklahoma bioretention cell demonstration project." *Appl. Eng. Agric.* 31(1), 63–71.

- Chavez, R. A., Brown, G. O., and Storm, D. E. (2013). "Impact of variable hydraulic conductivity on bioretention cell performance and implications for construction standards." *J. of Hydraul. Eng.* 139(7), 707–715.
- Clary, J., Jones, J., Leisenring, M., Hobson, P., and Strecker, E. (2017). *International stormwater BMP database: 2016 summary statistics*. Water Environment & Reuse Foundation, Alexandria, VA.
- Cording, A., Hurley, S., and Adair, C. (2018). "Influence of critical bioretention design factors and projected increases in precipitation due to climate change on roadside bioretention performance." *J. Environ. Eng.* 144(9), 04018082.
- Cucarella, V., and Renman, G. (2009). "Phosphorus sorption capacity of filter materials used for on-site wastewater treatment determined in batch experiments: A comparative study." *J. Environ. Qual.* 38(2), 381–392.
- Davis, A. P., Hunt, W. F., Traver, R. G., and Clar, M. (2009). "Bioretention technology: Overview of current practice and future needs." *J. Environ. Eng.* 135(3), 109–117.
- Davis, A. P., Shokouhian, M., Sharma, H., and Minami, C. (2006). "Water quality improvement through bioretention media: Nitrogen and phosphorus removal." *Water Environ. Res.* 78(3), 284–293.
- Ding, B., Rezanezhad, F., Gharedaghlou, B., Van Cappellen, P., and Passeport, E. (2019). "Bioretention cells under cold climate conditions: Effects of freezing and thawing on water infiltration, soil structure, and nutrient removal." *Sci. Total Environ.* 649, 749–759.
- Duranceau, S. J., and Biscardi, P. G. (2015). "Comparing adsorptive media use for the direct treatment of phosphorous-impaired surface water." *J. Environ. Eng.* 141(8), 04015012.
- Elliott, H. A., O'Connor, G. A., Lu, P., and Brinton, S. (2002). "Influence of water treatment residuals on phosphorus solubility and leaching." *J. Environ. Qual.* 31(4), 1362–1369.
- Erickson, A. J., Gulliver, J. S., and Weiss, P. T. (2007). "Enhanced sand filtration for storm water phosphorus removal." *J. Environ. Eng.* 133(5), 485–497.
- Erickson, A. J., Gulliver, J. S., and Weiss, P. T. (2012). "Capturing phosphates with iron enhanced sand filtration." *Water Res.* 46(9), 3032–3042.
- Erickson, A. J., Gulliver, J. S., and Weiss, P. T. (2017). "Phosphate removal from agricultural tile drainage with iron enhanced sand." *Water*, 9(9), 1–17.
- Erickson, A. J., Weiss, P. T., and Gulliver, J. S. (2018). "Monitoring and maintenance of phosphate adsorbing filters." *J. Environ. Eng.* 144(1), 05017007.
- Glaister, B. J., Fletcher, T. D., Cook, P. L. M., and Hatt, B. E. (2014). "Co-optimisation of phosphorus and nitrogen removal in stormwater biofilters: The role of filter media, vegetation and saturated zone." *Water Sci. Technol.* 69(9), 1961–1969.

- Goh, H. W., Lau, T. L., Foo, K. Y., Chang, C. K., and Zakaria, N. A. (2015). "Influence of hydraulic conductivity and organic matter content in different bioretention media on nutrient removal." *Appl. Mech. Mater.* 802, 448–453.
- Goh, H. W., Zakaria, N. A., Lau, T. L., Foo, K. Y., Chang, C. K., and Leow, C. S. (2017). "Mesocosm study of enhanced bioretention media in treating nutrient rich stormwater for mixed development area." *Urban Water J.* 14(2), 134–142.
- Greenway, M. (2016). "Media for enhanced phosphorus removal from secondary wastewater effluent." *Proc., World Environmental and Water Resources Congress 2016: Water, Wastewater and Stormwater, and Urban Watershed Symposium*, ASCE, West Palm Beach, FL, 408–418.
- Guo, H., Lim, F. Y., Zhang, Y., Lee, L. Y., Hu, J. Y., Ong, S. L., Yau, W. K., and Ong, G. S. (2015). "Soil column studies on the performance evaluation of engineered soil mixes for bioretention systems." *Desalin. Water Treat.* 54(13), 3661–3667.
- Hatt, B. E., Fletcher, T. D., and Deletic, A. (2009). "Pollutant removal performance of field-scale stormwater biofiltration systems." *Water Sci. Technol.* 59(8), 1567–1576.
- Hood, A., Chopra, M., and Wanielista, M. (2013). "Assessment of biosorption activated media under roadside swales for the removal of phosphorus from stormwater." *Water*, 5(1), 53–66.
- Houle, J. J., Ballestoero, T. P., and Puls, T. A. (2017). "The performance analysis of two relatively small capacity urban retrofit stormwater controls." *J. Water Manage. Model.* 25, C417.
- Hsieh, C.-H., and Davis, A. P. (2005). "Evaluation and optimization of bioretention media for treatment of urban storm water runoff." *J. Environ. Eng.* 131(11), 1521–1531.
- Hsieh, C.-H., Davis, A. P., and Needelman, B. A. (2007). "Bioretention column studies of phosphorus removal from urban stormwater runoff." *Water Environ. Res.* 79(2), 177–184.
- Hunt, W. F., Jarrett, A. R., Smith, J. T., and Sharkey, L. J. (2006). "Evaluating bioretention hydrology and nutrient removal at three field sites in North Carolina." *J. Irrig. Drain. Eng.* 132(6), 600–608.
- Jay, J. G., Brown, S. L., Kurtz, K., and Grothkopp, F. (2017). "Predictors of phosphorus leaching from bioretention soil media." *J. Environ. Qual.* 46(5), 1098–1105.
- Johnson, J. P., and Hunt, W. F. (2016). "Evaluating the spatial distribution of pollutants and associated maintenance requirements in an 11 year-old bioretention cell in urban Charlotte, NC." *J. Environ. Manage.* 184, 363–370.
- Jones, J., Chang, N.-B., and Wanielista, M. P. (2015). "Reliability analysis of nutrient removal from stormwater runoff with green sorption media under varying influent conditions." *Sci. Total Environ.* 502, 434–447.

- Kadlec, R. H., and Wallace, S. (2008). "Phosphorus." Chapter 10 in *Treatment Wetlands*, 2nd Ed. CRC Press, Boca Raton, FL, 349–402.
- Kandel, S., Vogel, J., Penn, C., and Brown, G. (2017). "Phosphorus retention by fly ash amended filter media in aged bioretention cells." *Water*, 9(10), 746.
- Kim, H. J., Choi, J.-W., Kim, T.-H., Park, J.-S., and An, B. (2018). "Effect of TSS removal from stormwater by mixed media column on T-N, T-P, and organic material removal." *Water*, 10(8), 1069.
- Klimeski, A., Uusitalo, R., and Turtola, E. (2014). "Screening of Ca- and Fe-rich materials for their applicability as phosphate-retaining filters." *Ecol. Eng.* 68, 143–154.
- Komlos, J., and Traver, R. G. (2012). "Long-term orthophosphate removal in a field-scale stormwater bioinfiltration rain garden." *J. Environ. Eng.* 138(10), 991–998.
- Kratky, H., Li, Z., Li, X., and Yu, T. (2018). "Laboratory study on the performance of bioretention for stormwater management in cold climates." *Proc., International Low Impact Development Conference 2018: Getting in Tune with Green Infrastructure*, ASCE, Nashville, TN, 90–100.
- Lee, L. Y., Wang, B., Guo, H., Hu, J. Y., and Ong, S. L. (2015). "Aluminum-based water treatment residue reuse for phosphorus removal." *Water*, 7(4), 1480–1496.
- LeFevre, G. H., Paus, K. H., Natarajan, P., Gulliver, J. S., Novak, P. J., and Hozalski, R. M. (2015). "Review of dissolved pollutants in urban storm water and their removal and fate in bioretention cells." *J. Environ. Eng.* 141(1), 04014050.
- Li, B., and Brett, M. T. (2013). "The influence of dissolved phosphorus molecular form on recalcitrance and bioavailability." *Environ. Pollut.* 182, 37–44.
- Li, J., and Davis, A. P. (2016). "A unified look at phosphorus treatment using bioretention." *Water Res.* 90, 141–155.
- Li, J., Jiang, C., Lei, T., and Li, Y. (2016a). "Experimental study and simulation of water quality purification of urban surface runoff using non-vegetated bioswales." *Ecol. Eng.* 95, 706–713.
- Li, J., Li, L., Dong, W., and Li, H. (2018a). "Purification effects of amended bioretention columns on phosphorus in urban rainfall runoff." *Water Sci. Technol.* 78(9), 1937–1945.
- Li, J., Li, Y., Zhang, J., and Li, Y. (2016b). "Bioswale column experiments and simulation of pollutant removal from urban road stormwater runoff." *Desalin. Water Treat.* 57(52), 24894–24912.
- Li, J., Liang, Z., Li, Y., Li, P., and Jiang, C. (2018b). "Experimental study and simulation of phosphorus purification effects of bioretention systems on urban surface runoff." *PLoS One*, 13(5), e0196339.

- Line, D. E., and White, N. M. (2007). "Effects of development on runoff and pollutant export." *Water Environ. Res.* 79(2), 185–190.
- Liu, F., Zuo, J., Chi, T., Wang, P., and Yang, B. (2015). "Removing phosphorus from aqueous solutions by using iron-modified corn straw biochar." *Front. Environ. Sci. Eng.* 9(6), 1066–1075.
- Liu, J., and Davis, A. P. (2014). "Phosphorus speciation and treatment using enhanced phosphorus removal bioretention." *Environ. Sci. Technol.* 48(1), 607–614.
- Liu, J., Sample, D. J., Owen, J. S., Li, J., and Evanylo, G. (2014). "Assessment of selected bioretention blends for nutrient retention using mesocosm experiments." *J. Environ. Qual.* 43(5), 1754–1763.
- Lucas, W. C., and Greenway, M. (2008). "Nutrient retention in vegetated and nonvegetated bioretention mesocosms." *J. Irrig. Drain. Eng.* 134(5), 613–623.
- Lucas, W. C., and Greenway, M. (2011). "Phosphorus retention by bioretention mesocosms using media formulated for phosphorus sorption: Response to accelerated loads." *J. Irrig. Drain. Eng.* 137(3), 144–153.
- Lyngsie, G., Penn, C. J., Pedersen, H. L., Borggaard, O. K., and Hansen, H. C. B. (2015). "Modelling of phosphate retention by Ca- and Fe-rich filter materials under flow-through conditions." *Ecol. Eng.* 75, 93–102.
- Ma, J., and Sansalone, J. (2007). "Mass transfer behavior of media for treatment of stormwater phosphorus." *Proc., World Environmental and Water Resources Congress 2007: Restoring Our Natural Habitat*, ASCE, Tampa, FL.
- McTaggart, C., Farago, L., Jegatheesan, V., and Shu, L. (2015). "Storm water harvesting and reuse in Australia: enhanced sand filtration for the treatment of storm water." *Desalin. Water Treat.* 54(4–5), 1327–1333.
- Mendelssohn, I. A., Kleiss, B. A., and Wakeley, J. S. (1995). "Factors controlling the formation of oxidized root channels: A review." *Wetlands*, 15(1), 37–46.
- Mitsch, W. J., and Gosselink, J. G. (2015). "Wetland Biogeochemistry." Chapter 6 in *Wetlands*, 5th Ed. John Wiley & Sons, Hoboken, NJ, 179–214.
- Muerdter, C., Ozkok, E., Li, L., Davis, A. P., Özkök, E., Li, L., and Davis, A. P. (2016). "Vegetation and media characteristics of an effective bioretention cell." *J. Sustainable Water Built Environ.* 2(1), 04015008.
- O'Neill, S. W., and Davis, A. P. (2012a). "Water treatment residual as a bioretention amendment for phosphorus. I: Evaluation studies." *J. Environ. Eng.* 138(3), 318–327.
- O'Neill, S. W., and Davis, A. P. (2012b). "Water treatment residual as a bioretention amendment for phosphorus. II: Long-term column studies." *J. Environ. Eng.* 138(3), 328–336.

- Palmer, E. T., Poor, C. J., Hinman, C., and Stark, J. D. (2013). "Nitrate and phosphate removal through enhanced bioretention media: Mesocosm study." *Water Environ. Res.* 85(9), 823–832.
- Passeport, E., Hunt, W. F., Line, D. E., Smith, R. A., and Brown, R. A. (2009). "Field study of the ability of two grassed bioretention cells to reduce storm-water runoff pollution." *J. Irrig. Drain. Eng.* 135(4), 505–510.
- Paul, M. J., and Meyer, J. L. (2001). "Streams in the urban landscape." *Annu. Rev. Ecol. Syst.* 32(1), 333–365.
- Penn, C., Chagas, I., Klimeski, A., and Lyngsie, G. (2017). "A review of phosphorus removal structures: How to assess and compare their performance." *Water*, 9(8), 583.
- Poor, C., Balmes, C., Freudenthaler, M., and Martinez, A. (2018). "Role of mycelium in bioretention systems: Evaluation of nutrient and metal retention in mycorrhizae-inoculated mesocosms." *J. Environ. Eng.* 144(6), 04018034.
- Poor, C. J., Conkle, K., MacDonald, A., and Duncan, K. (2018). "Water treatment residuals in bioretention planters to reduce phosphorus levels in stormwater." *Environ. Eng. Sci.*
- Randall, M. T., and Bradford, A. (2013). "Bioretention gardens for improved nutrient removal." *Water Qual. Res. J. Can.* 48(4), 372–386.
- Ryccewicz-Borecki, M., McLean, J. E., and Dupont, R. R. (2017). "Nitrogen and phosphorus mass balance, retention and uptake in six plant species grown in stormwater bioretention microcosms." *Ecol. Eng.* 99, 409–416.
- Sanford, J. R., and Larson, R. A. (2016). "Evaluation of phosphorus filter media for an inline subsurface drainage treatment system." *J. Environ. Qual.* 45(6), 1919–1925.
- Sellner, B. M., Hua, G., and Ahiablame, L. M. (2019). "Fixed bed column evaluation of phosphate adsorption and recovery from aqueous solutions using recycled steel byproducts." *J. Environ. Manage.* 233, 595–602.
- Shober, A. L., and Sims, J. T. (2009). "Evaluating phosphorus release from biosolids and manure-amended soils under anoxic conditions." *J. Environ. Qual.* 38(1), 309–318.
- Shrestha, P., Hurley, S. E., and Wemple, B. C. (2018). "Effects of different soil media, vegetation, and hydrologic treatments on nutrient and sediment removal in roadside bioretention systems." *Ecol. Eng.* 112, 116–131.
- Soleimanifar, H., Deng, Y., Wu, L., and Sarkar, D. (2016). "Water treatment residual (WTR)-coated wood mulch for alleviation of toxic metals and phosphorus from polluted urban stormwater runoff." *Chemosphere*, 154, 289–292.
- Stevenson, F. J., and Cole, M. A. (1999). "The phosphorus cycle." Chapter 9 in *Cycles of soils: Carbon, nitrogen, phosphorus, sulfur, micronutrients*, 2nd Ed. John Wiley & Sons, New York, NY, 279–329.

- Stoner, D., Penn, C., McGrath, J., and Warren, J. (2012). "Phosphorus removal with by-products in a flow-through setting." *J. Environ. Qual.* 41(3), 654–663.
- Stumm, W., and Morgan, J. J. (1996). "Precipitation and dissolution." Chapter 7 in *Aquatic chemistry: Chemical equilibria and rates in natural waters*, 3rd Ed. John Wiley & Sons, New York, NY, 349–424.
- Taylor, A., Wetzel, J., Mudrock, E., King, K., Cameron, J., Davis, J., and McIntyre, J. (2018). "Engineering analysis of plant and fungal contributions to bioretention performance." *Water*, 10(9), 1226.
- U.S. Environmental Protection Agency (USEPA). (1999). *Preliminary data summary of urban storm water best management practices*. EPA-821-R-99-012, Office of Water (4303), Washington, DC.
- U.S. Environmental Protection Agency (USEPA). (2015). *National pollutant discharge elimination system (NPDES) multi-sector general permit for stormwater discharges associated with industrial activity (MSGP)*. Washington, DC.
- Van Tichelen, K. K., and Colpaert, J. V. (2000). "Kinetics of phosphate absorption by mycorrhizal and non-mycorrhizal Scots pine seedlings." *Physiol. Plant.* 110(1), 96–103.
- Vandermoere, S., Ralaizafisolaoarivony, N. A., Van Ranst, E., and De Neve, S. (2018). "Reducing phosphorus (P) losses from drained agricultural fields with iron coated sand (-glaucanite) filters." *Water Res.* 141, 329–339.
- Wang, D. Q., Chai, G. D., Shan, J. Q., Yang, Z. J., Li, H. E., Li, J. K., and Lin, Y. S. (2018). "Impact of pyrene on pollutant removal and microbial enzyme activities in bioretention systems." *Proc., IOP Conference Series: Earth and Environmental Science*, 191, IOP Publishing, 012108.
- Waschbusch, R. J., Selbig, W. R., and Bannerman, R. T. (1999). "Sources of phosphorus in stormwater and street dirt from two urban residential basins in Madison, Wisconsin, 1994-95." *Water Resources Investigation Rep. 99-4021*, U.S. Geological Survey, Middleton, WI.
- Weiss, P. T., Aljobeh, Z. Y., Bradford, C., and Breitzke, E. A. (2016). "An iron-enhanced rain garden for dissolved phosphorus removal." *Proc., World Environmental and Water Resources Congress 2016: Water, Wastewater and Stormwater, and Urban Watershed Symposium*, ASCE, West Palm Beach, FL, 185–194.
- Wendling, L. A., Douglas, G. B., Coleman, S., and Yuan, Z. (2013). "Nutrient and dissolved organic carbon removal from natural waters using industrial by-products." *Sci. Total Environ.* 442, 63–72.
- Willard, L. L., Wynn-Thompson, T., Krometis, L. H., Neher, T. P., and Badgley, B. D. (2017). "Does it pay to be mature? Evaluation of bioretention cell performance seven years postconstruction." *J. Environ. Eng.* 143(9), 04017041.

- Wium-Andersen, T., Nielsen, A. H., Hvitved-Jacobsen, T., Kristensen, N. K., Brix, H., Arias, C., and Vollertsen, J. (2012). "Sorptions media for stormwater treatment - A laboratory evaluation of five low-cost media for their ability to remove metals and phosphorus from artificial stormwater." *Water Environ. Res.* 84(7), 605–616.
- Yan, Q., James, B. R., and Davis, A. P. (2017). "Lab-scale column studies for enhanced phosphorus sorption from synthetic urban stormwater using modified bioretention media." *J. Environ. Eng.* 143(1), 04016073.
- Yan, Q., James, B. R., and Davis, A. P. (2018). "Bioretention media for enhanced permeability and phosphorus sorption from synthetic urban stormwater." *J. Sustainable Water Built Environ.* 4(1), 04017013.
- Zhang, B., Li, J., Li, Y., and Li, H. (2018). "Adsorption characteristics of several bioretention-modified fillers for phosphorus." *Water*, 10(7), 831.
- Zhang, W., Brown, G. O., Storm, D. E., and Zhang, H. (2008). "Fly-ash-amended sand as filter media in bioretention cells to improve phosphorus removal." *Water Environ. Res.* 80(6), 507–516.
- Zhou, Z., Xu, P., Cao, X., Zhou, Y., and Song, C. (2016). "Efficiency promotion and its mechanisms of simultaneous nitrogen and phosphorus removal in stormwater biofilters." *Bioresour. Technol.* 218, 842–849.